Control of power electronic converters in microgrids

Jesús Doval-Gandoy
jdoval@uvigo.es
http://jdoval.webs.uvigo.es

Contents

- Background of microgrids
- AC current control of grid-connected converters
  - Plant model
  - Interface filter
  - Classical controllers
- Limitations of classical current controllers
- State-space based techniques applied to current controllers
- AC voltage control of standalone or weak grid-tied converters

Contents

- Background of microgrids
- AC current control of grid-connected converters
  - Plant model
  - Interface filter
  - Classical controllers
- Limitations of classical current controllers
- State-space based techniques applied to current controllers
- AC voltage control of standalone or weak grid-tied converters

Centralized grid vs. distributed grid

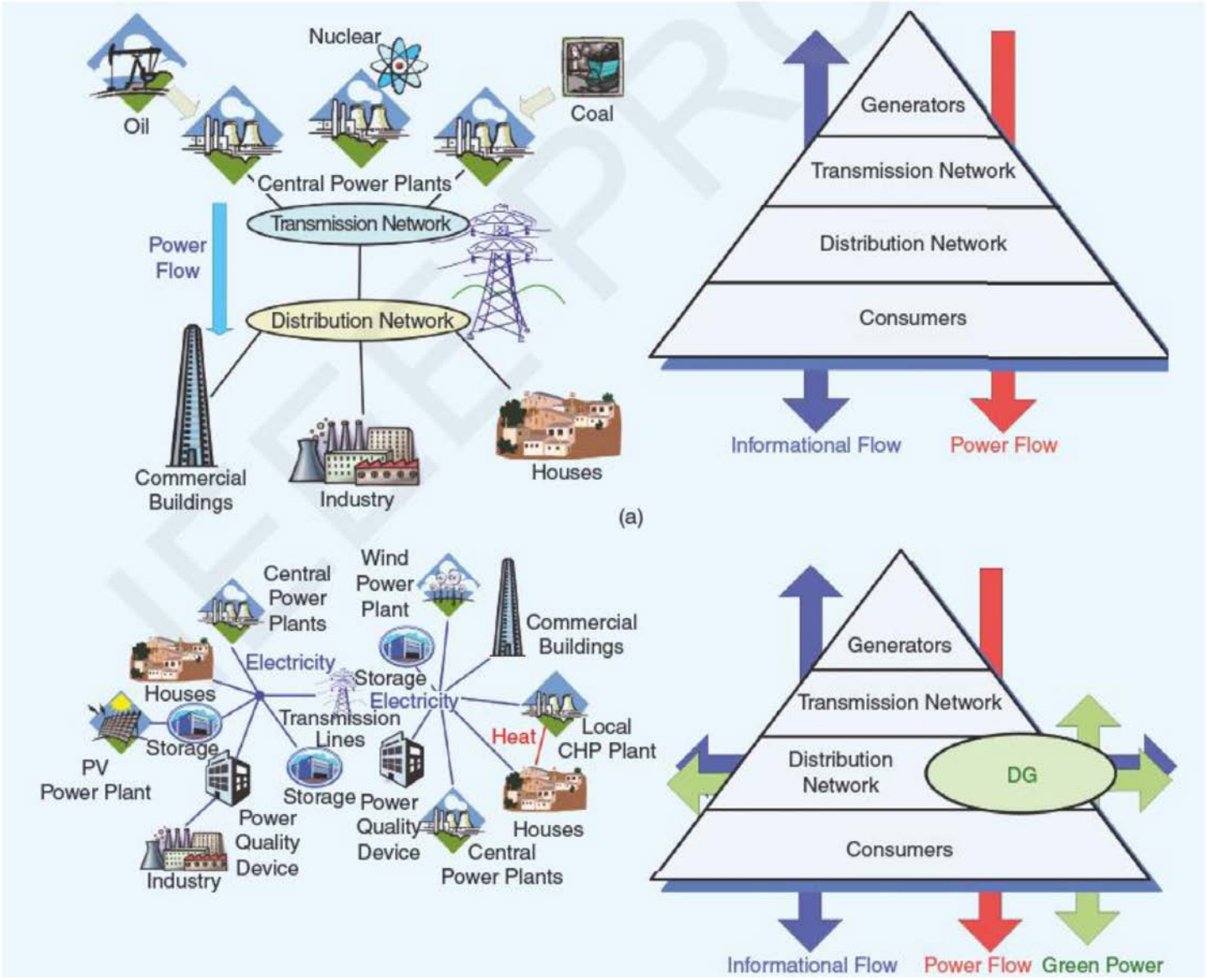

Distributed power generation

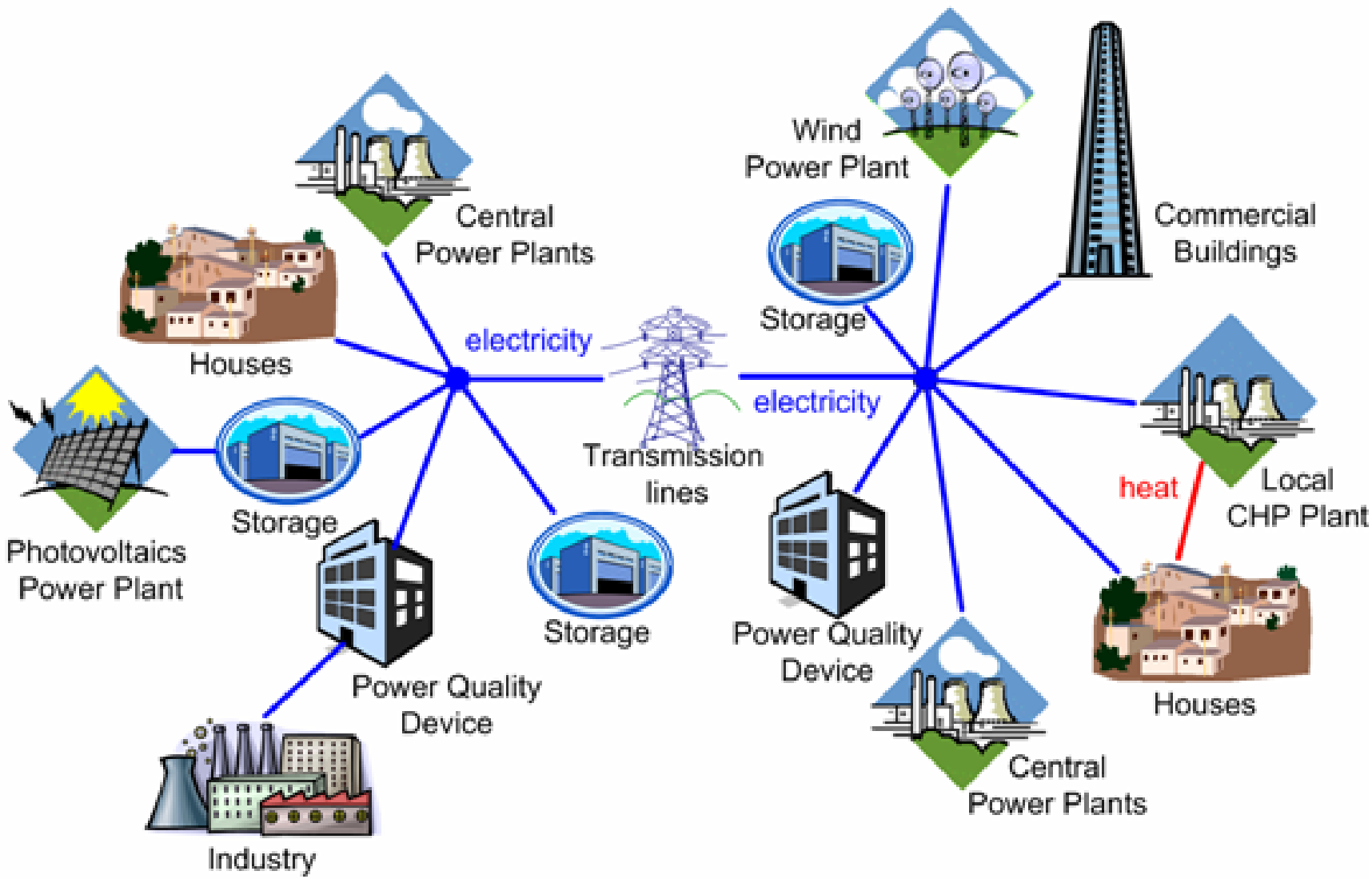

Power system evolution

- Active distribution grids with medium-scale and small-scale generators (hundreds kW to tens MW).
- Involving conventional& renewable technologies, together with storage systems
- Flexible high-voltage transportation systems connecting those grids with lower cost and ROW (Right Of Way) restrictions

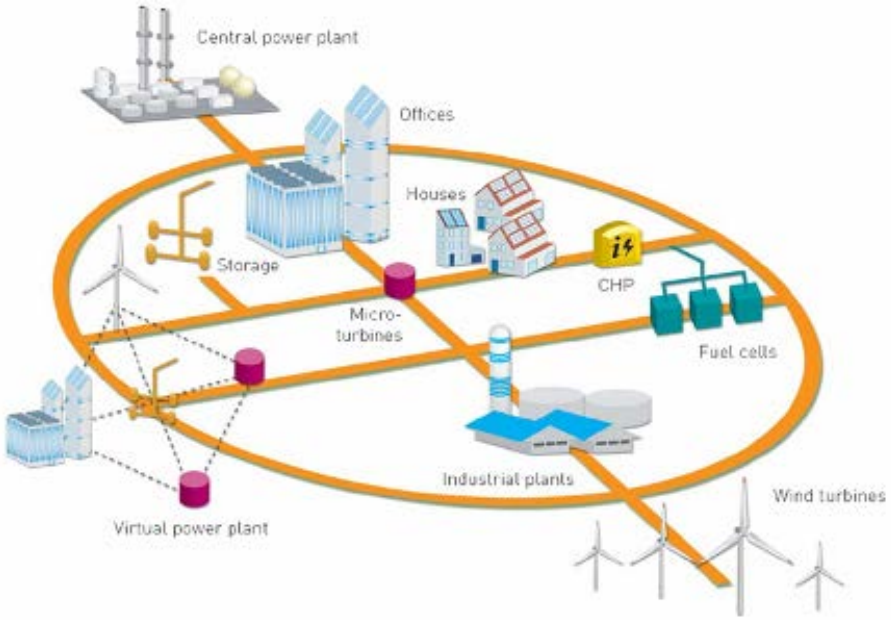

Future: Operation of system will be shared between central and distributed generators. Control of distributed generators could be aggregated to form microgrids or 'virtual' power plants to facilitate their integration both in the physical system and in the market.

- Renewable energy:
  - Photovoltaic
  - Wind
  - Hydrogen
  - Micro-turbines
- Small energy storage systems:
  - UPS (static & dynamic)
  - Flywheels
  - Supercapacitors
  - Compressed air energy storage system CAES
  - Mini-hydraulics
  - Superconducting Magnetic Energy Storage (SMES)
  - Batteries
- Energy production decentralization

Microgrid definition

Traditional grid	Microgrid
Centralized generation	Generation everywhere
Power flows downhill	Power flows from everywhere
Utility controls connections	Anyone may participate
Behavior: predictable	Behavior: chaotic

Microgrid components

- Operation modes
- Energy management systems
- Advanced metering infrastructure
- Energy storage systems
- Distributed generation
- Power electronics interfaces
- Comunications
- Protections

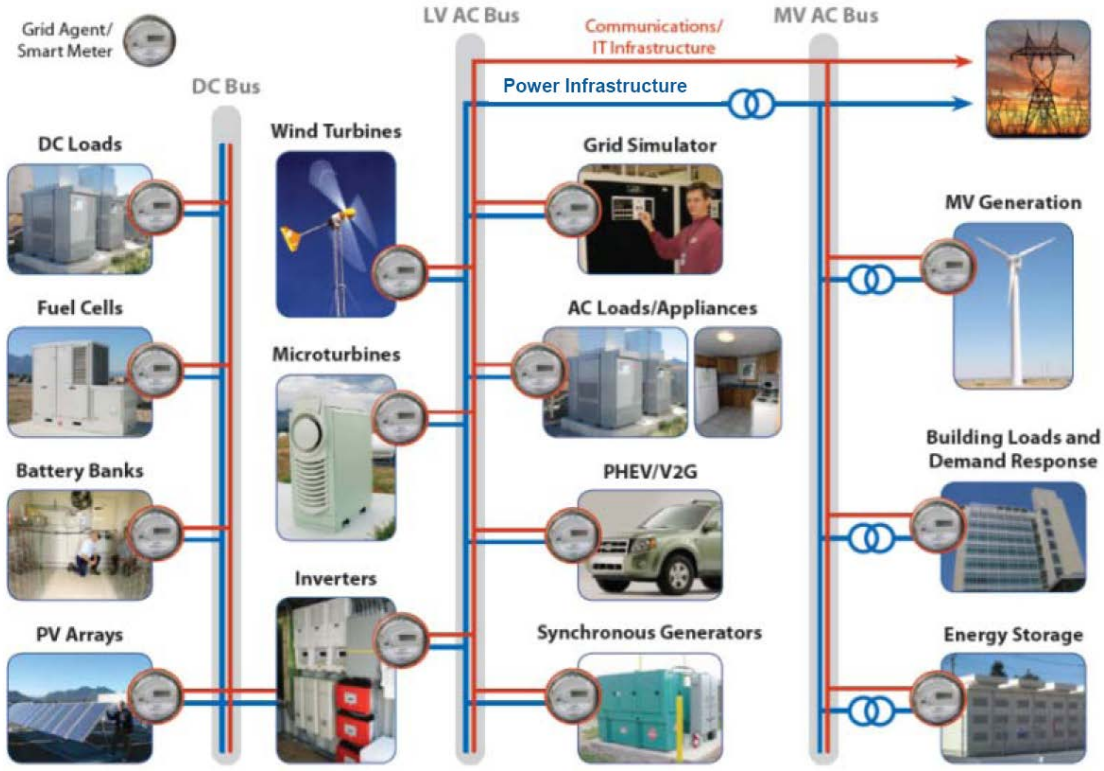

Hierarchical control for microgrids

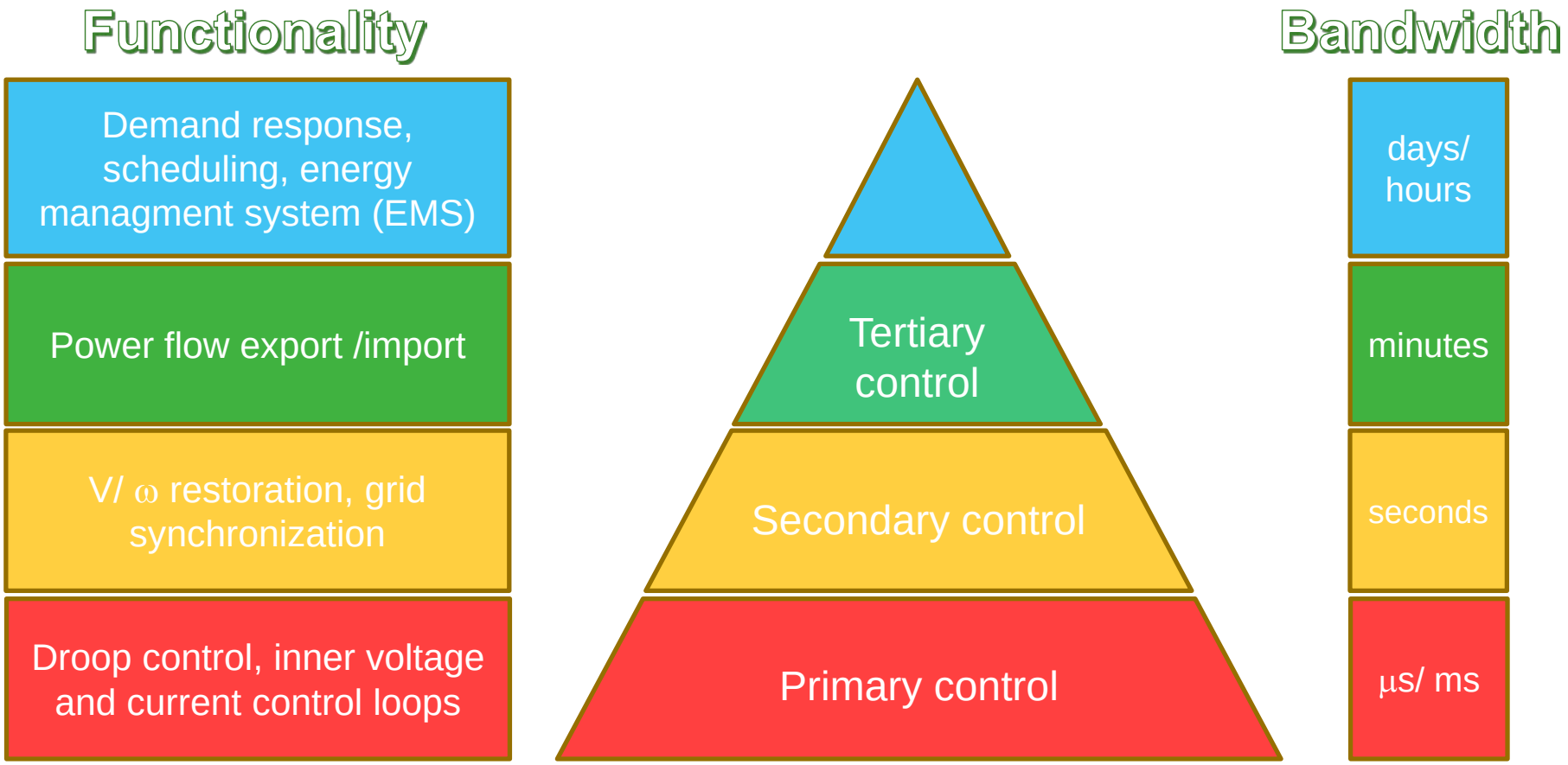

Power electronics converter as interface

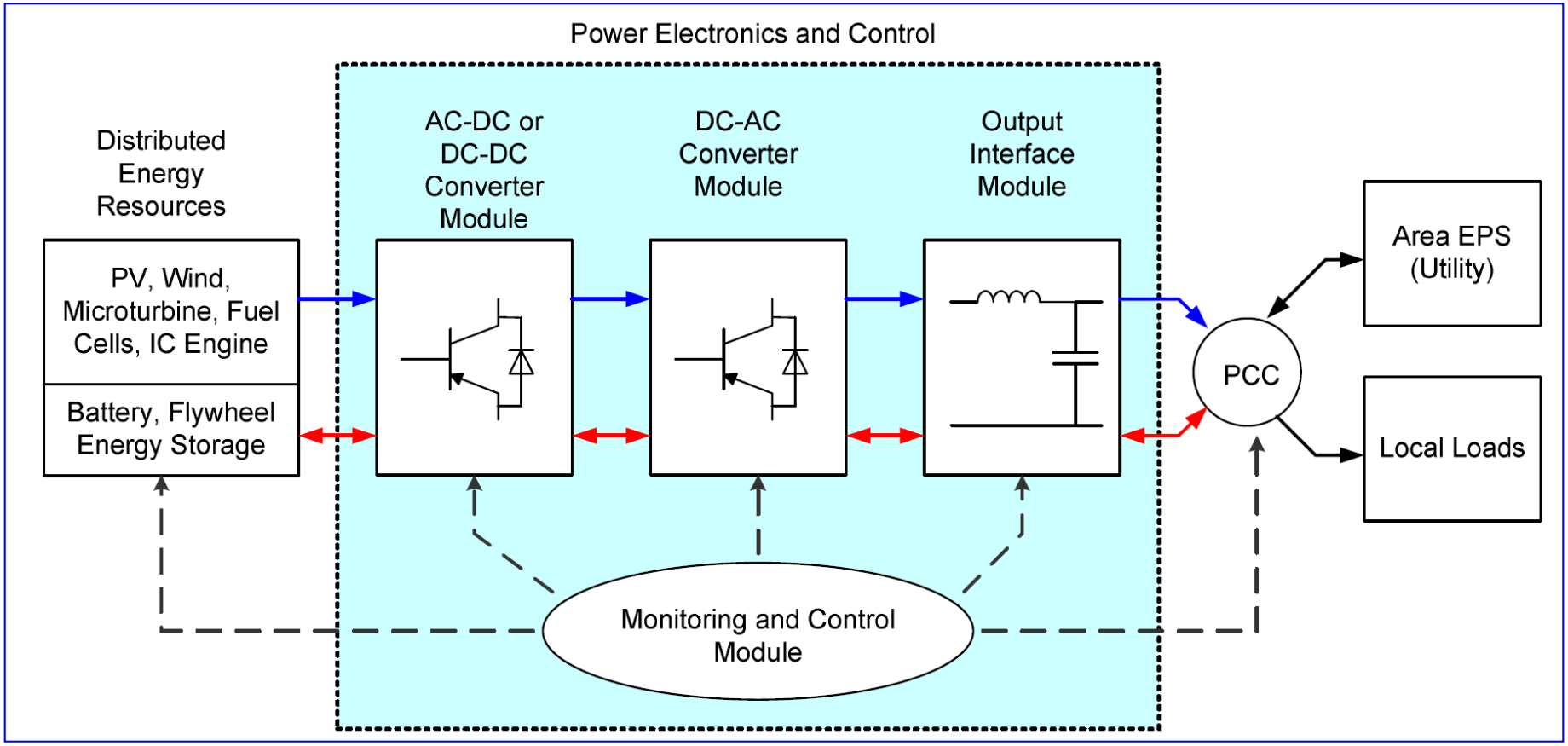

Background

- Increasing penetration of distributed power generation systems.
- Power converters should regulate the voltage/current within the elements that conform the grid/microgrid (sources and loads).

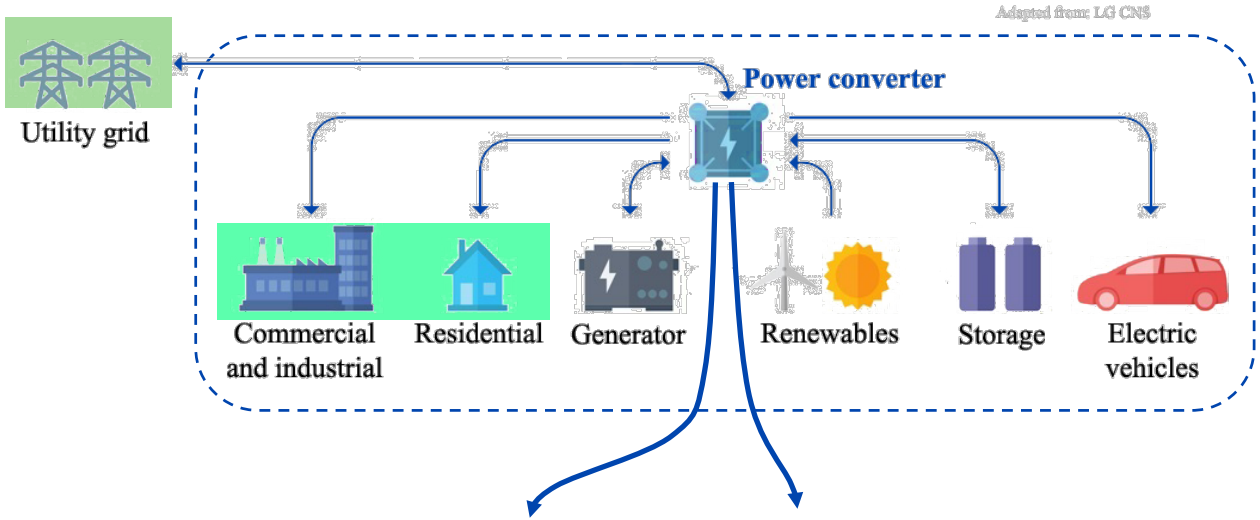

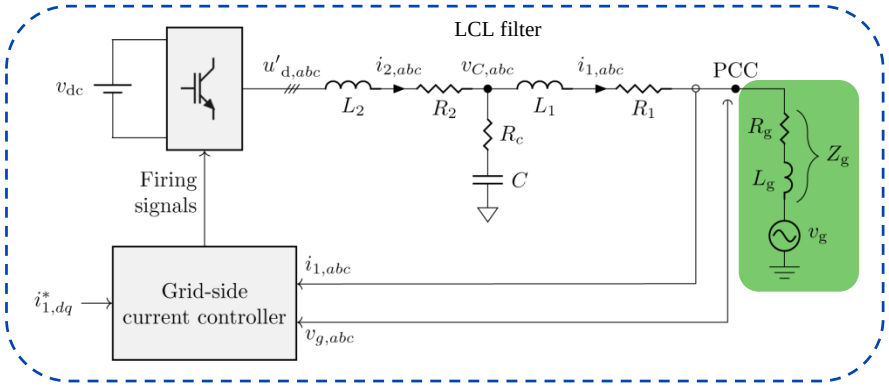

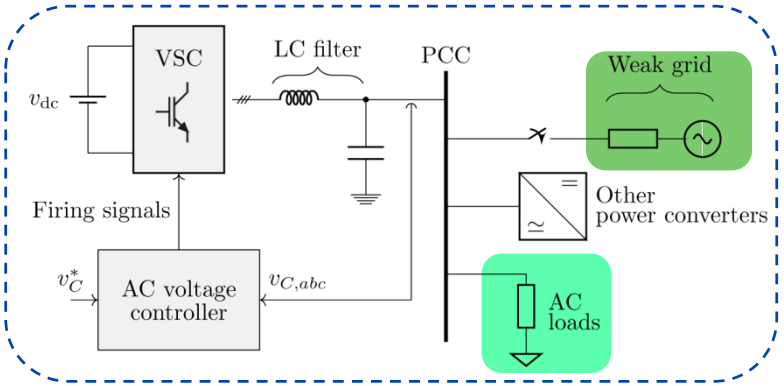

Contents

- Background of microgrids
- AC current control of grid-connected converters
  - Plant model
  - Interface filter
  - Classical controllers
- Limitations of classical current controllers
- State-space based techniques applied to current controllers
- AC voltage control of standalone or weak grid-tied converters

Control loops in a grid-tied converter

- Implementation
  - Modulation stage
  - Multiple cascaded loops of linear controllers
  - Outer power/ dc-link voltage controllers
  - Inner current controllers
    - Appropriate power factor
    - Harmonic rejection
    - Disturbance rejection (faults)
    - Fast transient response

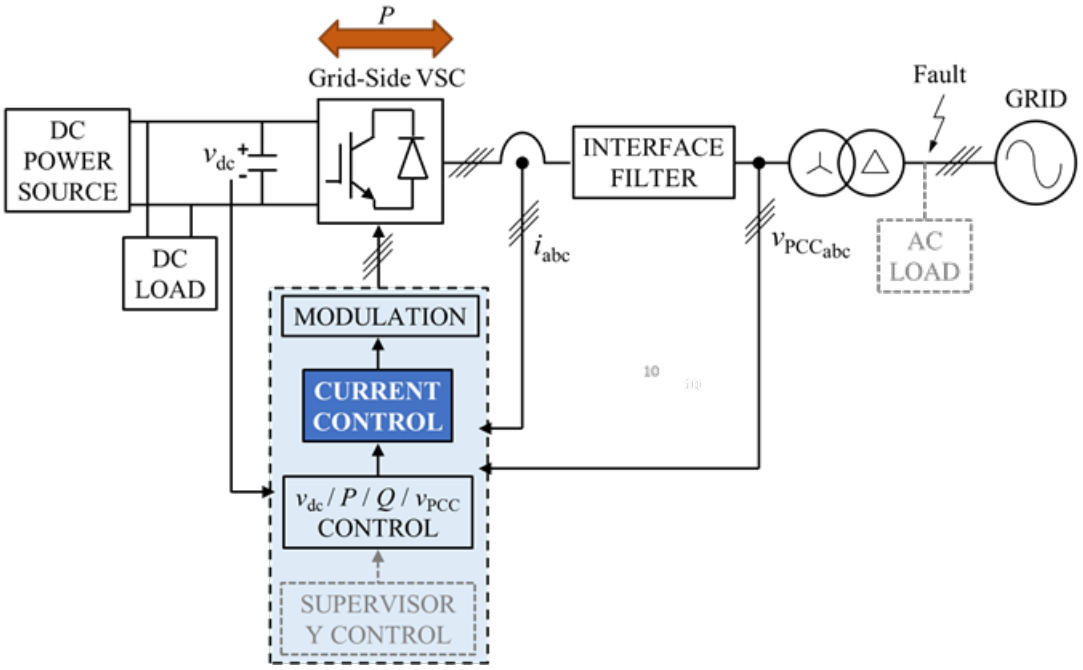

Design and implementation of the control technique

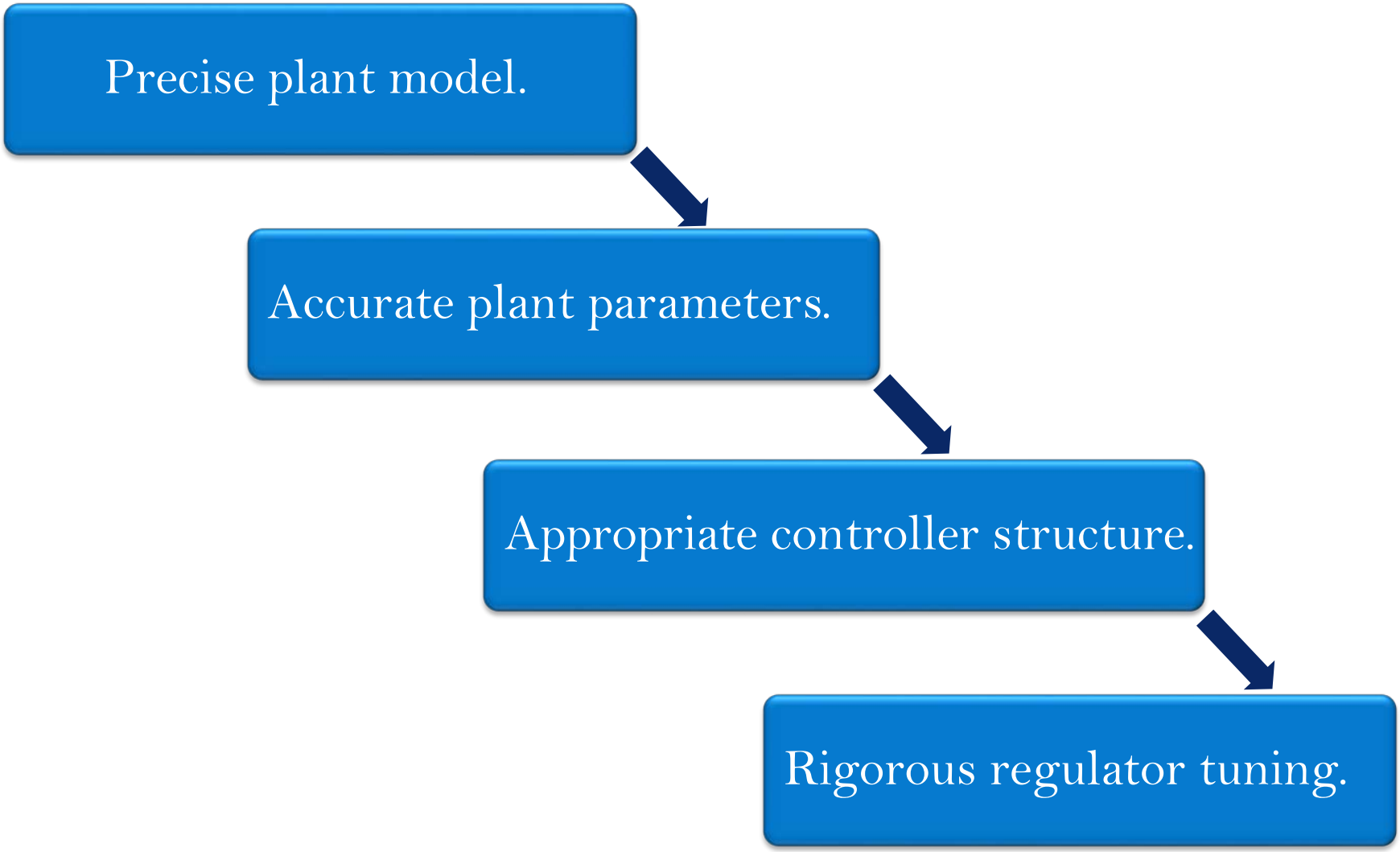

Plant model. Grid-connected converter

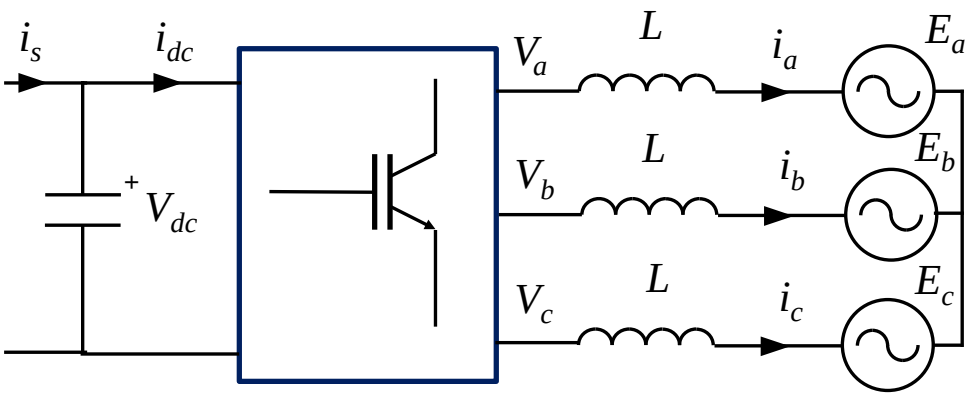

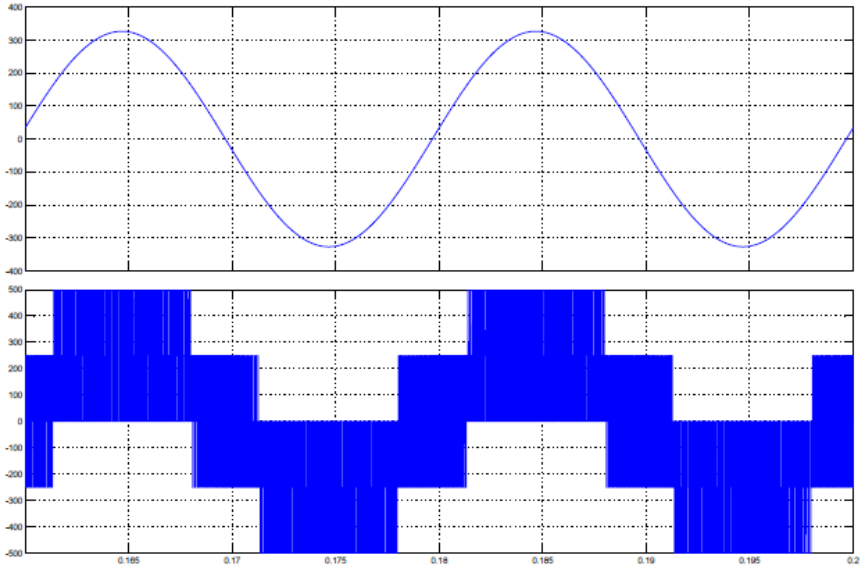

$$V_a = R_L i_a + L\frac{di_a}{dt} + E_a$$
$$V_b = R_L i_b + L\frac{di_b}{dt} + E_b$$
$$V_c = R_L i_c + L\frac{di_c}{dt} + E_c$$

$$E_a = \hat{E}\sin(\omega t)$$
$$E_b = \hat{E}\sin\left(\omega t - \frac{2}{3}\pi\right)$$
$$E_c = \hat{E}\sin\left(\omega t + \frac{2}{3}\pi\right)$$

$$i_a = \hat{I}\sin(\omega t - \varphi)$$
$$i_b = \hat{I}\sin\left(\omega t - \frac{2}{3}\pi - \varphi\right)$$
$$i_c = \hat{I}\sin\left(\omega t + \frac{2}{3}\pi - \varphi\right)$$

Plant model. Grid-connected converter

- Interfacing power production, consumption, storage and transportation within the power system based on microgrids.
- Based on semiconductor technology and signal processing.

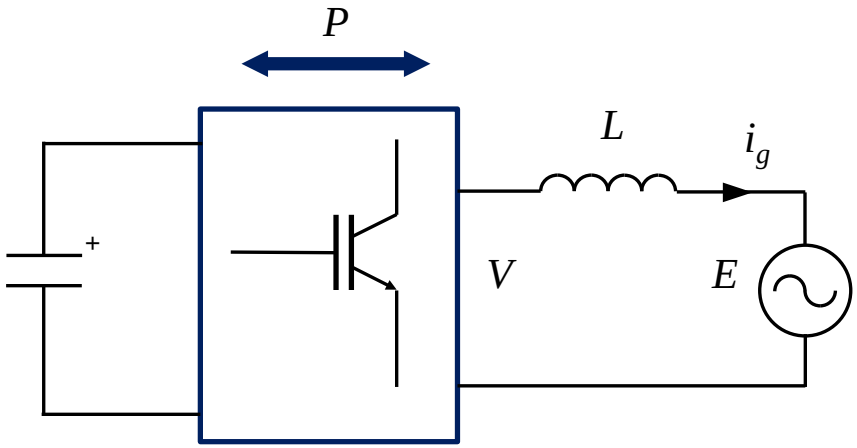

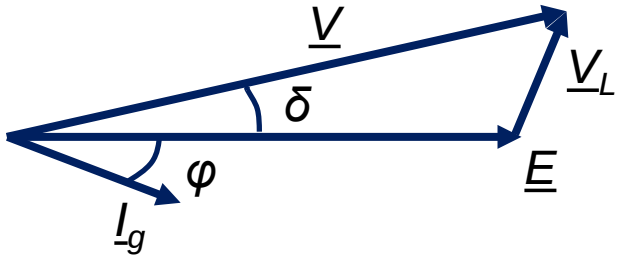

$$P = \frac{v \cdot e}{X_L} \cdot \sin\delta \approx \frac{v \cdot e}{X_L} \cdot \delta$$

$$Q = \frac{v \cdot (v - e \cdot \cos\delta)}{X_L} \cdot \cos\delta \approx \frac{v \cdot (v - e)}{X_L}$$

Plant model. Interface filter

- Passive filters are employed as the interface between the VSCs and the grid. They mitigate the switching harmonics that result from the modulation, and hence, reduce the losses and help meeting the connection requirements. In addition, their inductive character allows for proper operation of the grid-tied VSC, since the amplitude and phase imposed by the control at its output is able to regulate the active and reactive power flow. Interface filters can be mainly classified into first-order, second-order and third-order ones, i.e., L, LC and LCL filters, respectively.

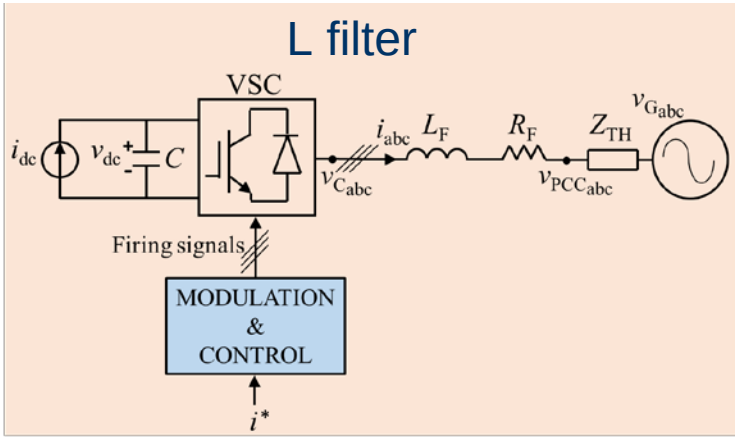

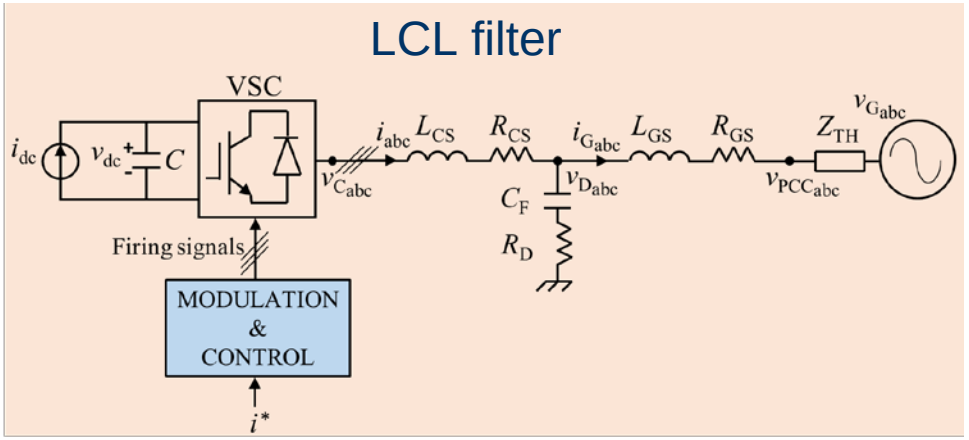

Plant model. Interface filter

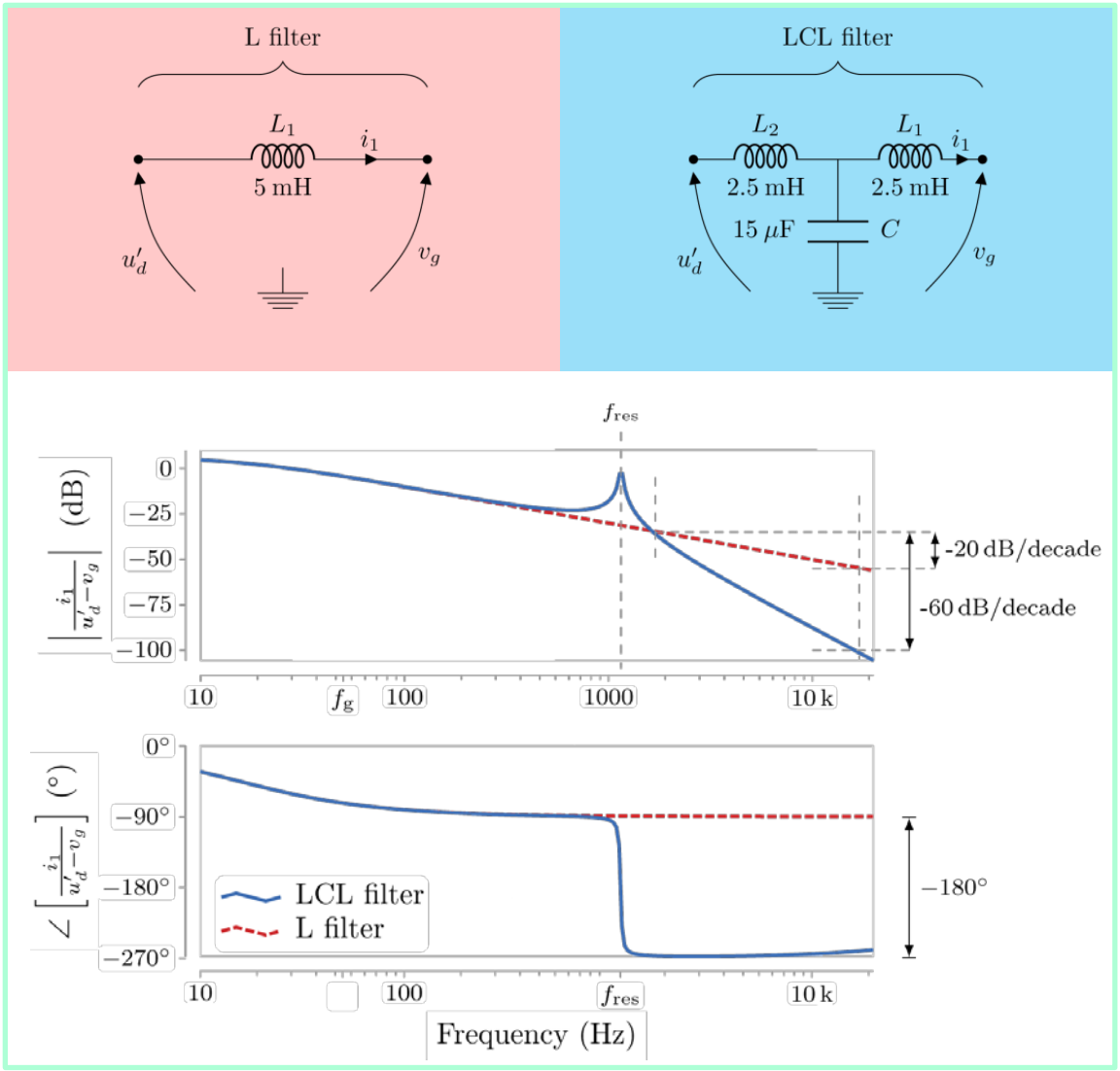

Plant model. Interface filter

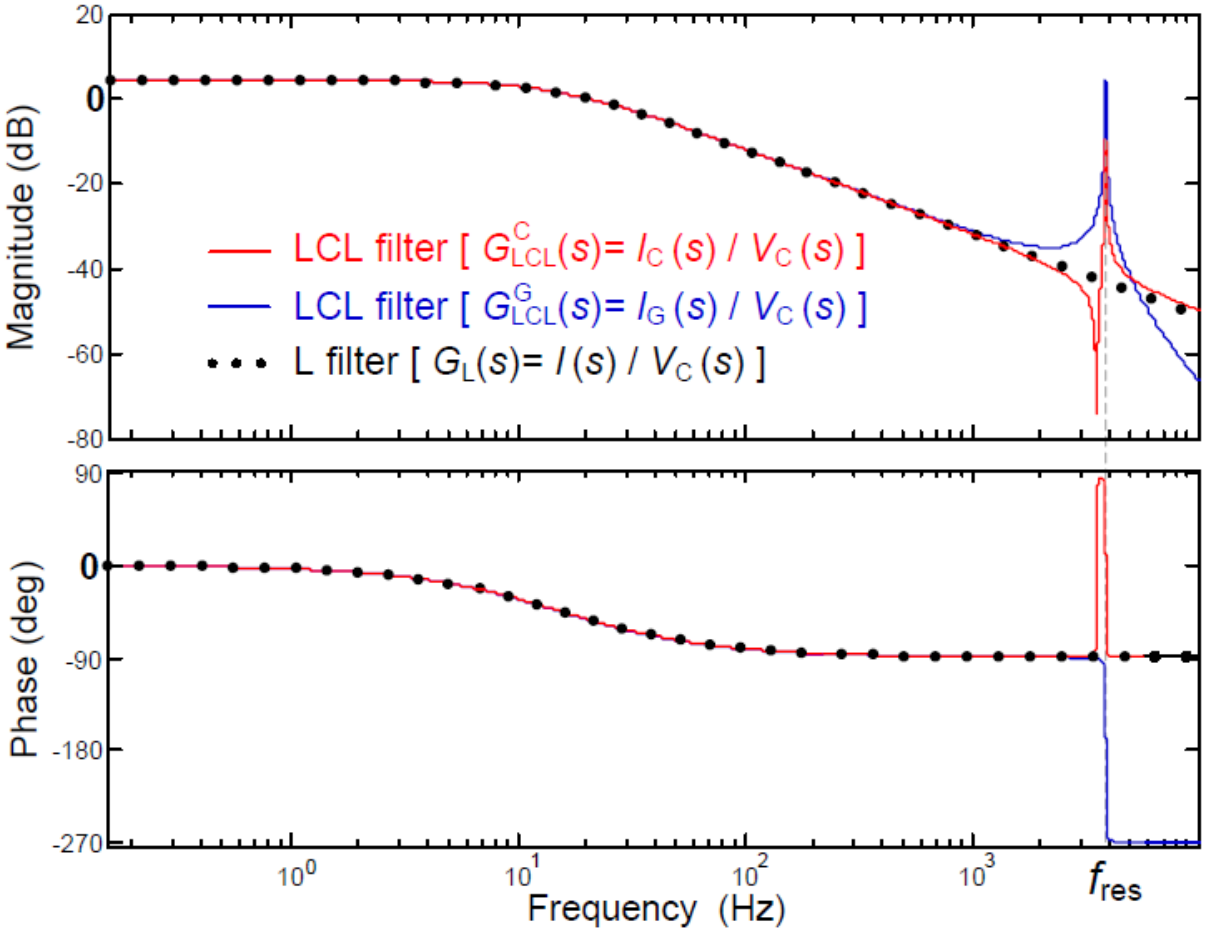

Figure 1.3: Bode diagrams of L and LCL filters, with equivalent parameters at low frequencies (i.e., $L_F = L_C + L_G$ and $R_F = R_C + R_G$). Parameters: $L_F = 6\,\text{mH}$, $R_F = 0.6\,\Omega$, $L_C = 5\,\text{mH}$, $R_C = 0.5\,\Omega$, $L_G = 1\,\text{mH}$, $R_G = 0.1\,\Omega$, $R_D = 0$, $C = 2\,\mu\text{F}$.

Reference frame

- With the aim of transforming the three-phase sinusoidal system into a continuous one, and thus, simplifying its analysis and control, it is possible to define a synchronous reference frame (SRF) rotating with the frequency of the former

$$\begin{pmatrix} u_\alpha \\ u_\beta \end{pmatrix} = \underbrace{\frac{2}{3}\begin{pmatrix} 1 & -\frac{1}{2} & -\frac{1}{2} \\ 0 & \frac{\sqrt{3}}{2} & -\frac{\sqrt{3}}{2} \end{pmatrix}}_{\mathbf{C}} \cdot \begin{pmatrix} u_a \\ u_b \\ u_c \end{pmatrix}$$

$$\begin{pmatrix} u_d \\ u_q \end{pmatrix} = \underbrace{\frac{2}{3}\begin{pmatrix} \cos(\theta_1) & \cos(\theta_1 - \frac{2\pi}{3}) & \cos(\theta_1 + \frac{2\pi}{3}) \\ -\sin(\theta_1) & -\sin(\theta_1 - \frac{2\pi}{3}) & -\sin(\theta_1 + \frac{2\pi}{3}) \end{pmatrix}}_{\mathbf{P}} \cdot \begin{pmatrix} u_a \\ u_b \\ u_c \end{pmatrix}$$

$$u_{\alpha\beta} = u_{dq}\, e^{j\omega_1 t} = u_{dq}\,[\cos(\omega_1 t) + j\,\sin(\omega_1 t)]$$
$$u_{dq} = u_{\alpha\beta}\, e^{-j\omega_1 t} = u_{\alpha\beta}\,[\cos(\omega_1 t) - j\,\sin(\omega_1 t)]$$

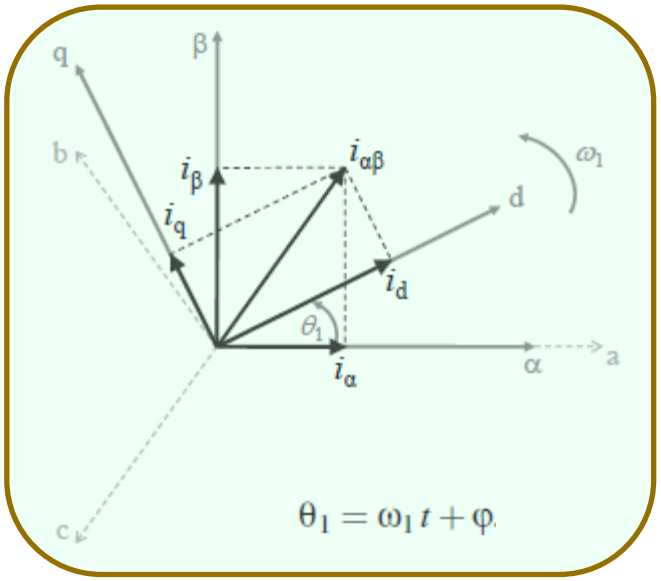

Plant model. L filter

- The plant admittance can be modeled in the stationary reference frame or in Synchronous Reference Frame (SRF).
- The plant model $G_L(s)$ is transformed to a positive-sequence SRF rotating with angular speed $w_o = hw_1$ by application of the substitution $s \rightarrow s + jhw_1$

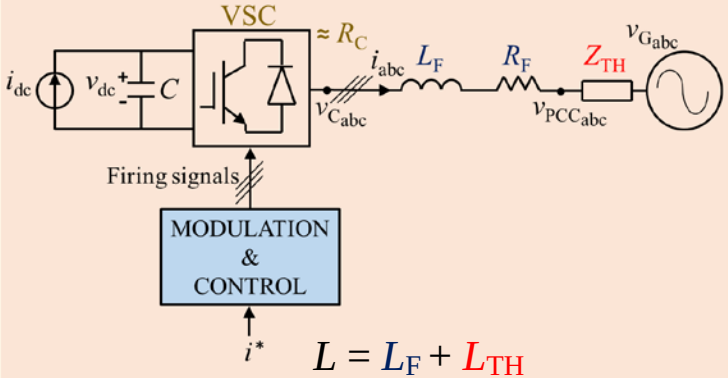

$$L = L_F + L_{TH}$$

$$R = R_F + R_{TH} + R_C$$

$$G_{L_{\alpha\beta}}(s) = \frac{I_{\alpha\beta}(s)}{V_{C_{\alpha\beta}}(s)} = \frac{1}{sL+R}$$

$$G_{L_{dq}}(s) = \frac{I_{dq}(s)}{V_{C_{dq}}(s)} = \frac{1}{sL+R+j\omega_1 L}$$

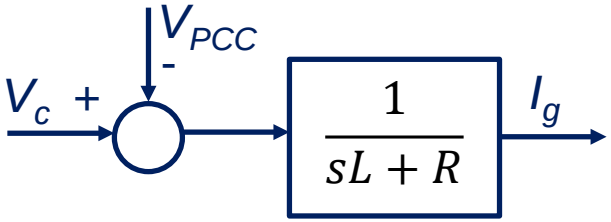

Plant model. LCL filter

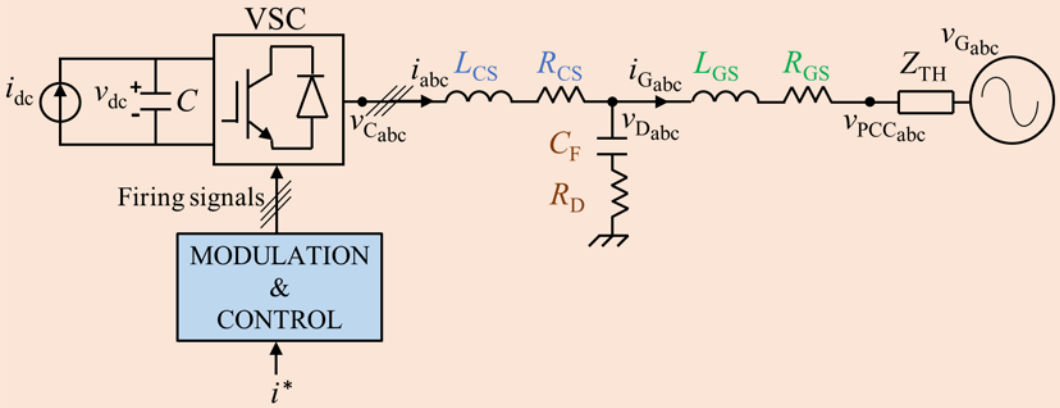

$$G_{LCL_{\alpha\beta}}(s) = \frac{I_{\alpha\beta}(s)}{V_{C_{\alpha\beta}}(s)} = \frac{Y_{CS}(s)\,[1 + Y_{GS}(s)\,Z_D(s)]}{1 + Y_{CS}(s)\,Z_D(s) + Y_{GS}(s)\,Z_D(s)}$$

$$Y_{CS_{\alpha\beta}}(s) = \frac{I_{\alpha\beta}(s)}{V_{C_{\alpha\beta}}(s) - V_{D_{\alpha\beta}}(s)} = \frac{1}{s\,L_{CS} + (R_{CS} + R_C)}$$

$$Y_{GS_{\alpha\beta}}(s) = \frac{I_{G_{\alpha\beta}}(s)}{V_{D_{\alpha\beta}}(s) - V_{G_{\alpha\beta}}(s)} = \frac{1}{s\,(L_{GS} + L_{TH}) + (R_{GS} + R_{TH})}$$

$$Z_{D_{\alpha\beta}}(s) = \frac{V_{D_{\alpha\beta}}(s)}{I_{\alpha\beta}(s) - I_{G_{\alpha\beta}}(s)} = \frac{1}{s\,C_F} + R_D.$$

Plant model. LCL filter

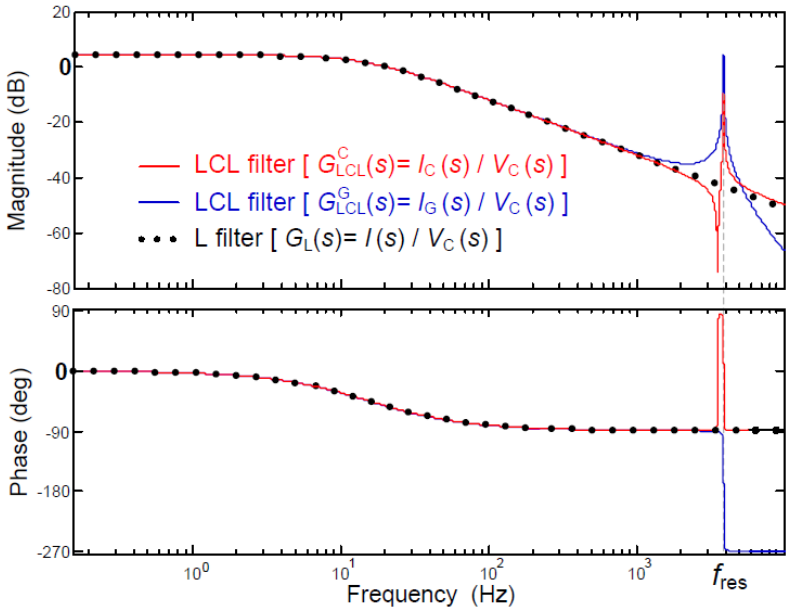

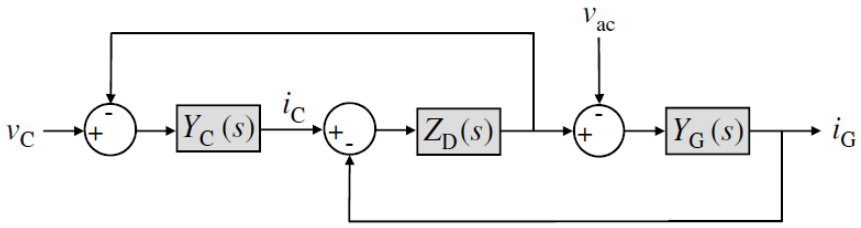

Block diagram of LCL filter

$$\frac{I_C(s)}{V_C(s)-V_D(s)} = \frac{1}{sL_C+R_C} = Y^C(s)$$

$$\frac{I_G(s)}{V_D(s)-V_{ac}(s)} = \frac{1}{sL_G+R_G} = Y^G(s)$$

$$\frac{V_D(s)}{I_C(s)-I_G(s)} = \frac{1}{sC} + R_D = Z^D(s).$$

$$G^C_{LCL}(s) = \frac{I_C(s)}{V_C(s)} = \frac{Y^C(s)\,[1+Y^G(s)Z^D(s)]}{1+Y^C(s)Z^D(s)+Y^G(s)Z^D(s)}$$

$$G^G_{LCL}(s) = \frac{I_G(s)}{V_C(s)} = \frac{Y^C(s)Y^G(s)Z^D(s)}{1+Y^C(s)Z^D(s)+Y^G(s)Z^D(s)}.$$

$$f_{res} = \frac{1}{2\pi}\sqrt{\frac{L_{CS}+L_{GS}}{C_F L_{CS} L_{GS}}}$$

Model for the current control in stationary frame

- The computational delay
- The regularly sampled pulse-width modulation (PWM) introduces half a sample delay when employing a triangular carrier, which can be modeled with good precision by a zero-order hold (ZOH)
- The current controller should present an infinite open-loop gain at the frequency of the PCC voltage, so that a perfect rejection of this disturbance is assured in steady state. In most cases, this voltage may be measured and fedforward at the output of the current controller to further improve the transient performance in the presence of grid faults

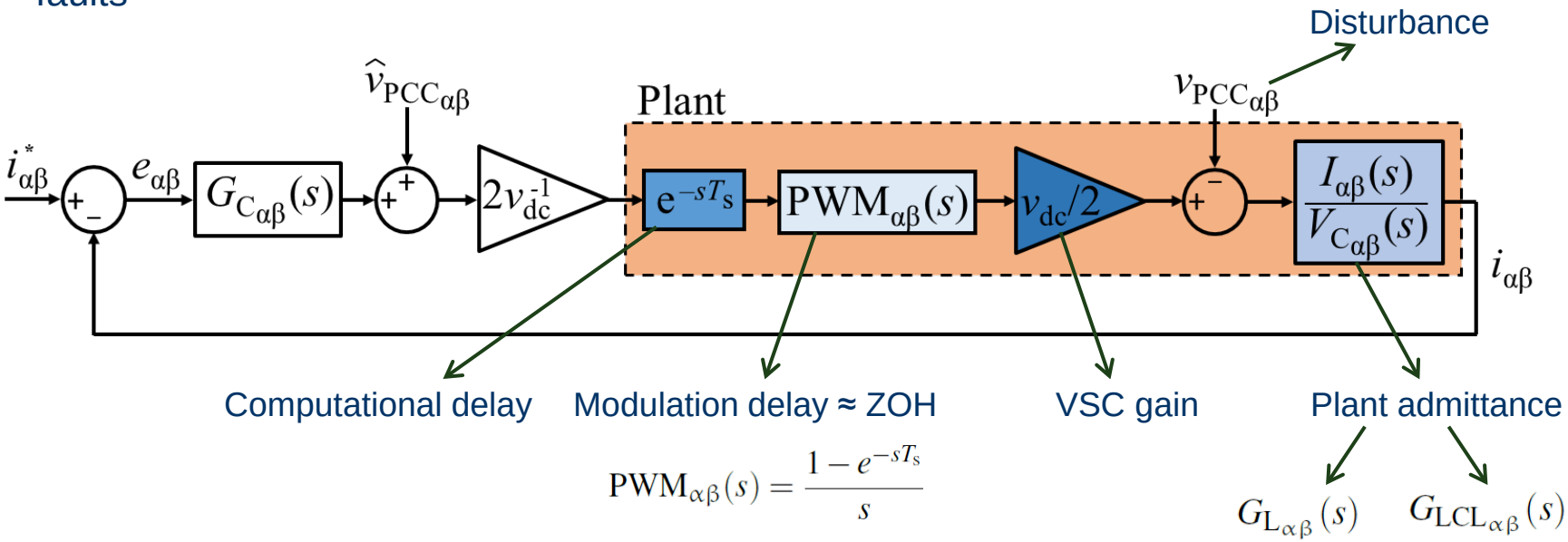

$$\mathrm{PWM}_{\alpha\beta}(s) = \frac{1 - e^{-sT_\mathrm{s}}}{s}$$

Model for the current control in stationary frame

- Overall transfer function of the control loop

$$I_{\alpha\beta}(s) = G_{\mathrm{CL}_{\alpha\beta}}(s) I^{*}_{\alpha\beta}(s) + G_{\mathrm{DR}_{\alpha\beta}}(s) V_{\mathrm{PCC}_{\alpha\beta}}(s)$$

- Closed-loop transfer functions of command tracking and disturbance rejection can be respectively expressed as follows

$$G_{\mathrm{CL}_{\alpha\beta}}(s) = \frac{G_{\mathrm{C}_{\alpha\beta}}(s)\, \mathrm{e}^{-sT_s}\, \mathrm{PWM}_{\alpha\beta}(s) G_{\mathrm{L}_{\alpha\beta}}(s)}{1 + G_{\mathrm{C}_{\alpha\beta}}(s)\, \mathrm{e}^{-sT_s}\, \mathrm{PWM}_{\alpha\beta}(s) G_{\mathrm{L}_{\alpha\beta}}(s)}$$

$$G_{\mathrm{DR}_{\alpha\beta}}(s) = -\frac{G_{\mathrm{L}_{\alpha\beta}}(s)}{1 + G_{\mathrm{C}_{\alpha\beta}}(s)\, \mathrm{e}^{-sT_s}\, \mathrm{PWM}_{\alpha\beta}(s) G_{\mathrm{L}_{\alpha\beta}}(s)}$$

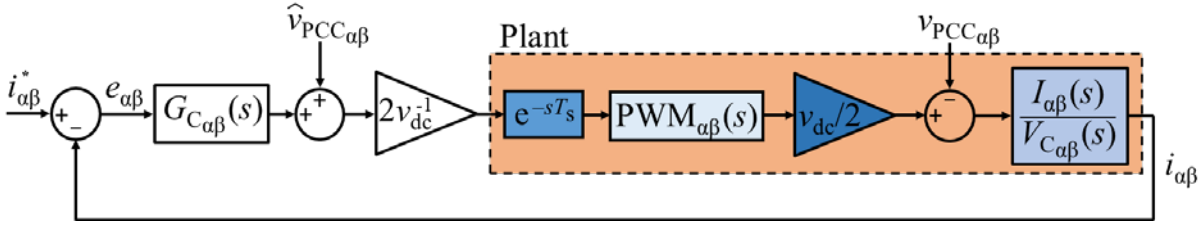

Current control techniques

- Several options. Linear/nonlinear techniques
  - Proportional integral
  - Resonant
  - Pole placement
  - …
  - Hysteresis
  - Deadbeat
  - Repetitive
  - …
  - Model predictive
  - Sliding mode
  - …

PI controller with cross-coupling decoupling. (PICCD)

- If the IMC principle is adopted, which is aimed at canceling the plant pole by the controller zero, the latter transfer function can be further simplified.
- $G_{OL}(s) = K_h/s$, where *alpha_c*=K_h coincides with the controller bandwidth and is the only degree of freedom of the resulting regulator. This involves selecting the PI controller gains as $K_{Ph}/K_{Ih} = L/R$ and $K_{Ph} = K_h L$.
- $K_p = K_h * L$, $K_i = K_h * R$. (BW= K_h = 4%-10% ws)

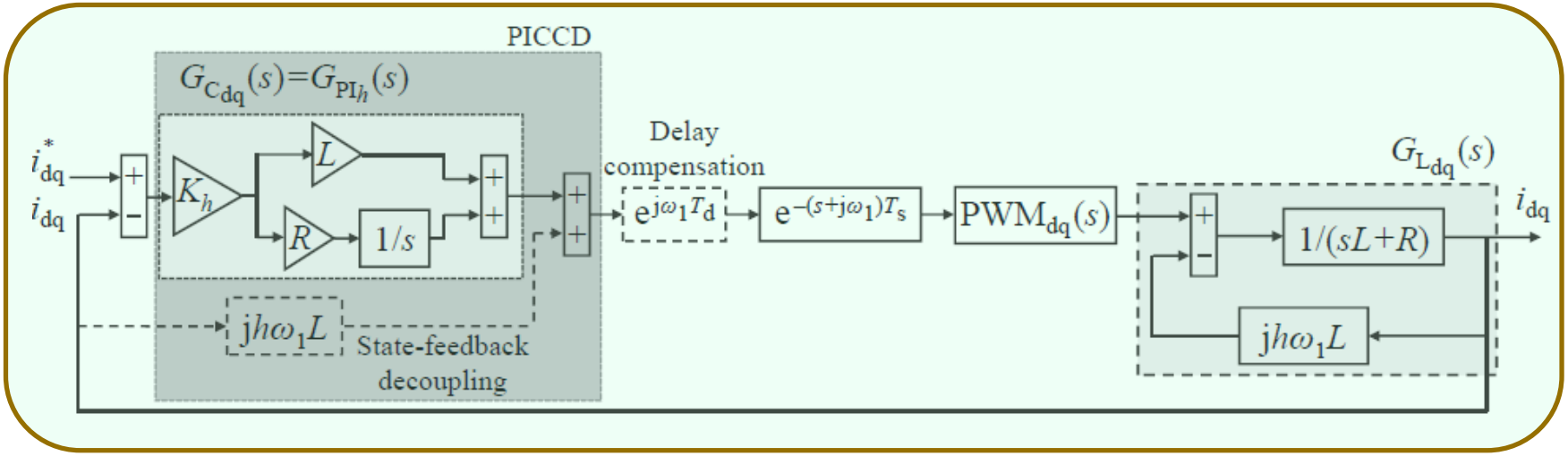

A. G. Yepes, A. Vidal, J. Malvar, O. López and J. Doval-Gandoy, "Tuning Method Aimed at Optimized Settling Time and Overshoot for Synchronous Proportional-Integral Current Control in Electric Machines", IEEE Transactions on Power Electronics, vol. 29, no. 6, pp. 3041-3054, Jun. 2014.

Complex Vector PI

- Instead of moving the plant pole to the real axis, as the classical PICCD does, it is also possible to match the complex pole of $G_{Ldq}(s)$ by a complex zero in the controller. Thus, the complex vector PI controller was proposed
- In case of plant parameter mismatches, the closed-loop frequency response with the PICCD would be more degraded around hw_1, i.e., at the vicinity of the frequency to be controlled, whereas with $G_{cPIh}(s)$ it would be altered around 0 Hz, which is more favorable.

$$G_{\mathrm{cPI}_h}(s) = \frac{s K_{\mathrm{P}_h} + K_{\mathrm{I}_h} + jh\omega_1 K_{\mathrm{P}_h}}{s} = K_h \frac{sL + R + jh\omega_1 L}{s}$$

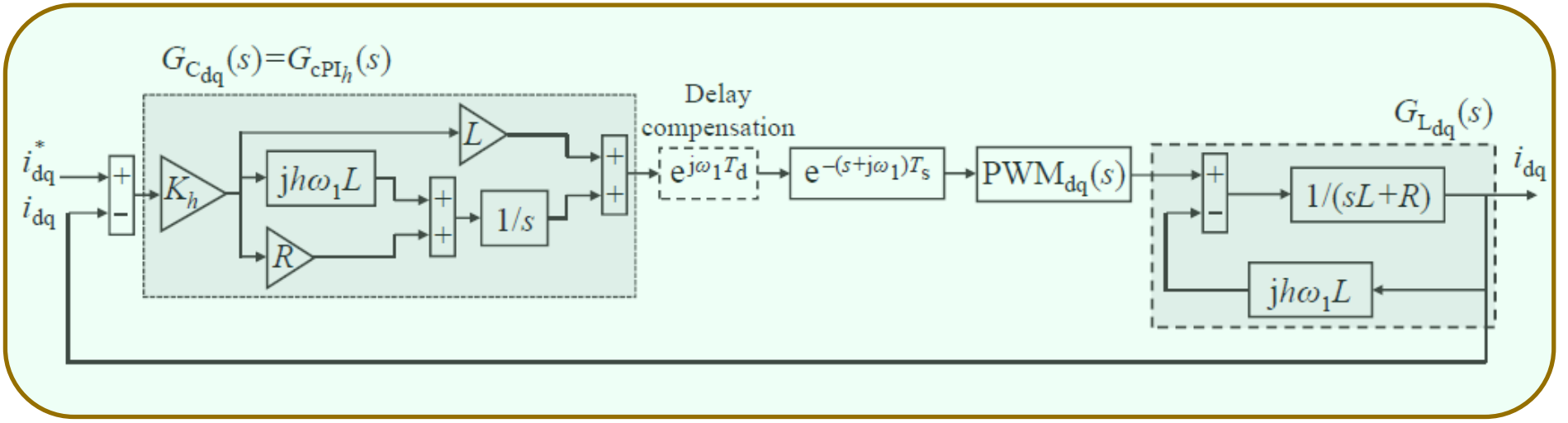

- F. Briz, M. Degner, and R. Lorenz, “Analysis and design of current regulators using complex vectors,” IEEE Trans. Ind. Appl., vol. 36, no. 3, pp. 817–825, May/Jun. 2000.

- H. Kim, M. Degner, J. Guerrero, F. Briz, and R. Lorenz, “Discrete-time current regulator design for ac machine drives,” IEEE Trans. Ind. Appl.,vol. 46, no. 4, pp. 1425–1435, Jul./Aug. 2010.

Decoupling in DSRF current control

- Decoupling Between Orthogonal Axes in Double Synchronous Reference Frame Current Control.
- In case of imbalance, the single SRF is commonly replaced by PI controllers in a pair of SRFs rotating with opposite sequences, which is known as double SRF control (DSRFC).

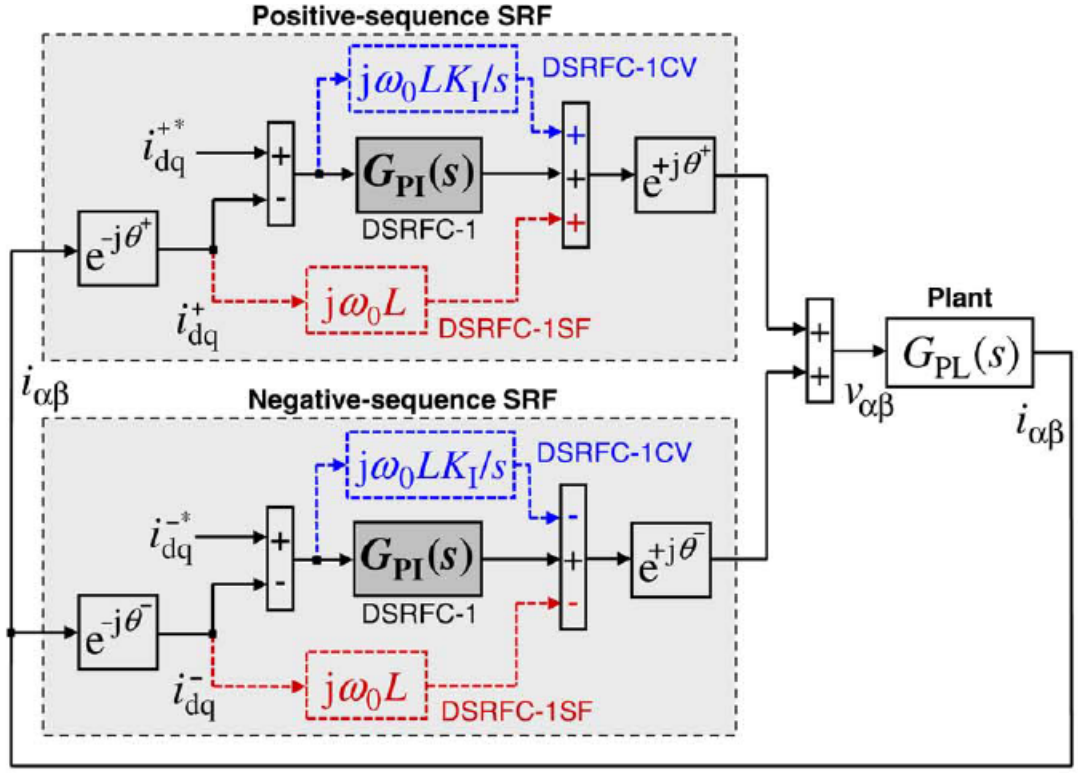

A. G. Yepes, A. Vidal, O. López and J. Doval-Gandoy, "Evaluation of Techniques for Cross-Coupling Decoupling Between Orthogonal Axes in Double Synchronous Reference Frame Current Control," in IEEE Transactions on Industrial Electronics, vol. 61, no. 7, pp. 3527-3531, July 2014.

Decoupling in DSRF current control

- It is generally assumed that the state feedback decoupling strategy can be applied to decouple the cross-coupling between the orthogonal axes of each SRF in DSRFC, as for a single SRF structure.
- SF technique does not produce a noticeable improvement in DSRFC, because the terms added to each SRF interfere with those added to the opposite-sequence SRF.
- It has been demonstrated that the CV decoupling strategy, when applied to DSRFC, provides an enhancement in axes decoupling for low bandwidth values.

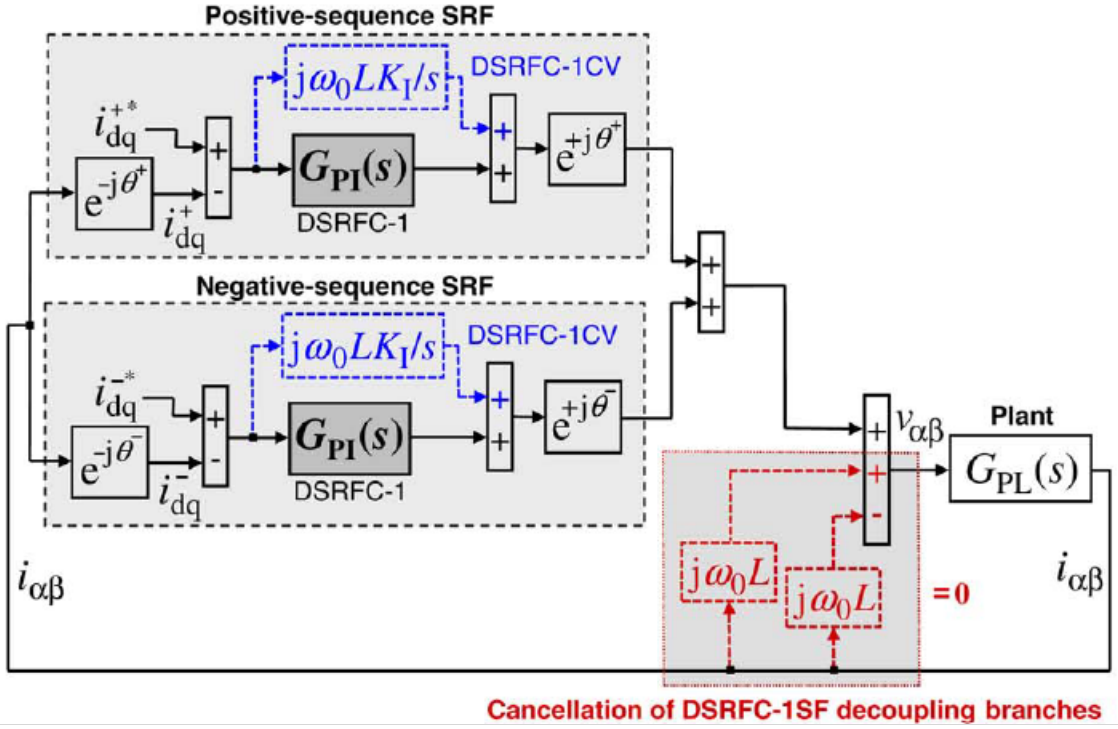

A. G. Yepes, A. Vidal, O. López
Current Control," in IEEE Trans

Synchronous Reference Frame

Proportional resonant controller

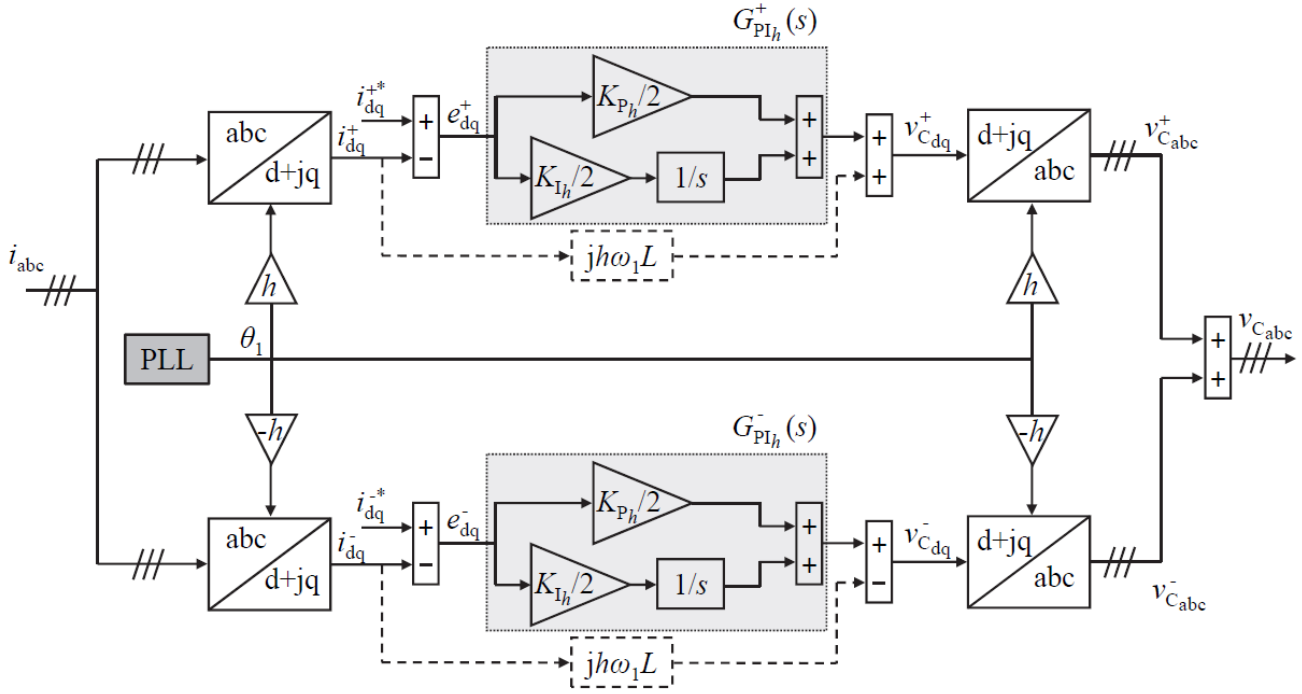

(a) Double SRF with classical PI controllers (with cross-coupling decoupling (PICCD)) and Park transforms.

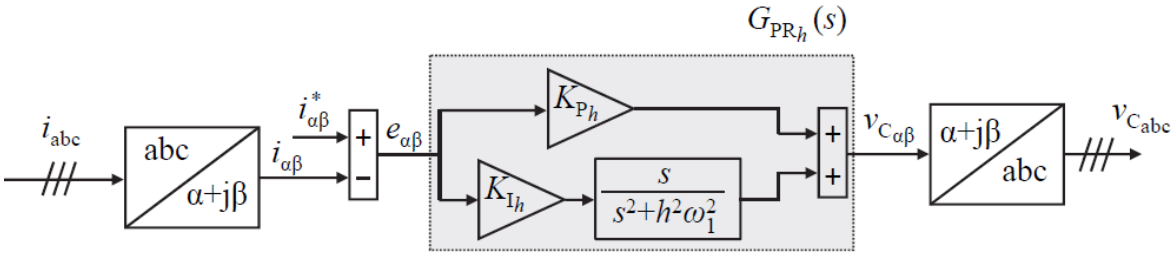

(b) PR controller and Clarke transforms.

Proportional resonant controller

- With the aim of regulating different harmonics, several PR controllers can be implemented in parallel, yielding to the following expression.

$$G_{\mathrm{PR}}(s) = K_{\mathrm{P_T}} + \sum_{h=1,5,7\ldots} K_{\mathrm{I}_h} \frac{s}{s^2 + h^2\omega_1^2}$$

$$K_{\mathrm{P_T}} = \sum_{h=1,5,7\ldots} K_{\mathrm{P}_h}$$

- In order to compensate the time delay at the vicinity of the resonant frequency, a delay compensation technique may also be added to these controllers. To compensate system delays, the zero at the origin can be displaced, so that a phase lead Φ_h is introduced at the vicinity of the synchronous frequency.

$$G^{\mathrm{d}}_{\mathrm{PR}_h}(s) = K_{\mathrm{P}_h} + K_{\mathrm{I}_h} \frac{s\cos(\phi'_h) - h\omega_1 \sin(\phi'_h)}{s^2 + h^2\omega_1^2}$$

Proportional resonant controller. Discretization

- Effect of discretization method (design from S-domain). Depending on the transformation method, different Z-domain transfer functions are obtained from transfer functions of the form $R(s)=s/(s^2+w^2)$.

Discretization method	Transfer function
Zero order hold	$R_{zoh}(z) = \frac{\sin(\omega_o T_s)}{\omega_o} \cdot \frac{z^{-1}-z^{-2}}{1-2z^{-1}\cos(\omega_o T_s)+z^{-2}}$
Forward Euler	$R_f(z) = T_s \cdot \frac{z^{-1}-z^{-2}}{1-2z^{-1}+z^{-2}(\omega_o^2 T_s^2+1)}$
Backward Euler	$R_b(z) = T_s \cdot \frac{1-z^{-1}}{(\omega_o^2 T_s^2+1)-2z^{-1}+z^{-2}}$
Trapezoid (Tustin)	$R_t(z) = 2T_s \cdot \frac{1-z^{-2}}{(\omega_o^2 T_s^2+4)+z^{-1}(2\omega_o^2 T_s^2-8)+z^{-2}(\omega_o^2 T_s^2+4)}$
Trapezoid with pre-warping	$R_{tp}(z) = \frac{\sin(\omega_o T_s)}{2\omega_o} \cdot \frac{1-z^{-2}}{1-2z^{-1}\cos(\omega_o T_s)+z^{-2}}$
Zero-pole matching	$R_{zpm}(z) = K_d \cdot \frac{z^{-1}-z^{-2}}{1-2z^{-1}\cos(\omega_o T_s)+z^{-2}}$
Impulse invariant	$R_{imp}(z) = T_s \cdot \frac{1-z^{-1}\cos(\omega_o T_s)}{1-2z^{-1}\cos(\omega_o T_s)+z^{-2}}$

- Poles and zeros are mapped to different placements. Since the resonant filters are very selective (narrow peaks), it is important to assess which method is more advantageous.

Proportional resonant controller. Tuning

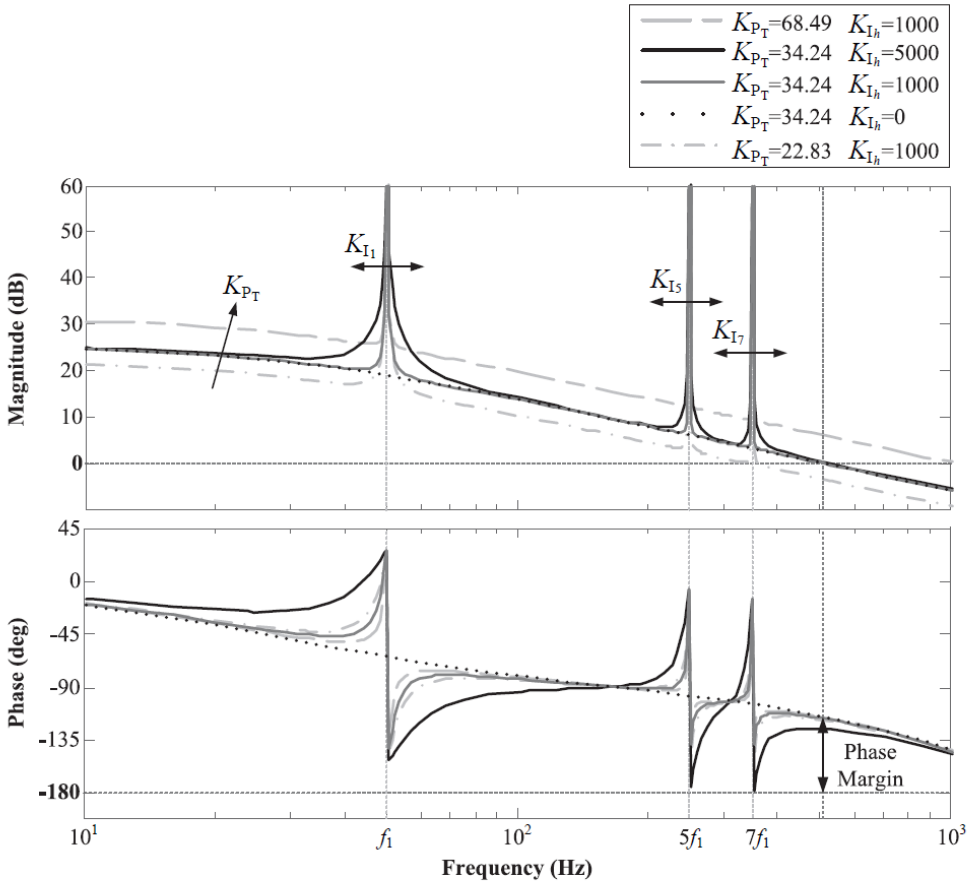

Figure 1.11: Open-loop Bode diagrams $G_{C_{\alpha\beta}}(z)z^{-1}G^{ZOH}_{L_{\alpha\beta}}(z)$ obtained with PR controllers without delay compensation, for different K_{P_T} and K_{I_h} values. The phase margin and crossover frequency is only indicated for those cases in which $K_{P_T} = 34.24$ (it is practically the same for the three K_{I_h} values). Parameters: $L = 10.9\,\text{mH}$, $R = 1.9\,\Omega$, $f_s = 10\,\text{kHz}$, $h \in \{1,5,7\}$, $f_1 = 50\,\text{Hz}$ and $K_{I_1} = K_{I_5} = K_{I_7} = K_{I_h}$.

Proportional resonant controller in SRF

- In three-phase systems, the most common current harmonics are negative-sequence 6k-1 harmonics and positive-sequence 6k+1 harmonic components, with k Є N.
- Each pair of positive-sequence 6k +1 and negative-sequence 6k-1 harmonics is combined into a single harmonic of order 6k when expressed in fundamental (positive-sequence) SRF.
- Both harmonics can be tracked by a single resonant controller tuned at h = 6k in fundamental SRF.

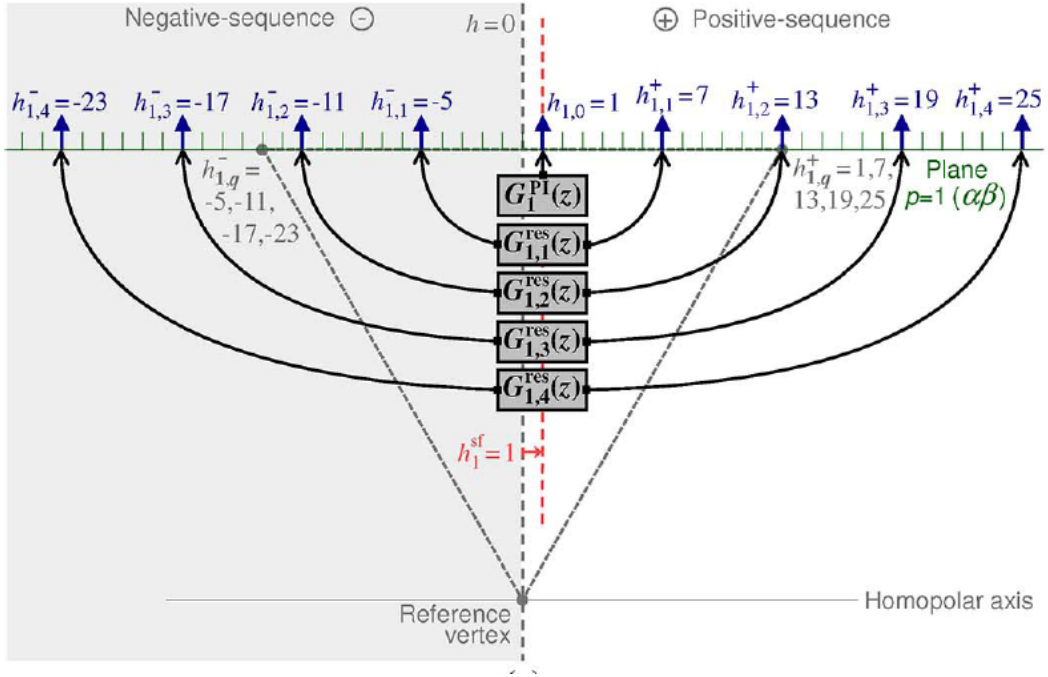

Control of grid-connected converter with LCL Filter

- Critical frequency. Ratio f_s/f_{res}
- They are unstable when
  - $f_{res} \leq {}^{f_s}/_{6}$ and grid-side current is controlled or
  - $f_{res} \geq {}^{f_s}/_{6}$ and converter-side current is controlled
- Therefore they require additional **damping mechanisms**.

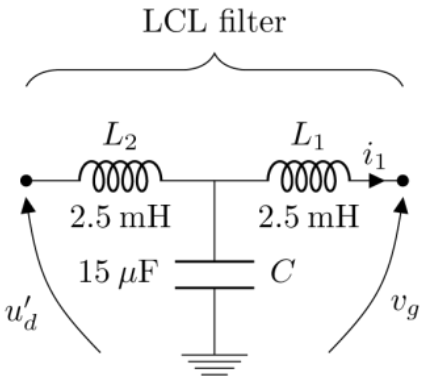

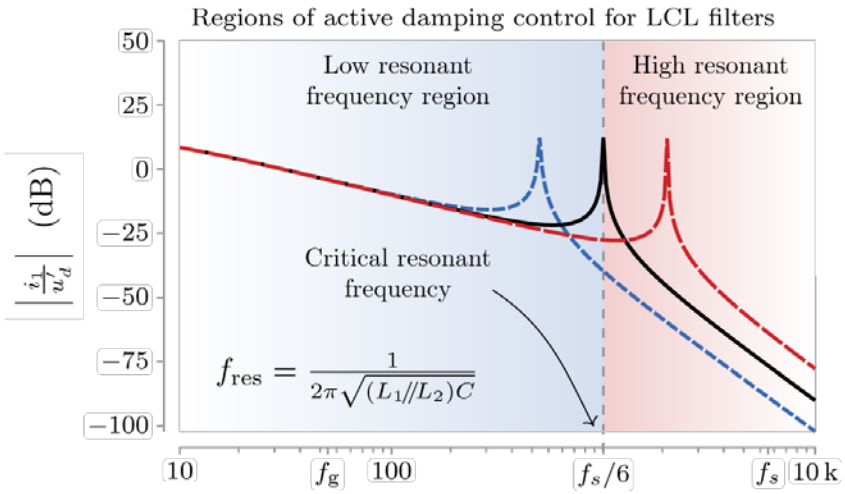

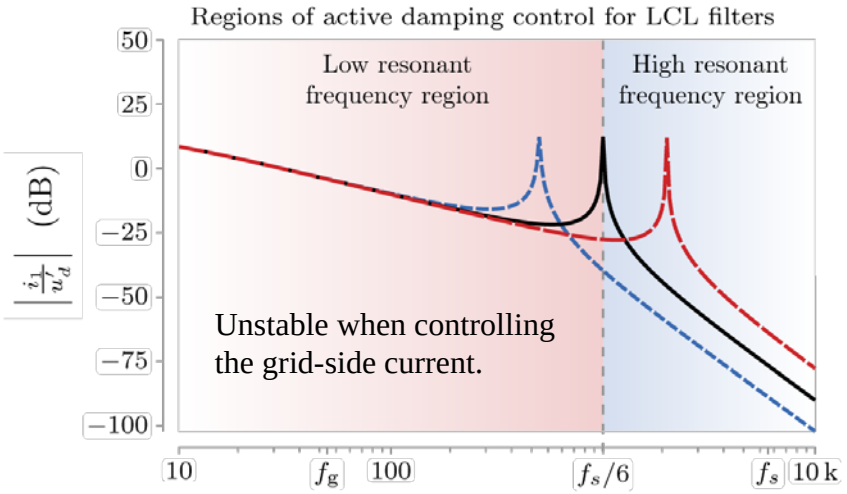

S. G. Parker,B. P.McGrath, and D. G. Holmes, “Regions of active damping control for LCL filters,” IEEE Trans. Ind. Appl., vol. 50, no. 1, pp. 424–432, Jan./Feb. 2014

Grid-connected converter with LCL filter. Passive damping

- Simple passive damping of the LCL filter involves placing a damping resistor in series with the filter capacitor. As the damping resistor size is increased the stability is also increased but the LCL filter effectiveness is decreased.
- LCL filter design. Passive damping.
  - Rdmin < Rd < Rdsw
  - Typically, Rd value is chosen as one-third the impedance of the filter capacitor at the resonant frequency.

$$R_{dsw} = \frac{1}{C_f 2\pi f_{sw}}$$

$$R_{dmin} = \frac{1}{3} f_s \frac{L_g^2}{(L + L_g)} = \frac{1}{6\pi} \frac{L_g}{L} \frac{f_s}{f_{res}} \left(\frac{1}{C_f \omega_{res}} \right)$$

$$R_d = \frac{1}{3} \frac{1}{2\pi f_{res} C_f}$$

Grid-connected converter with LCL filter. Passive damping

- To overcome both the loss aspect and the reduction in filter effectiveness of passive damping, several improved passive damping networks have been proposed.

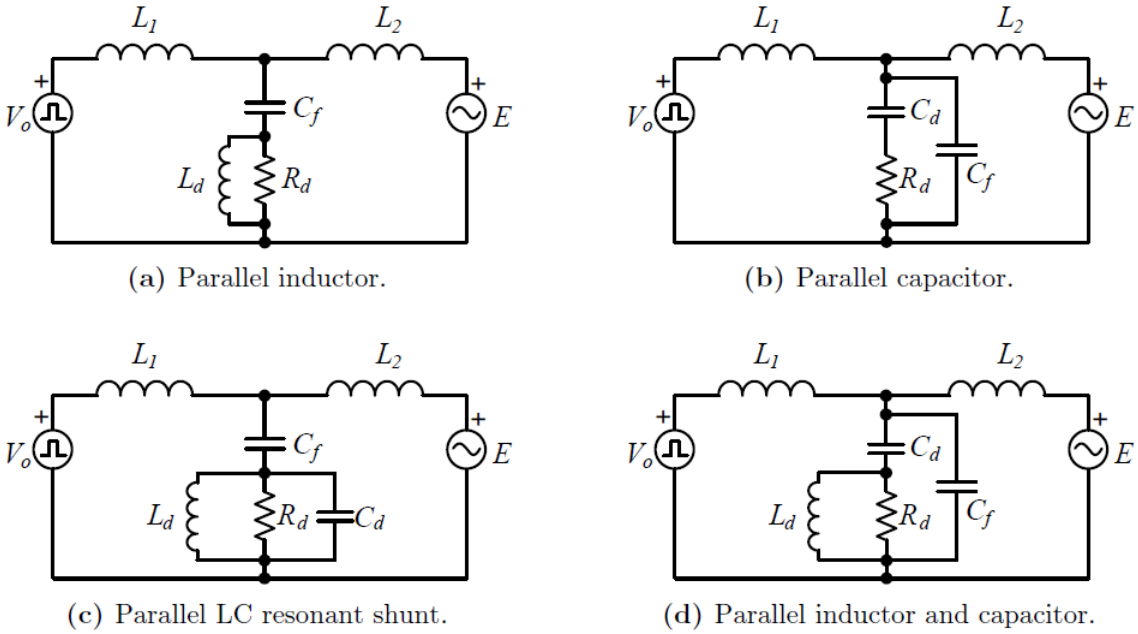

(a) Parallel inductor.

(b) Parallel capacitor.

(c) Parallel LC resonant shunt.

(d) Parallel inductor and capacitor.

S. Parker, "Discrete Time Current Regulation of Grid Connected Converters with LCL Filters", PhD Thesis, RMIT University, 2014.

Grid-connected converter with LCL filter. Active damping

- Active damping can be achieved by feeding back a signal proportional to the output current of the converter or to the capacitor current. In effect, these feedbacks emulate the presence of a virtual resistor, connected in series with L_2 or C, respectively, resulting in the damping of the resonance.

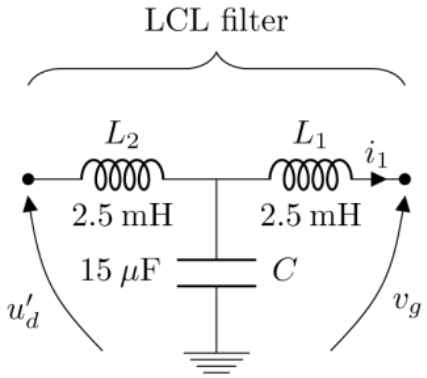

- An alternative method to feedback the capacitor current is to feedback the derivative of the capacitor voltage with respect to time. While both approaches are identical in continuous time, they differ in discrete time, and many times the damping is not possible when the resonance frequency is low.
- Damping techniques based on capacitor voltage feedback would however demand a noise-sensitive derivative term. Digital implementation of this derivative term is generally a challenge.

Grid-Connected Converter with LCL Filter

- Active damping by means of the capacitor voltage

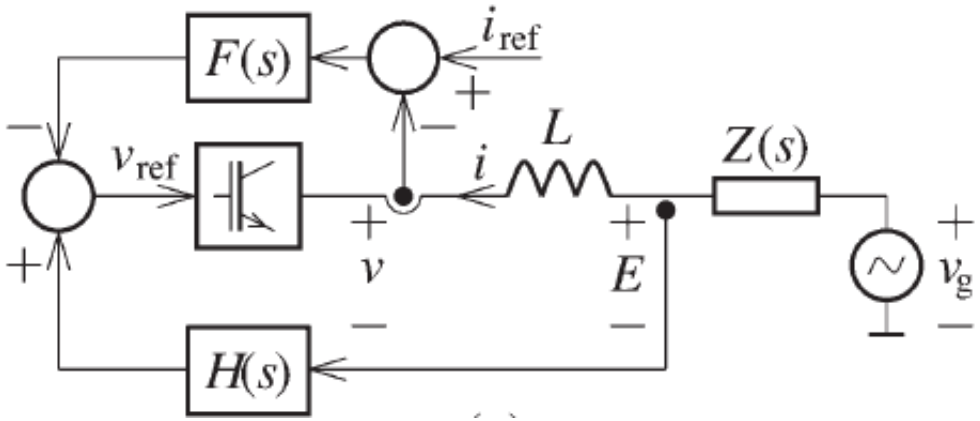

$$v_{\text{ref}} = -F(s)(i_{\text{ref}} - i) + H(s)E$$

$$H(s) = sK$$

$$K = \frac{4\alpha_c T_d^2}{\pi^2}$$

The negative-real-part region about ω = ωs/6 can be eliminated by modifying the "active damping" with a compensation filter Hc(s) as:

$$H(s) = sKH_c(s)$$

$$H_c(s) = \frac{s^2 + 2\zeta_z\omega_z s + \omega_z^2}{s^2 + 2\zeta_p\omega_p s + \omega_p^2}$$

$$\omega_p = 0.1\omega_s \quad \omega_z = 0.2\omega_s \quad \zeta_p = 2 \quad \zeta_z = 0.875$$

L. Harnefors, A. G. Yepes, A. Vidal and J. Doval-Gandoy, "Passivity-Based Controller Design of Grid-Connected VSCs for Prevention of Electrical Resonance Instability", IEEE Transactions on Industrial Electronics, vol. 62, no. 2, pp. 702-710, Feb. 2015

Grid-Connected Converter with LCL Filter

- Active damping by means of the capacitor current

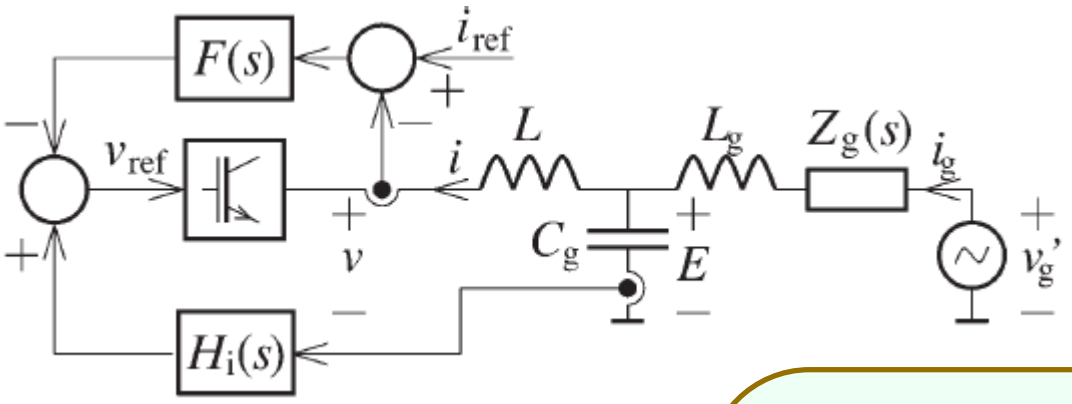

$$v_{\text{ref}} = -F(s)(i_{\text{ref}} - i) + H_i(s)(i_g - i)$$

$$E = \frac{1}{sC_g}(i_g - i)$$

$$H_i(s) = \frac{H(s)}{sC_g}$$

$$K = \frac{4\alpha_c T_d^2}{\pi^2}$$

$$H(s) = sKH_c(s)$$

$$H_c(s) = \frac{s^2 + 2\zeta_z\omega_z s + \omega_z^2}{s^2 + 2\zeta_p\omega_p s + \omega_p^2}$$

$$\omega_p = 0.1\omega_s \quad \omega_z = 0.2\omega_s \quad \zeta_p = 2$$

$$\zeta_z = 0.875$$

L. Harnefors, A. G. Yepes, A. Vidal and J. Doval-Gandoy, "Passivity-Based Controller Design of Grid-Connected VSCs for Prevention of Electrical Resonance Instability", IEEE Transactions on Industrial Electronics, vol. 62, no. 2, pp. 702-710, Feb. 2015

Contents

- Background of microgrids
- AC current control of grid-connected converters
  - Plant model
  - Interface filter
  - Classical controllers
- Limitations of classical current controllers
- State-space based techniques applied to current controllers
- AC voltage control of standalone or weak grid-tied converters

Limitations of previous classical current control methods

- Classical controllers do not have enough degrees of freedom to completely control the dynamics of a high-order plant model.
- Sensitivity function S describes the transfer function from external disturbance to process output. The sensitivity function tells us how the disturbances are influenced by feedback. Lower values suggest further attenuation of the external disturbance.
- Higher values of the system sensitivity correspond to a low robustness to plant parameter variations and a low disturbance-rejection bandwidth.

$$S(f) = \frac{i_1}{d_{i_1}}$$

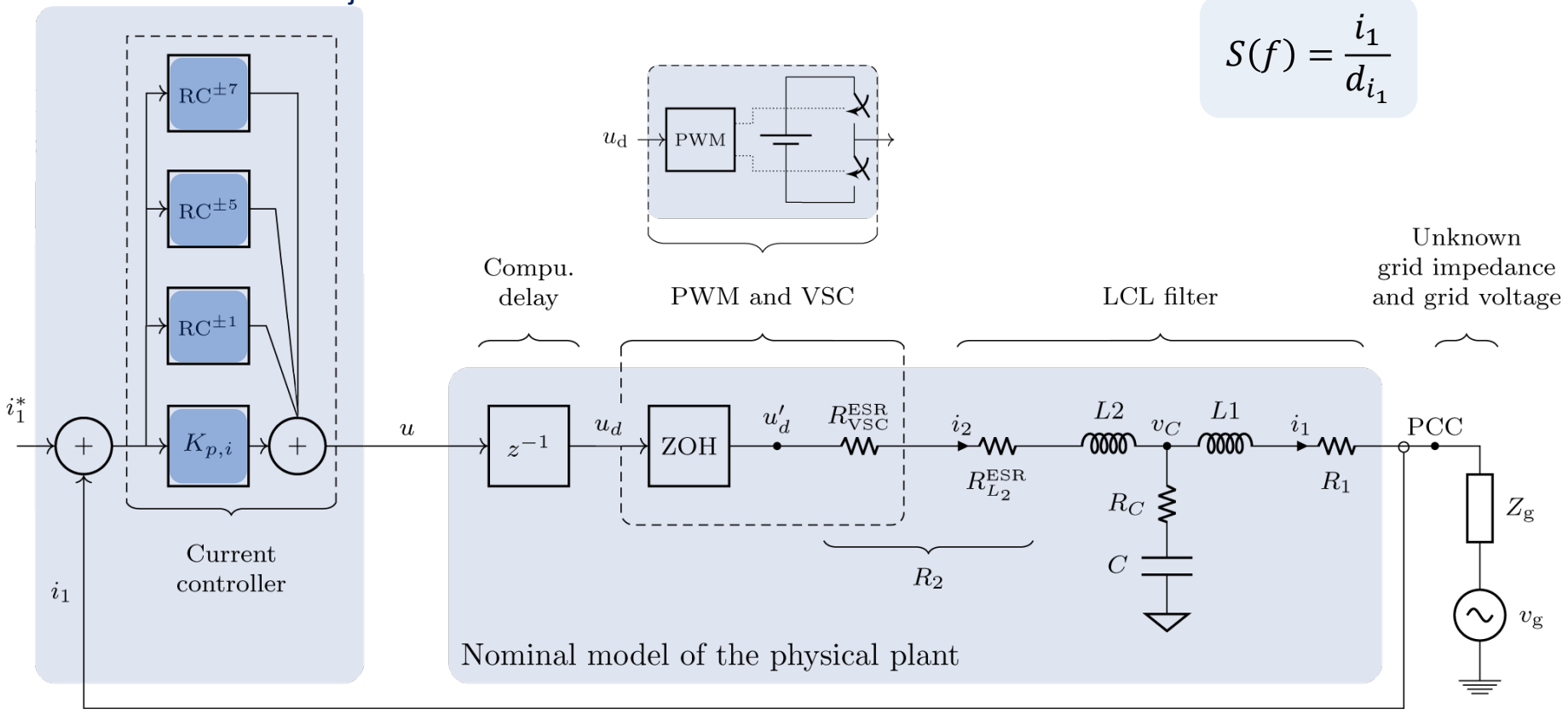

Limitations of previous classical current control methods

- Appearance of peaks in the system sensitivity function. The designer has little control over the width of the low sensitivity frequency regions.
- S < 1 : disturbances are reduced. S >1: disturbances are amplified by the feedback.
- Sensitivity peaks. Narrow low-sensitivity frequency regions.
- Stability depends on filter parameters and sampling frequency.
- Low robustness to plant parameter variations. Low disturbance-rejection bandwidth

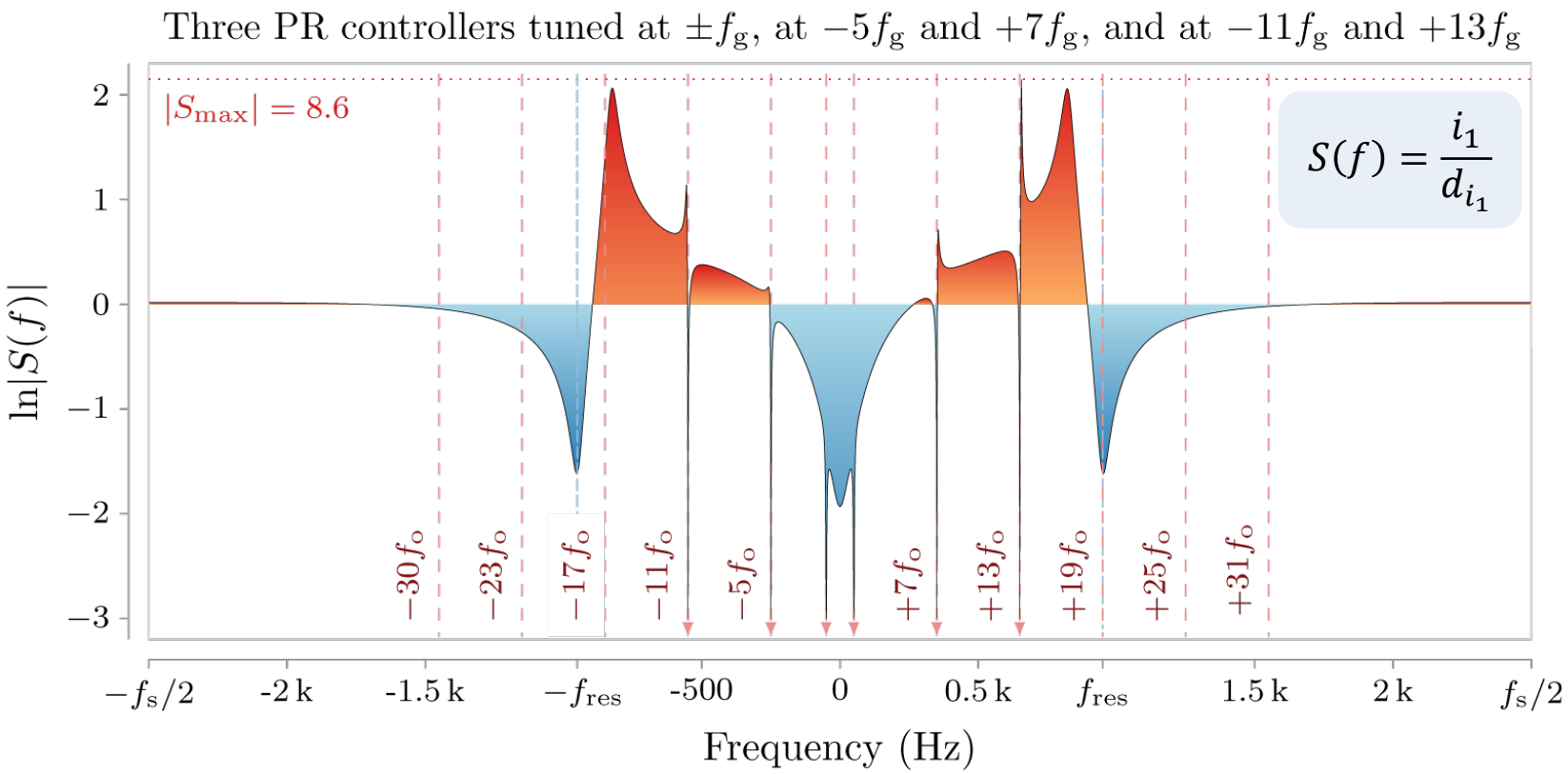

Limitations of previous classical current control methods

Conventional transfer-function-based controllers have stability problems when controlling a VSC with an LCL filter.

They are unstable when

- $f_{res} \leq f_s / 6$ and grid-side current is controlled or
- $f_{res} \geq f_s /6$ and converter-side current is controlled.

Therefore they require additional damping mechanisms.

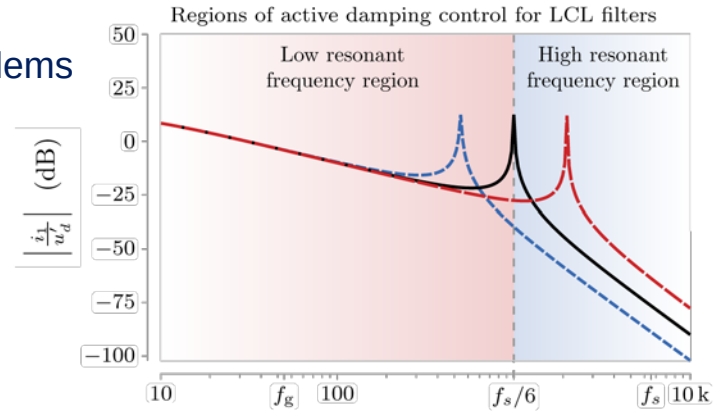

- They do not optimize the transient response in terms of speed, overshoot, or axis decoupling: frequency response is not flat.
- The designer cannot achieve a flat frequency response from reference to output, which ensures a fast and damped reference tracking response, with negligible overshoot or axis crosscoupling.

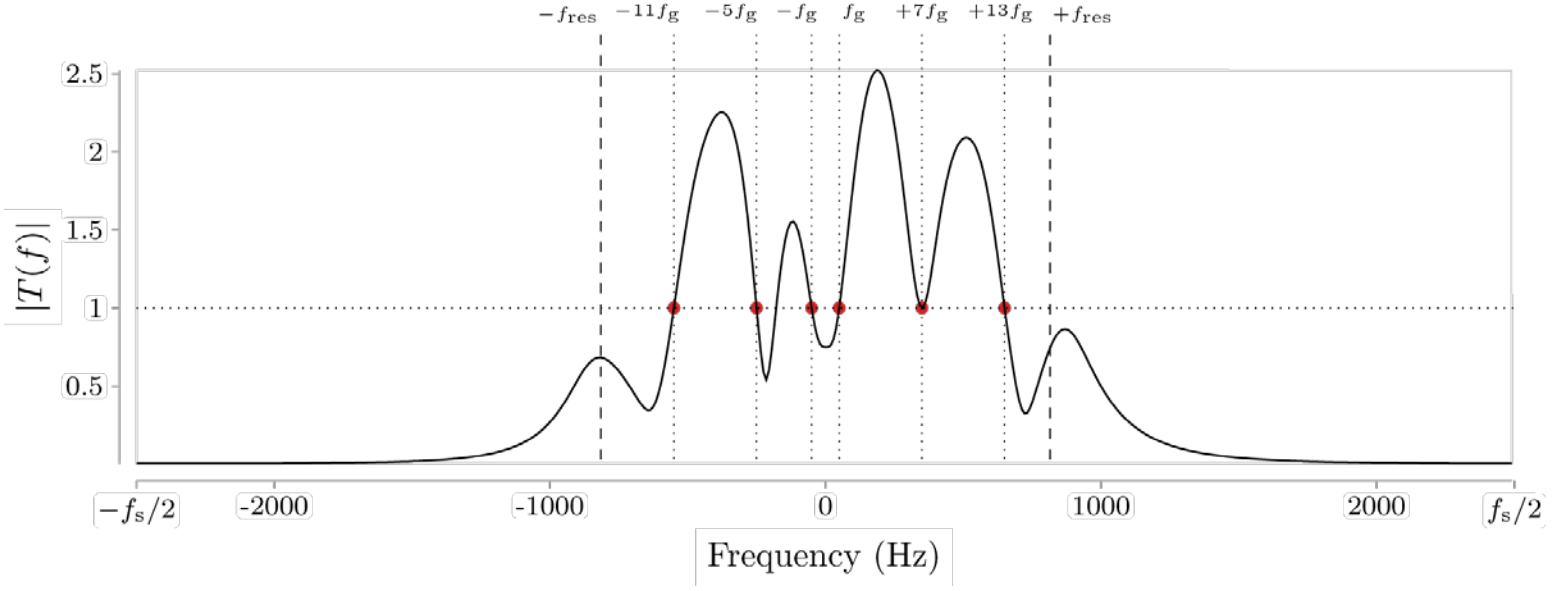

Limitations of previous classical current control methods

Is it possible to design a linear current controller that overcomes these limitations?

- A controller with the following characteristics:
- Fast reference-tracking and disturbance-rejection capability with negligible overshoot.
- Simple design process irrespectively of LCL filter values and sampling frequency.
- Stable and robust operation without additional damping methods even in the presence of plant parameter variations.

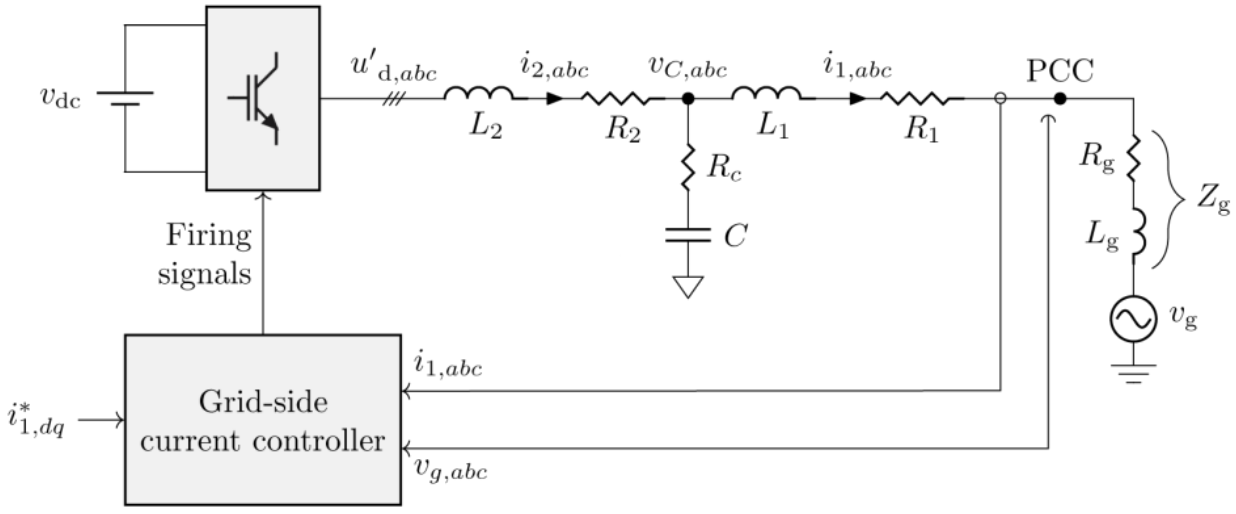

Contents

- Background of microgrids
- AC current control of grid-connected converters
  - Plant model
  - Interface filter
  - Classical controllers
- Limitations of classical current controllers
- State-space based techniques applied to current controllers
- AC voltage control of standalone or weak grid-tied converters

Space-state current controller

- In order to design the proposed controller the first step is to calculate a model of the physical system.
- A state-space model of the plant is calculated in the stationary frame.
- The model describes the following elements:
  - The LCL filter, including estimated ohmic losses from the reactive elements and the VSC.
  - The computational delay.
  - The PWM delay.

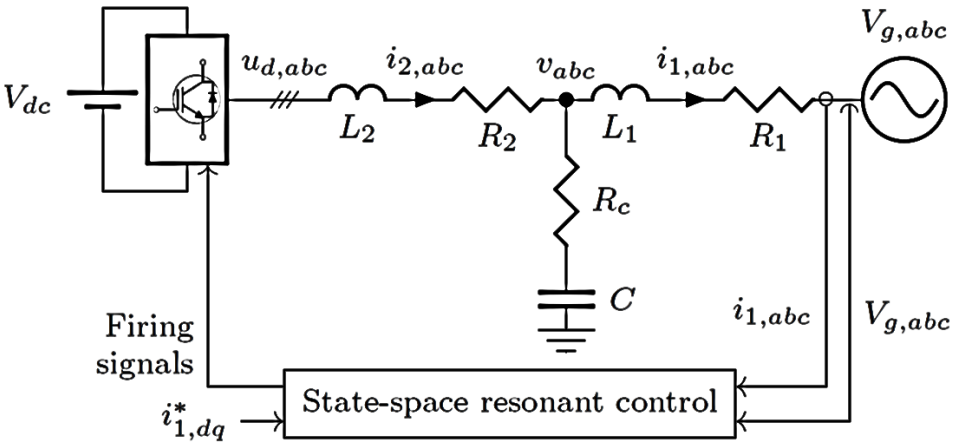

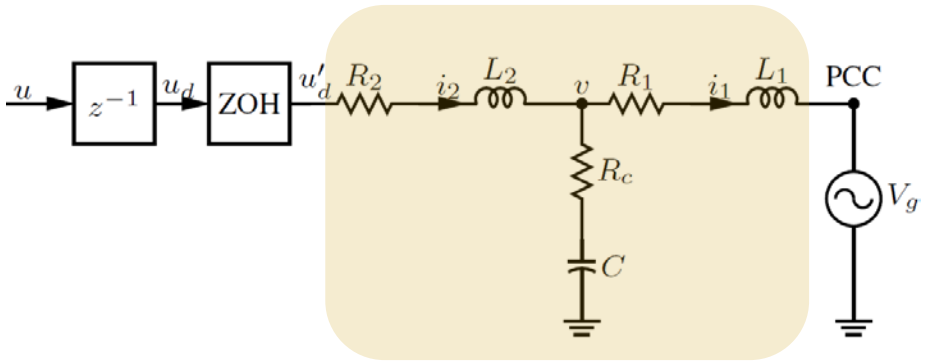

Model of the plant for the compensator

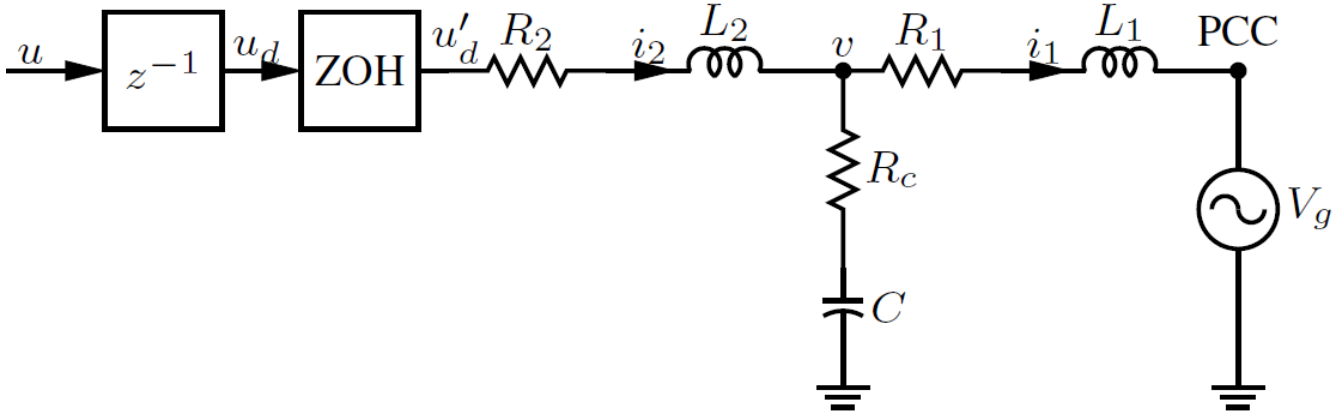

$$\frac{d\mathbf{x}(t)}{dt} = \underbrace{\begin{bmatrix} \frac{-R_1}{L_1} & 0 & \frac{1}{L_1} \\ 0 & \frac{-R_2}{L_2} & \frac{-1}{L_2} \\ \frac{CR_cR_1-L_1}{CL_1} & \frac{L_2-CR_cR_2}{CL_2} & \frac{-(R_cL_1+R_cL_2)}{L_1L_2} \end{bmatrix}}_{\mathbf{A}} \mathbf{x}(t) + \underbrace{\begin{bmatrix} 0 & \frac{1}{L_2} & \frac{R_c}{L_2} \end{bmatrix}^{\mathrm{T}}}_{\mathbf{B}} u'_d(t)$$

$$i_1(t) = \underbrace{\begin{bmatrix} 1 & 0 & 0 \end{bmatrix}}_{\mathbf{C}} \mathbf{x}(t) \qquad \mathbf{x}(t) = \begin{bmatrix} i_1 & i_2 & v \end{bmatrix}^{\mathrm{T}}$$

Model of the plant & disturbance for the observer

- A sinusoidal disturbance w(t) of frequency ω_g which contains both sequences (two complex conjugate poles in its model), is a solution of

$$\frac{d^2w(t)}{dt^2} = -\omega_g^2 w(t)$$

- The previous plant model is augmented with the disturbance model in order to include the resonant action.

$$\underbrace{\begin{bmatrix}\mathbf{x}_2(k+1)\\ \mathbf{r}(k+1)\end{bmatrix}}_{\mathbf{x}_3(k+1)} = \underbrace{\begin{bmatrix}\mathbf{F_2} & \mathbf{G_2H_d}\\ \mathbf{0} & \mathbf{F_d}\end{bmatrix}}_{\mathbf{F_3}} \underbrace{\begin{bmatrix}\mathbf{x}_2(k)\\ \mathbf{r}(k)\end{bmatrix}}_{\mathbf{x}_3(k)} + \underbrace{\begin{bmatrix}\mathbf{G_2}\\ \mathbf{0}\end{bmatrix}}_{\mathbf{G_3}} u(k)$$

$$i_1(k) = \underbrace{\begin{bmatrix}\mathbf{H_2} & \mathbf{0}\end{bmatrix}}_{\mathbf{H_3}} \underbrace{\begin{bmatrix}\mathbf{x}_2(k)\\ \mathbf{r}(k)\end{bmatrix}}_{\mathbf{x}_3(k)}$$

$$\mathbf{x}_3(k) = \begin{bmatrix} i_1 & i_2 & v & u_d & r_1 & r_2 \end{bmatrix}^{\mathrm{T}}$$

$$\mathbf{r}(t) = \begin{bmatrix} r_1 & r_2 \end{bmatrix}^{\mathrm{T}} = \begin{bmatrix} w & dw/dt \end{bmatrix}^{\mathrm{T}}$$

Space-state current controller. Controller architecture (I)

Two main components (principle of separation of estimation and control). The design of the observer and the design of the compensator is performed independently

The **compensator** provides:

- Consistent and fast **ref.-track. response**.
- Low controller effort.
- No overshoot.

The **observer** provides:

- Good **robustness** to **disturbances** and to variations in the grid impedance.

This controller structure **avoids wind-up** problems.

The above properties are guaranteed **irrespectively of the LCL filter** used and the **sampling frequency f_s**, provided that $f_{\text{res}} < f_s/2$.

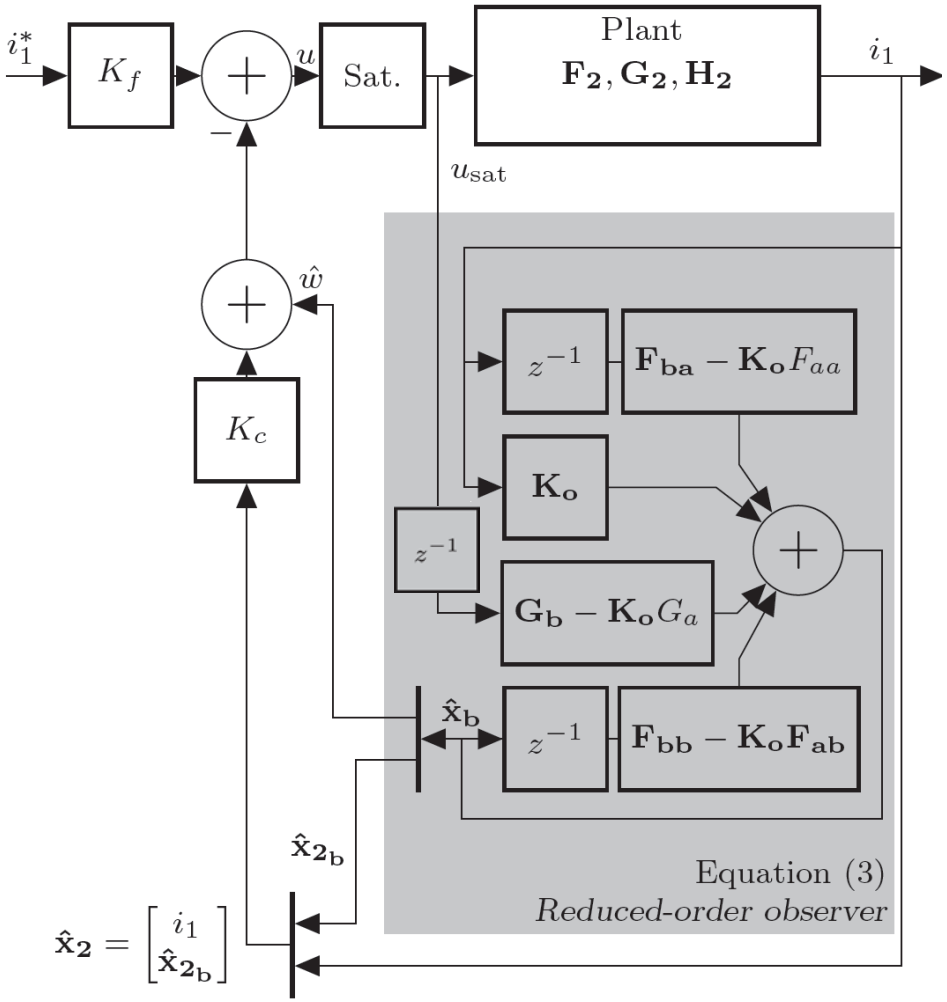

Space-state current controller. Controller architecture (I)

Two main components (principle of separation of estimation and control). The design of the observer and the design of the compensator is performed independently

$$u(k) = K_f i_1^* - \begin{bmatrix} \mathbf{K_c} & 1 & 0 \end{bmatrix} \begin{bmatrix} i_1 \\ \hat{\mathbf{x}}_\mathbf{b} \end{bmatrix}$$

$$x_a(k) = i_1(k)$$

$$\mathbf{x_b}(k) = \begin{bmatrix} i_2 & v & u_d & r_1 & r_2 \end{bmatrix}^{\mathrm{T}}$$

$$\underbrace{\begin{bmatrix} x_a(k+1) \\ \mathbf{x_b}(k+1) \end{bmatrix}}_{\mathbf{x_3}(k+1)} = \underbrace{\begin{bmatrix} F_{aa} & \mathbf{F_{ab}} \\ \mathbf{F_{ba}} & \mathbf{F_{bb}} \end{bmatrix}}_{\mathbf{F_3}} \underbrace{\begin{bmatrix} x_a(k) \\ \mathbf{x_b}(k) \end{bmatrix}}_{\mathbf{x_3}(k)} + \underbrace{\begin{bmatrix} G_a \\ \mathbf{G_b} \end{bmatrix}}_{\mathbf{G_3}} u$$

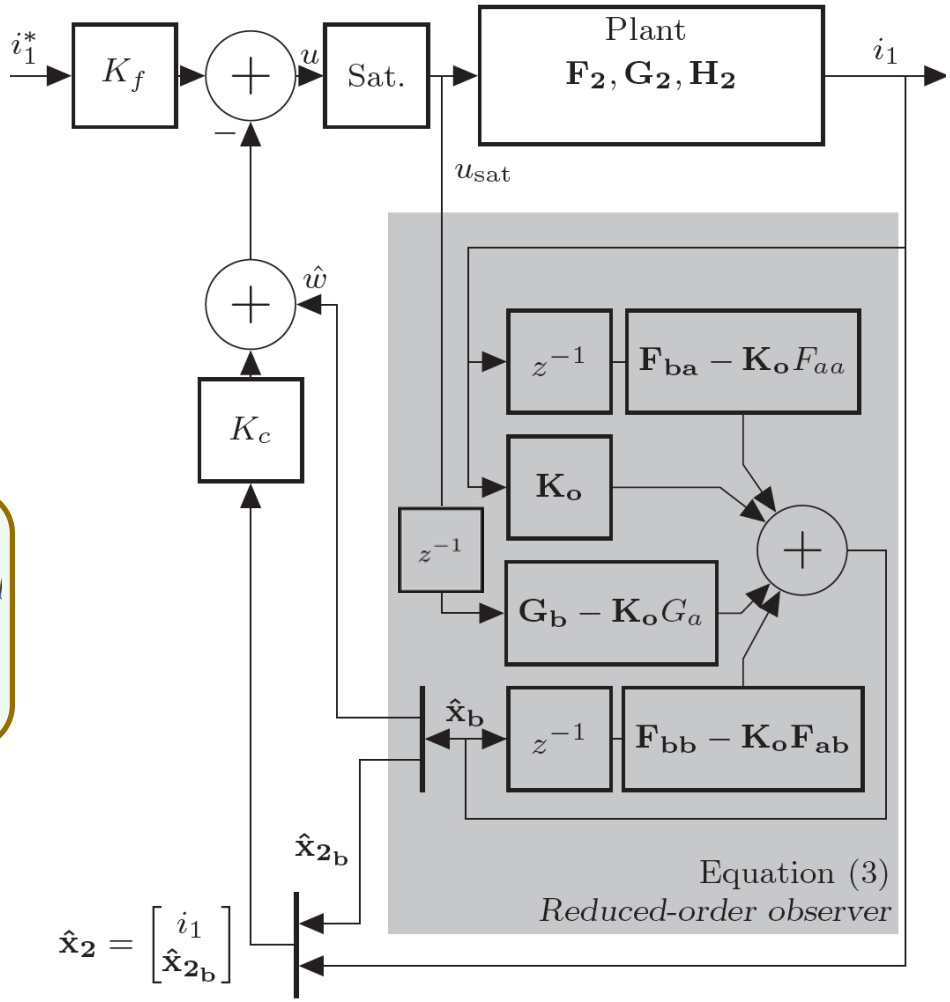

Design using pole placement

- The plant model has four poles.
  - LCL filter: 2 resonant poles + 1 real pole at zero freq.
  - Computational delay adds 1 pole at the origin of the z-plane.
- The compensator and the observer are designed using the pole placement method according to a radial projection of the resonant poles of the plant.

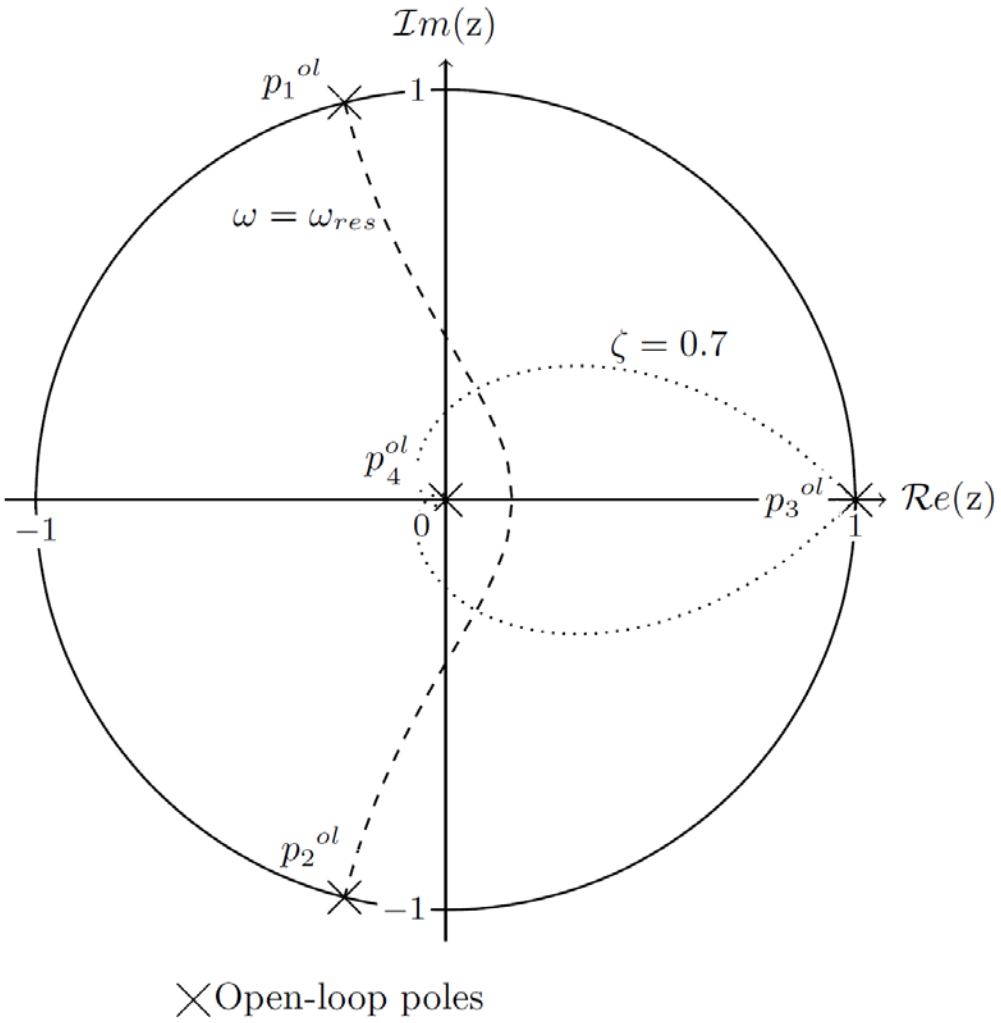

Design of the compensator

- The resonant poles of the plant are moved to a more damped region using a radial projection.
- The delay pole is kept in the same location.
- The DC pole is moved to a higher frequency and set as a dominant pole with the desired bandwidth. But a frequency fdom < fres/2 is recommended for the dominant pole because it ensures a negligible effect of the damped resonant poles on the system response

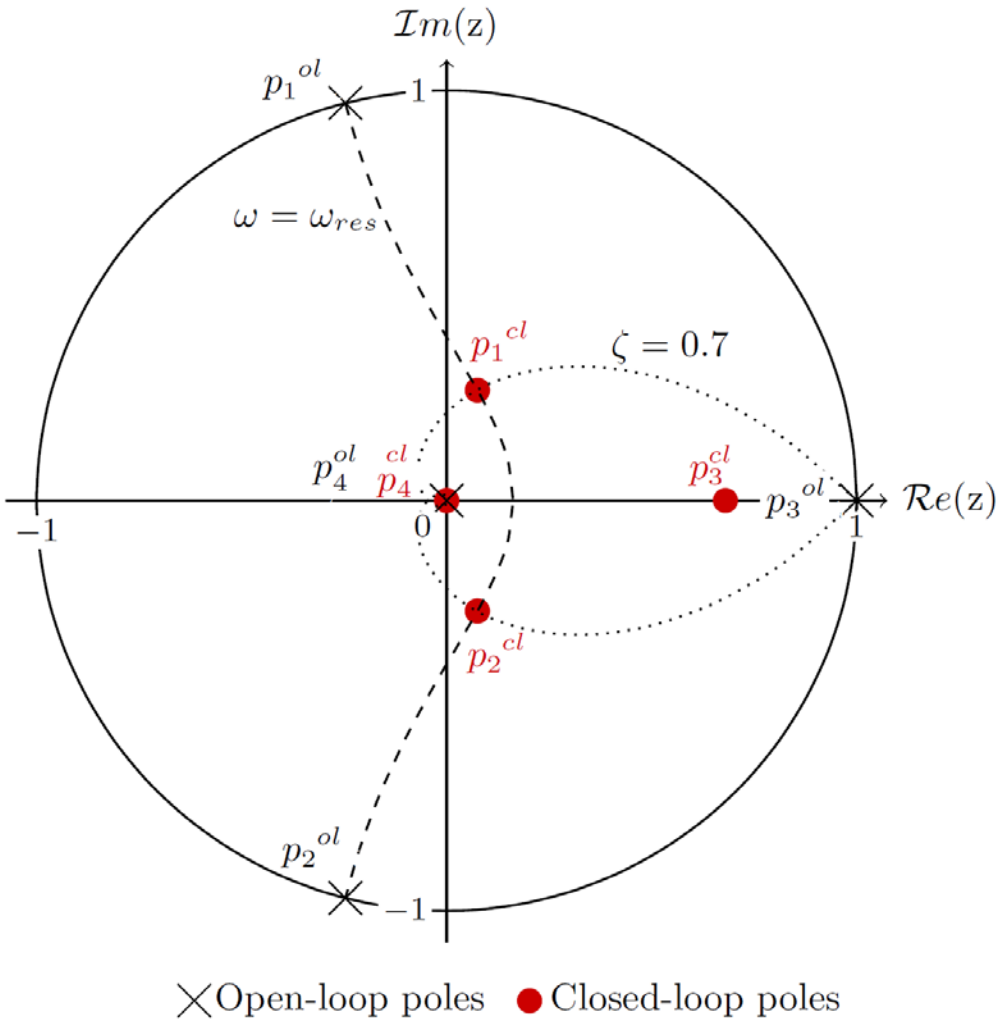

Design of the reduced-order observer

- The model of the plant and disturbance for the observer has six poles.
  - LCL filter

$$p_{5,6}^{ol} = e^{\pm j\omega_{res}T_s}$$
$$p_7^{ol} = 1$$

  - Computational delay

$$p_8^{ol} = 0$$

  - Resonant action

$$p_{9,10}^{ol} = e^{\pm j\omega_g T_s}$$

- Now the pole assignment is not restricted to yield a low control effort, because the observer does not drive any actuator, but simply calculates the state of the system.
- On the other hand, the observer poles are moved to a higher frequency, in order to ensure that the dynamics of the system are determined by the dominant pole

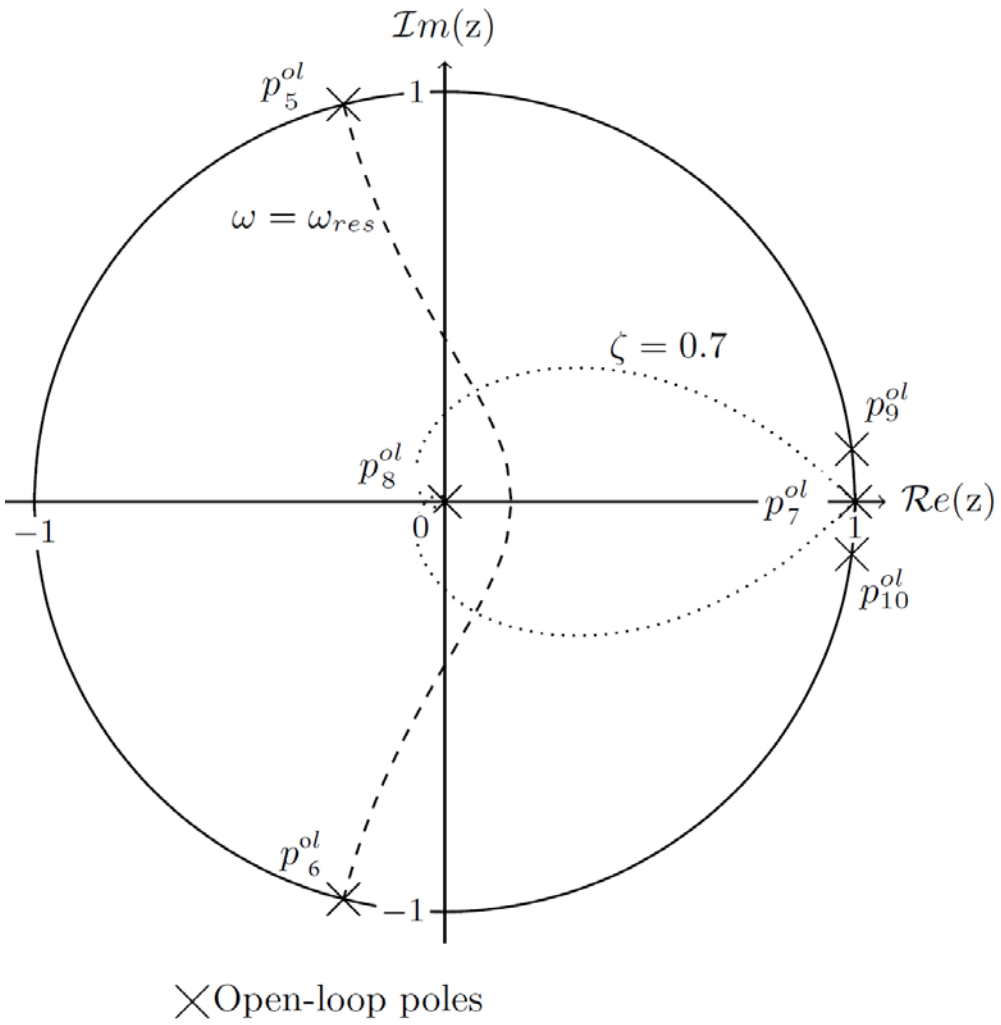

Design of the reduced-order observer

- Now the pole assignment is not restricted to yield a low control effort, because the observer does not drive any actuator, but simply calculates the state of the system.
- The reduced-order estimator eliminates one pole, making the response faster.
- A larger bandwidth can be set, and it is advisable to place the observer closed-loop poles at frequencies higher and damped than that of the dominant pole of the compensator so as to provide similar dynamics to those of the compensator alone.
- Moved to twice the frequency of the dominant pole.

$$p_7^{cl} = e^{-2\omega_{dom} T_s}$$

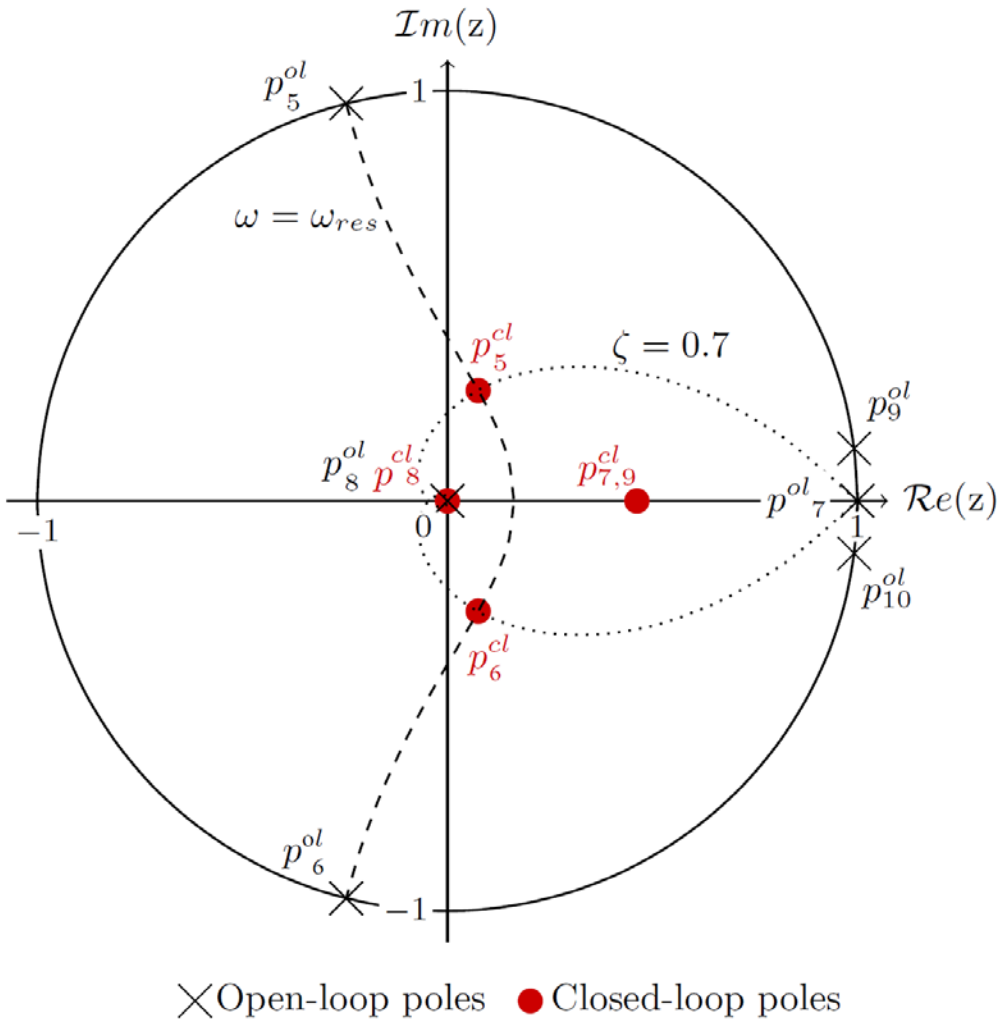

SS Current Controller. Robustness Analysis

High robustness to variations in the **filter parameters** and the **grid inductance**.

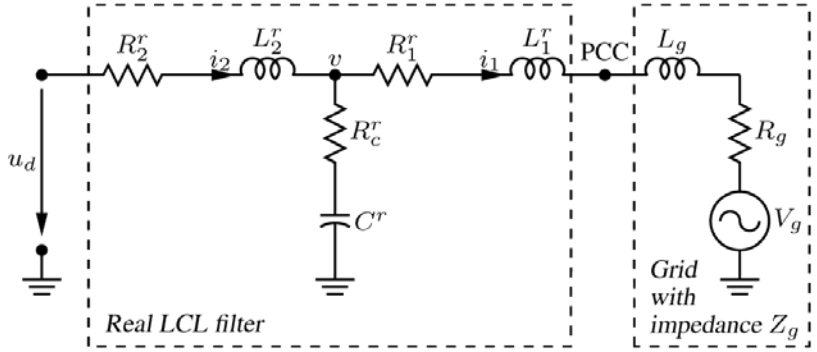

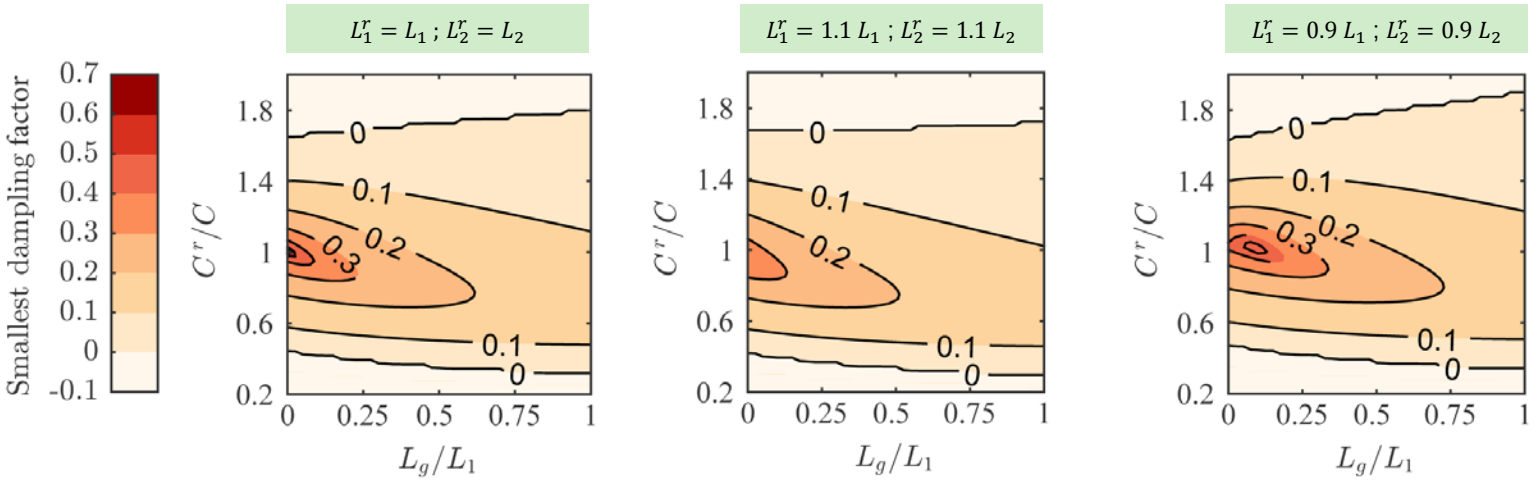

SS Current Controller. Experiments

* 20-kW VSC
* V_{AC} = 400 V
* V_{DC} = 700 V
* $f_s = f_{sw}$ = 2.5 kHz and **$f_s/6$ = 417 Hz**
* f_{dom} = 150Hz
* Two LCL filters f_{res} higher/lower than $f_s/6$
  1. Filter I: **f_{res} = 330 Hz**
  2. Filter II: **f_{res} = 707 Hz**

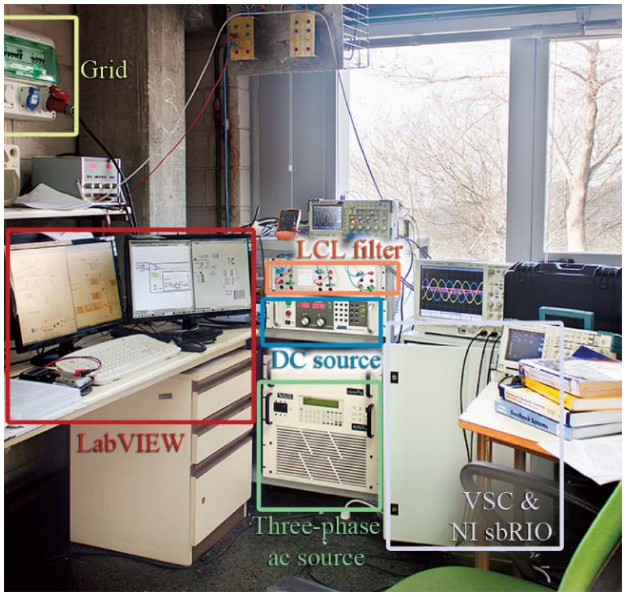

Tests:

- Reference tracking
- Disturbance rejection
- Parameters variation

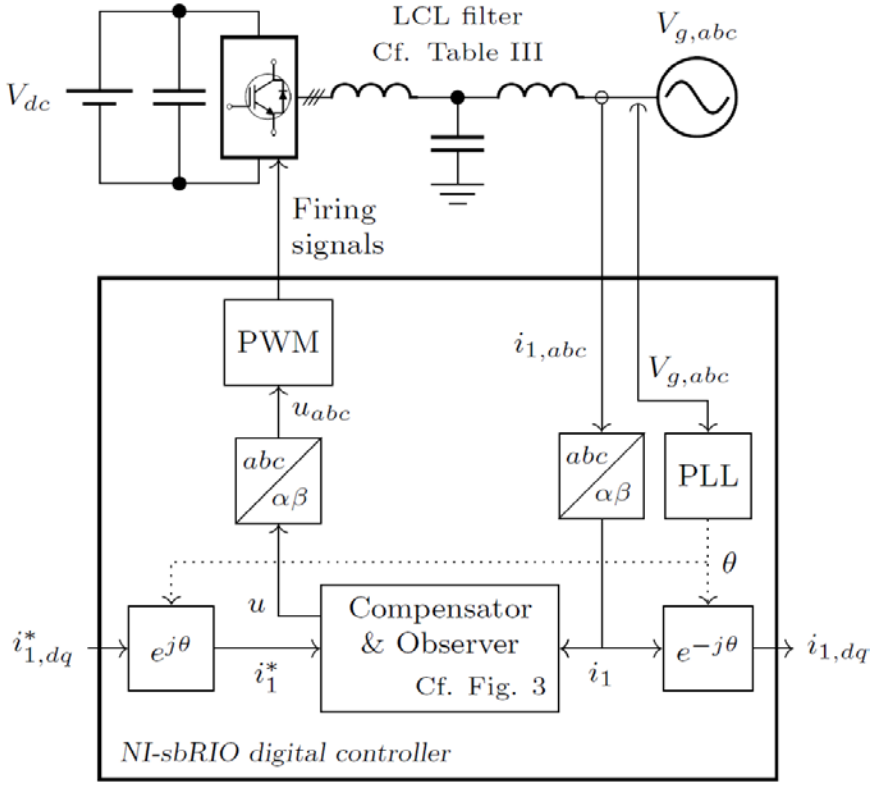

SS Current Controller. Ref. Tracking

- Reference step $i^*_{1,q+}$ in the positive synchronous frame dq⁺.
- Experimental and simulation waveforms ($i_{1,dq+}$ and $i^{sim}_{1,dq+}$ respectively).
- Dynamics equivalent to a first-order system.
- Rise time of approx. 2.5ms.

$$T_{10\%-90\%} = \ln|9| \,/(2\pi f_{dom}) = 2.33 \text{ ms}$$

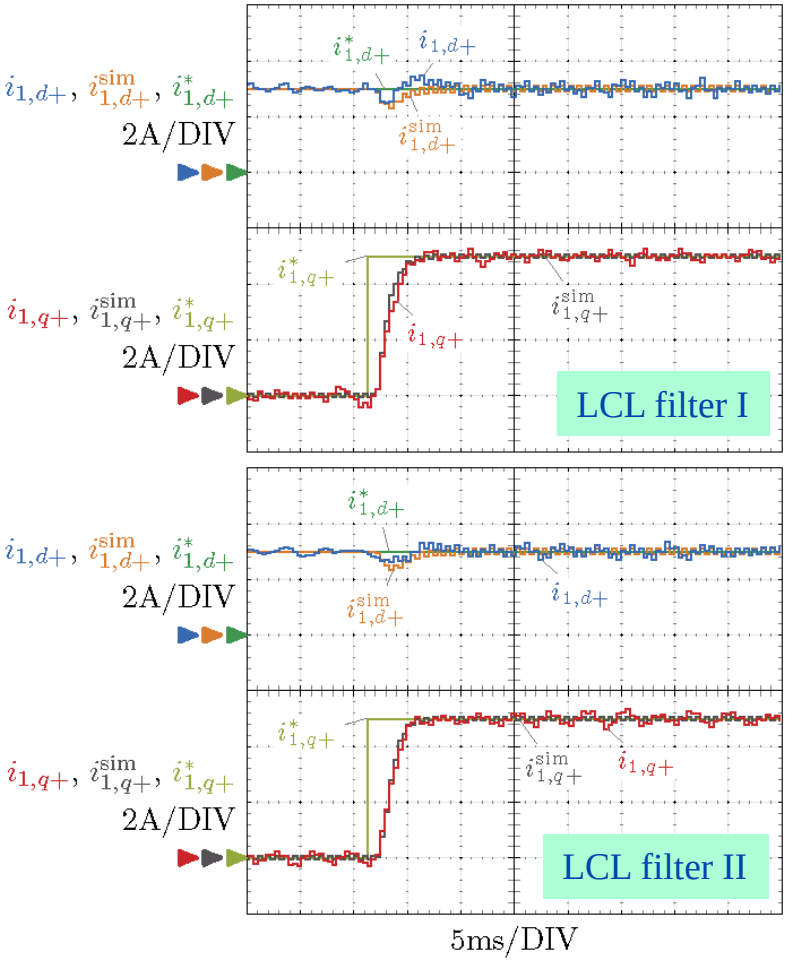

SS Current Controller. Ref. Tracking

- Reference step $i^*_{1,q+}$ in the negative synchronous frame dq-.
- Experimental and simulation waveforms ($i_{1,dq+}$ and $i^{sim}_{1,dq+}$ respectively).
- Dynamics equivalent to a first-order system.
- Rise time of approx. 2.5ms.

$$T_{10\%-90\%} = \ln|9| / (2\pi f_{dom}) = 2.33 \text{ ms}$$

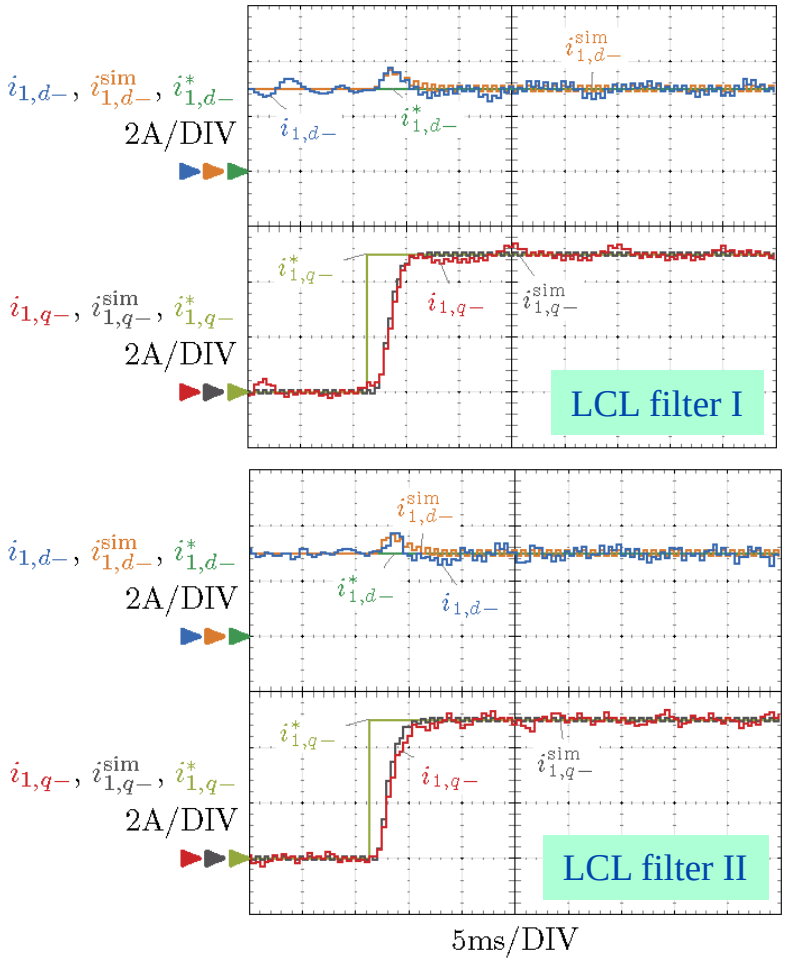

SS Current Controller. Disturbance Rejection

- 40%-depth, type-C voltage sag.
- Current references are maintained constant.
- Experimental and simulation waveforms ($i_{1,dq}$ and $i^{sim}_{1,dq}$).
- Dynamics of a first-order system.
- Settling time (2%), approx. 5ms.

$$T_{st} = -\ln|0.02| / (2\pi f_{dom}) = 4.15 \text{ ms}$$

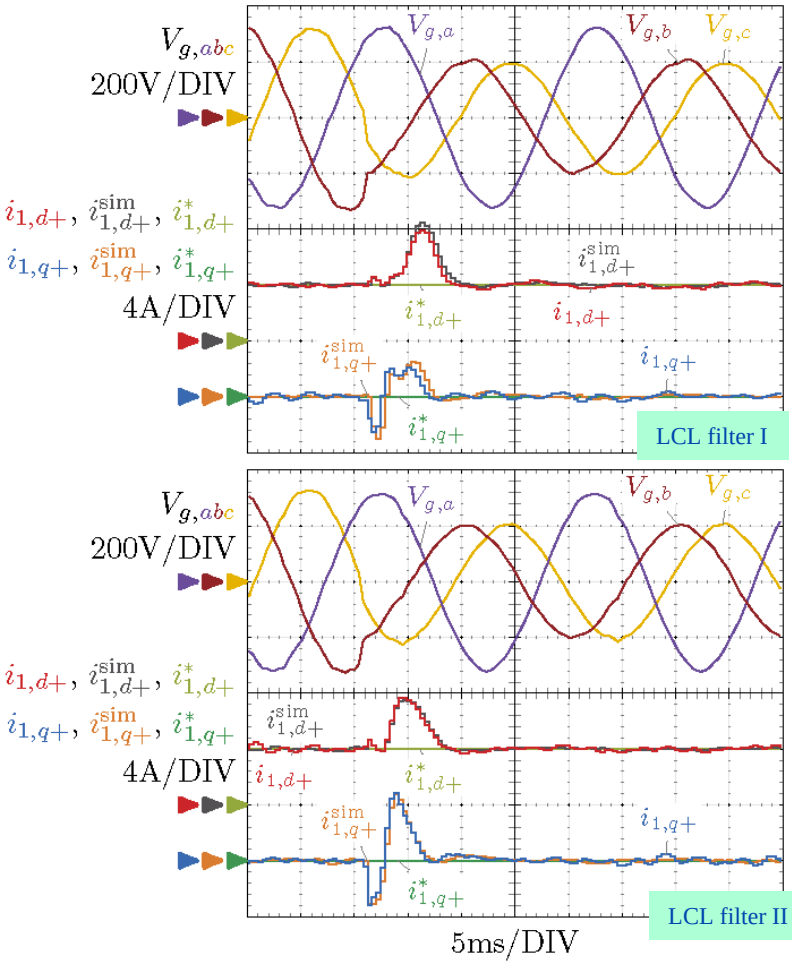

SS Current Controller. Refer. Tracking & Disturbance Rejection

- Robustness to voltage harmonics:
  - Grid voltage with harmonics (V_3 = 0.8 %; V_5 = 0.2 %; V_7 = 2.0 %; V_9 = 0.4%)
- Transient response not affected.
- Low steady-state error at the harmonic freq., mainly sixth harmonic current in dq-frame.

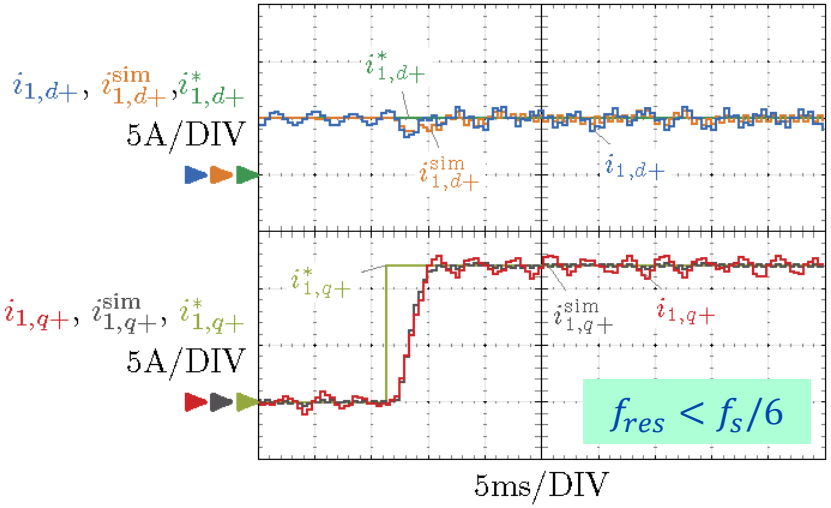

SS Current Controller. Conclusions

- A current controller of both positive and negative grid-side current sequences for grid-tied converters with LCL filter.
- Fast reference-tracking capability with negligible overshoot.
- Simple design process independently of the LCL filter and sampling freq. selected.
- Robust to disturbances such as low-order grid voltage harmonics and plant parameter variations.
- Avoids wind-up problems.
- Can be applied to control multiple frequencies with zero steady-state error.
- Low controller effort, regardless of the switching frequency and LCL filter used: fres above or below fs/6.
- Robust to disturbances and plant parameter variations: voltage sags, grid voltage harmonics.

SS Multifrequency Current Controller

- Previously presented controllers have proven to have a good transient response and inherent stability and robustness without additional active damping mechanisms. Nevertheless, they do not completely achieve zero steady-state error in the grid-side current at the low-order grid-frequency harmonics.
- In order to achieve this goal, the previous controller architecture is maintained, but now, the observer estimates multiple disturbances.
- A Kalman filter is used instead of a reduced-order observer.

The observer (Kalman filter) provides:

- Good disturbances rejection at multiple frequencies.
- Good robustness to variations in the grid impedance.

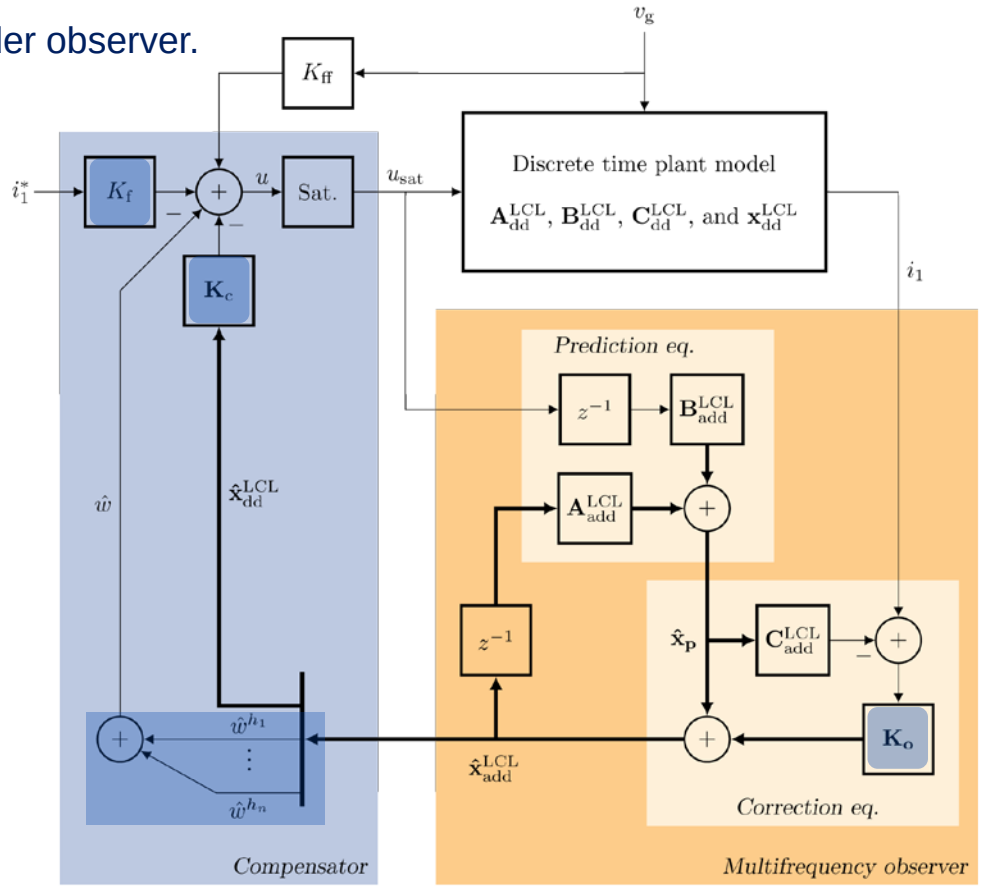

SS Multifrequency Current Controller. Disturbance Rejection

- Why a Kalman filter instead of a Luenberger observer?
- Observer design determines: transient response to disturbances and robustness to parameter variations.
- According to Bode's integral, on average, the amplification and attenuation of disturbance is zero. In graphical terms, this means that the red and blue regions are equal in area.

- Sensitivity function of a harmonic controller that removes the following current harmonics (+1, -1, +7, -5, +13, -11) using a Luenberger observer with a direct discrete-time pole-placement strategy which places the observer poles at twice the frequency of the dominant pole of the compensator.

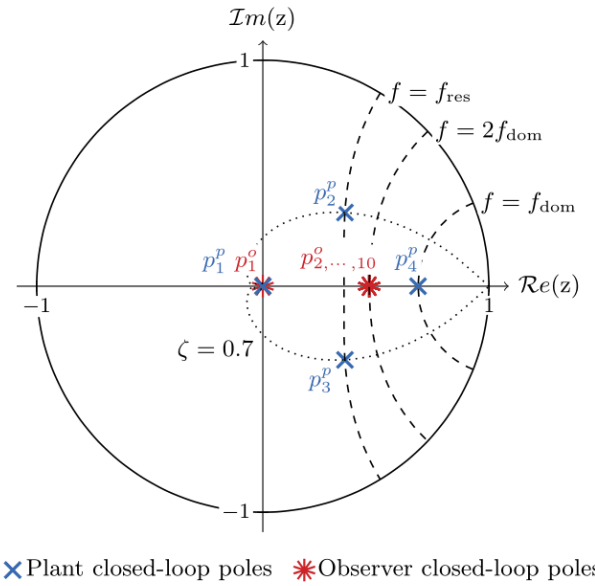

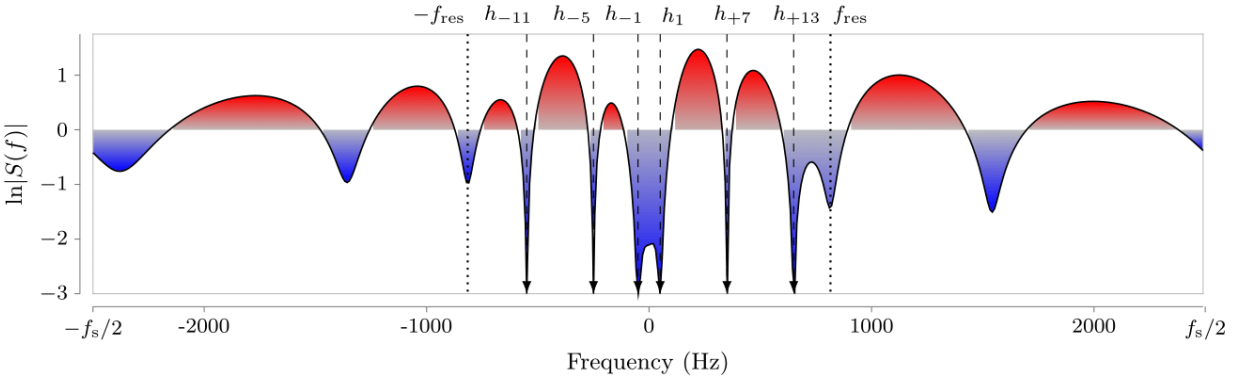

SS Multifrequency Current Controller. Disturbance Rejection

- **Limitations of this approach**
- High sensitivity (red areas in the sensitivity) at frequency ranges above the resonant frequency, which yields a low robustness because the controller should not respond to disturbance at such high frequencies where unmodeled dynamics are more common.
- Presence of useless low-sensitivity areas outside the targeted frequencies, which contribute to worsen the performance at other frequencies.
- An optimum sensitivity function should have sensitivities lower than unity only at the frequency regions of the targeted harmonics and at the resonant frequency of the LCL filter.

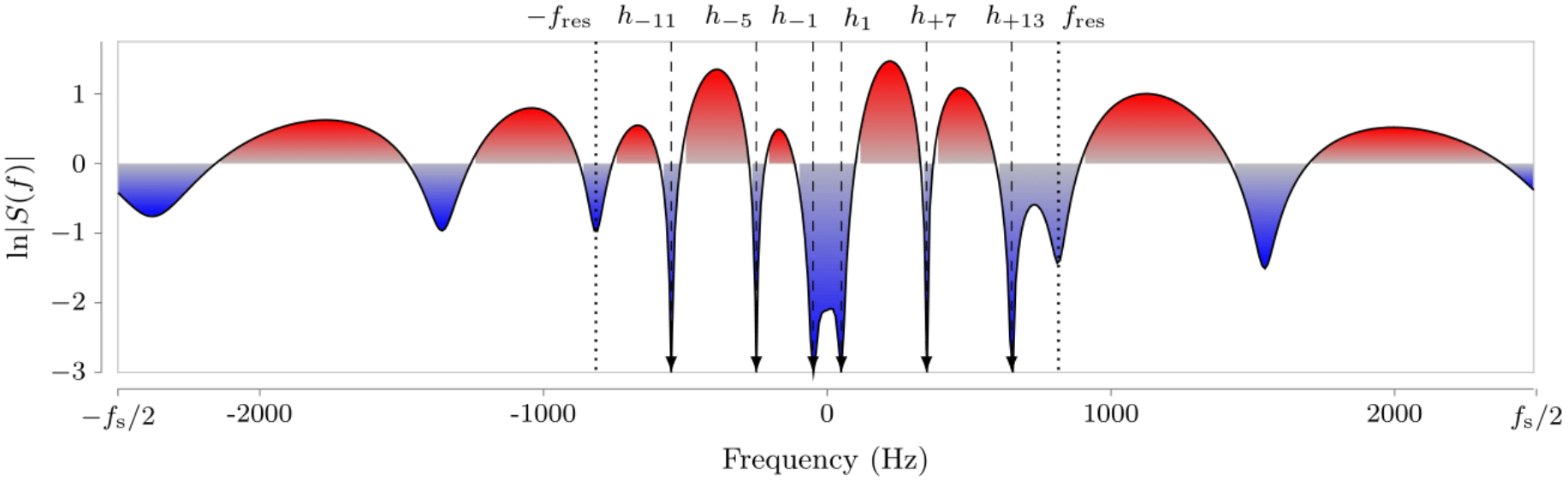

SS Multifrequency Current Controller. Disturbance Rejection

- **Limitations of this approach**
- In addition, sensitivities greater than one should be spread evenly in the rest of the frequency range where the controller operates, i.e., below the cut off frequency of the LCL filter, so as to avoid sensitivity peaks.
- From this analysis, it is clear that a better closed-loop pole-placement strategy is needed when a multi-frequency controller is considered.

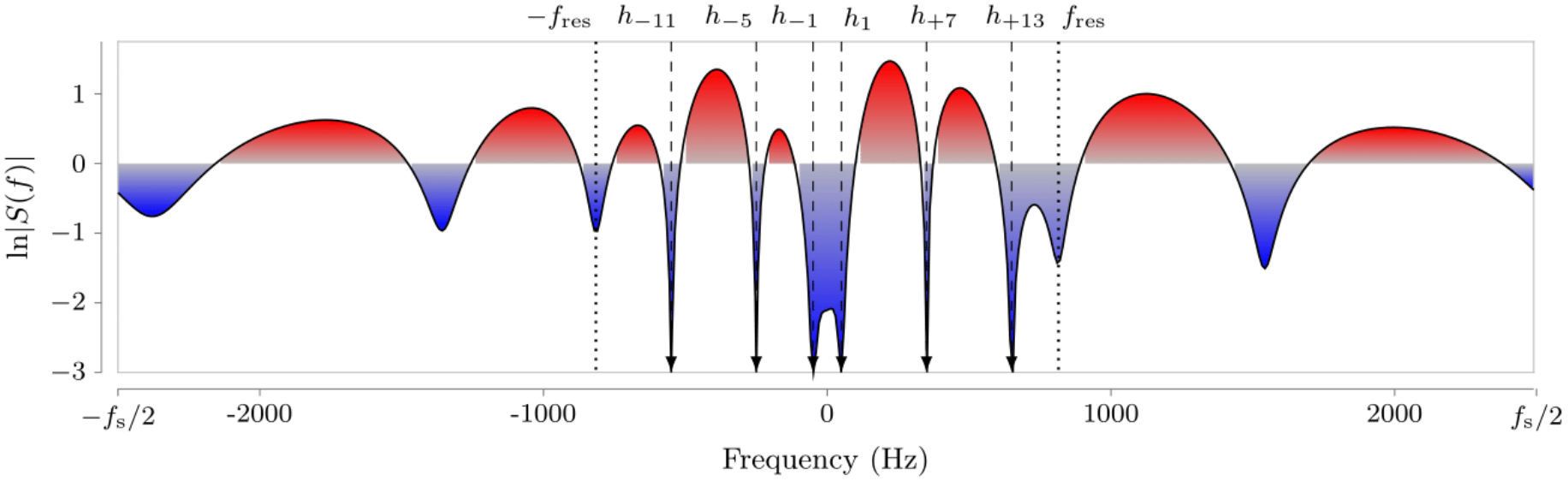

SS Multifrequency Current Controller. Disturbance Rejection

- Instead of designing the observer according to its dynamic characteristics (by placing its poles at high frequencies as shown in the previous slide), which results in a high sensitivity and a low robustness, the proposal adopts a Kalman filter.
- This method is particularly useful in this case, where a multi-frequency observer is considered, because it frees the designer from defining the multiple required closed-loop pole locations.
- In order to design a Kalman filter a parameter named process noise (Q) needs to be defined. The process noise parameter sets the bandwidth of the multi-frequency observer, which is defined by the width of the low-sensitivity regions around the frequencies of interest.

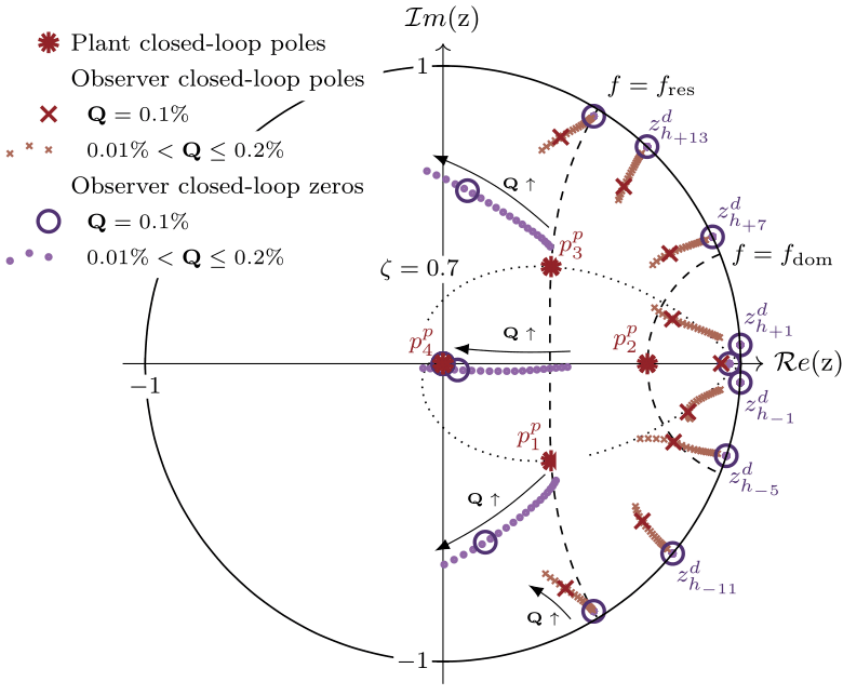

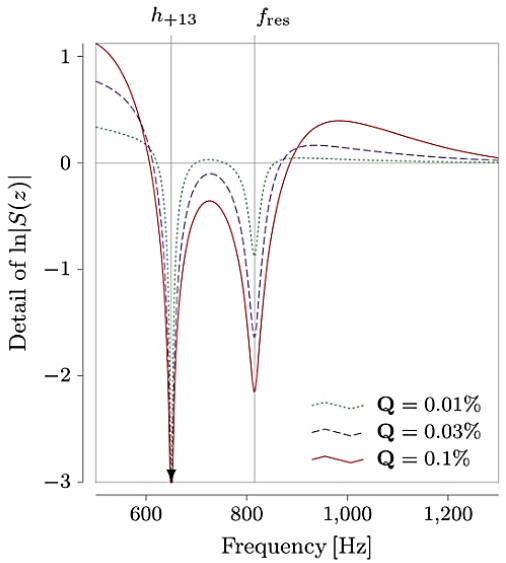

SS Multifrequency Current Controller. Disturbance Rejection

- Roots of the sensitivity transfer function S(f) for a sweep in the process noise Q.
- When Q increases, the observer closed-loop poles move away from the disturbance zeros, hence increasing the disturbance rejection bandwidth. It is recommended a value of 0.1.
  - If, for example, the voltage fluctuates significantly (at the fundamental or at harmonic frequencies) a higher value of Q is recommended to increase the bandwidth of the observer to quickly remove such disturbances.
  - Conversely, if the VSC is connected to a weak grid (where the plant parameters vary significantly from the nominal model), then a lower Q yields a more robust controller.

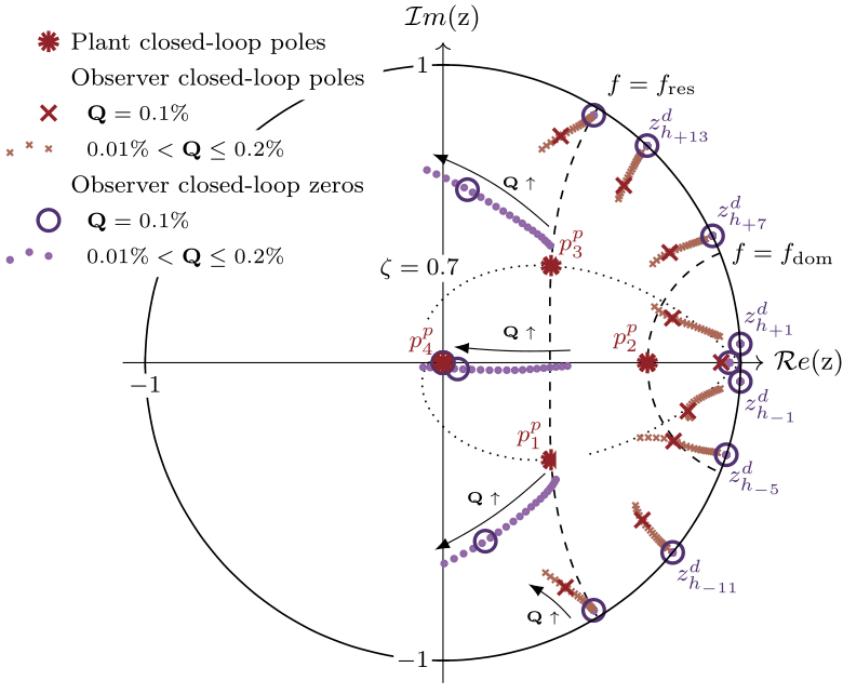

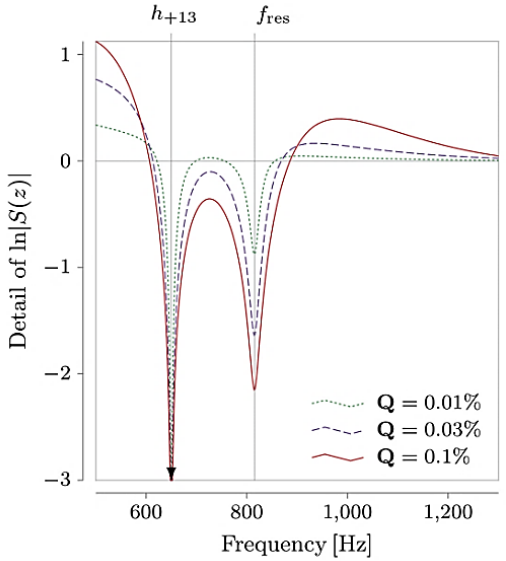

SS Multifrequency Current Controller. Disturbance Rejection

A controller with a reduced-order observer that is designed according to a direct discrete-time pole-placement strategy.

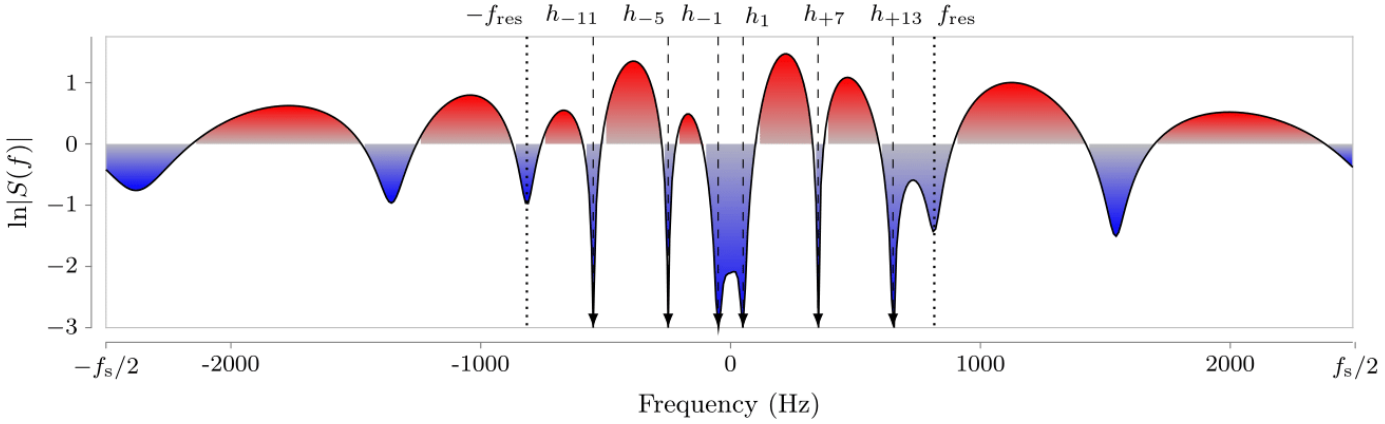

The multifrequency controller uses a Kalman filter.

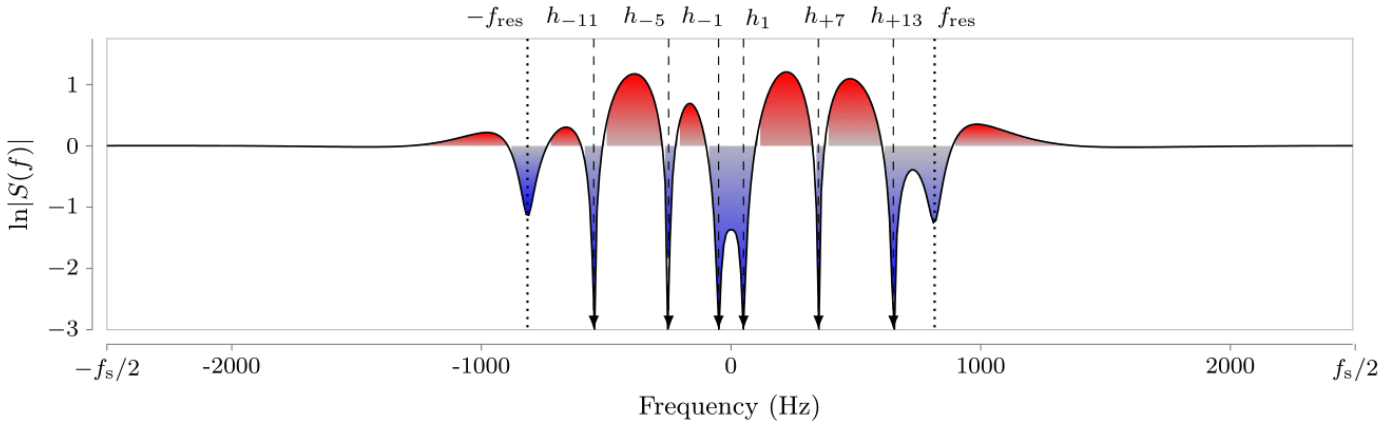

SS Multifrequency Current Controller. Reference Tracking

- Reference tracking capability

  output-error feedback structure VS **state-command structure**.

- Typically, classic transfer-function design adopts an output-error feedback structure.
  - When this structure is selected, the complementary sensitivity function T(f) of the system is the transfer function that determines the reference tracking performance.
  - This transfer function has unity gain at the frequencies controlled with zero steady-state error; however, it does not have a flat frequency response.
  - Depending on the harmonics controlled or the LCL filter installed, the response varies because this transfer function depends on the observer.

Output-error feedback structure

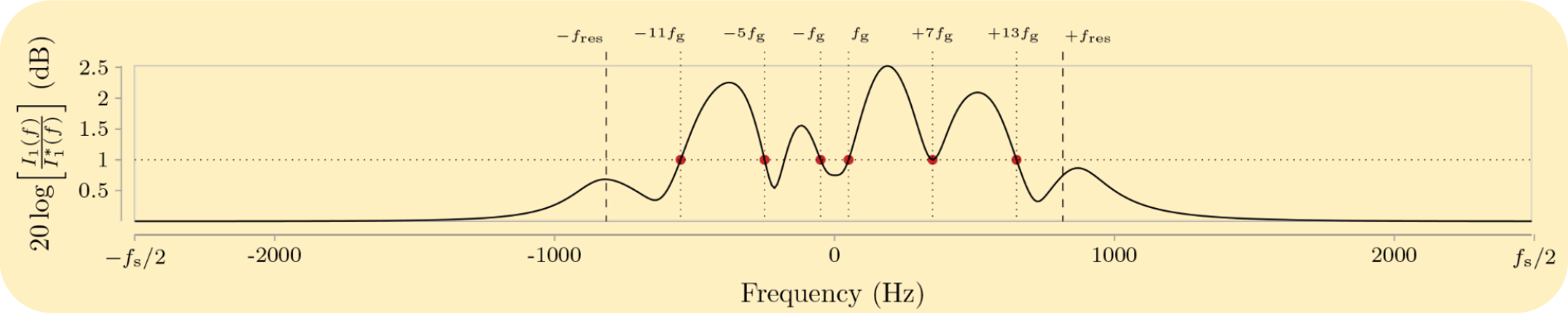

SS Multifrequency Current Controller. Reference Tracking

- Reference tracking capability

  output-error feedback structure VS **state-command structure**.

- State-command structure.
  - In this case, the transfer function that relates the grid-side current to the current reference is not T(f).
  - Now the reference-to-output transfer function only contains the closed-loop poles of the plant, irrespectively of the number of harmonics controlled.
  - Therefore, this transfer function has a flat frequency response

State-command structure with the proposed compensator design.

- Consistent and fast transient response.
- Low controller effort.
- No overshoot.

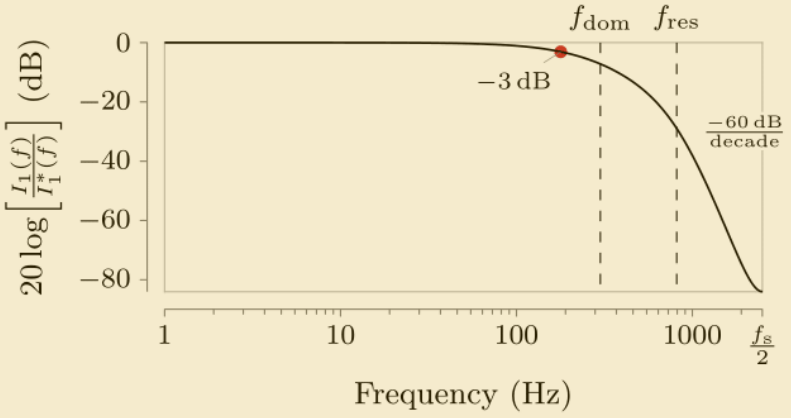

SS Multifrequency Current Controller. Experimental Results

Three tests

- Reference tracking.
- Disturbance rejection.
- Effect of the observer bandwidth (param. $\boldsymbol{Q}$)

10-kW VSC working as **inverter**.

$f_{sw} = 2.5$ kHz, $f_s = 5$ kHz

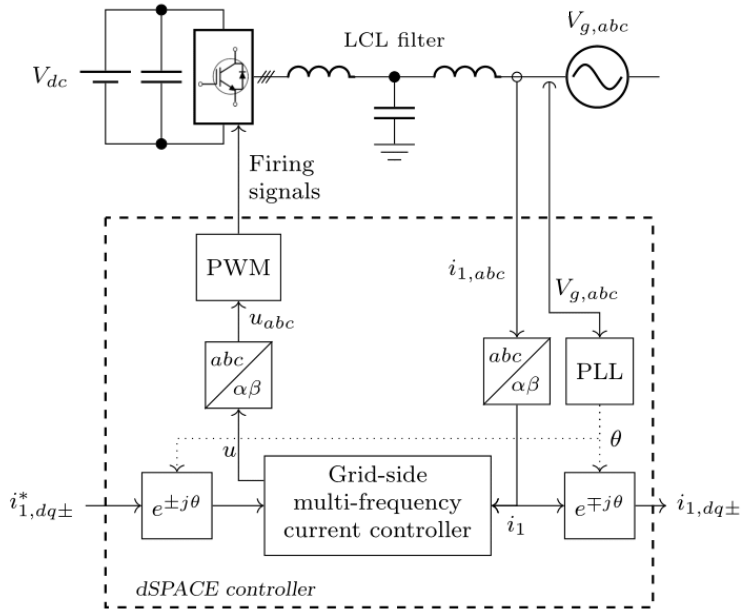

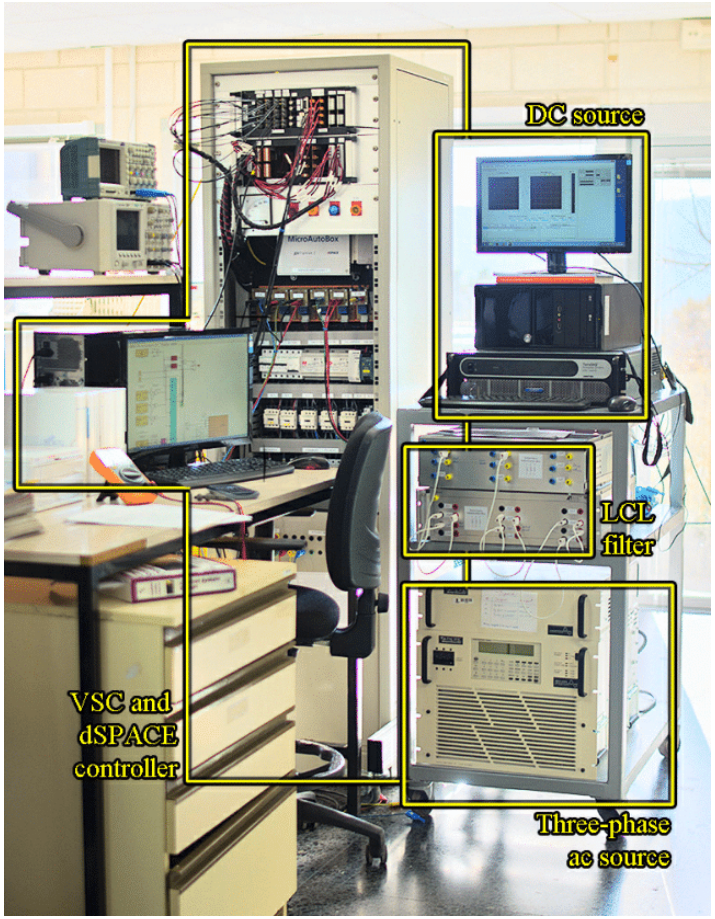

SS- Experimental Results. Reference Tracking

A reference step in the d axis is commanded.

- The compensator design defines the transient response:
  - Fast, damped, and without overshoot or axis crosscoupling
  - Zero steady-state error at the targeted harmonics

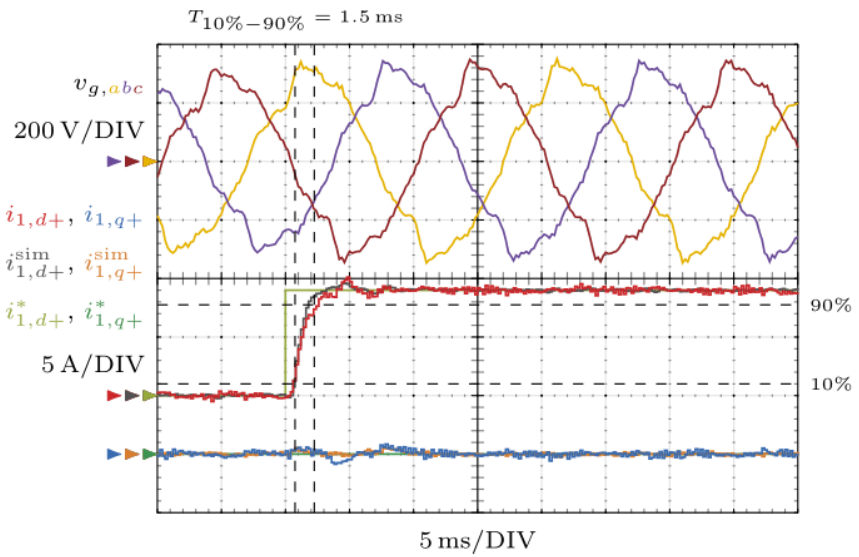

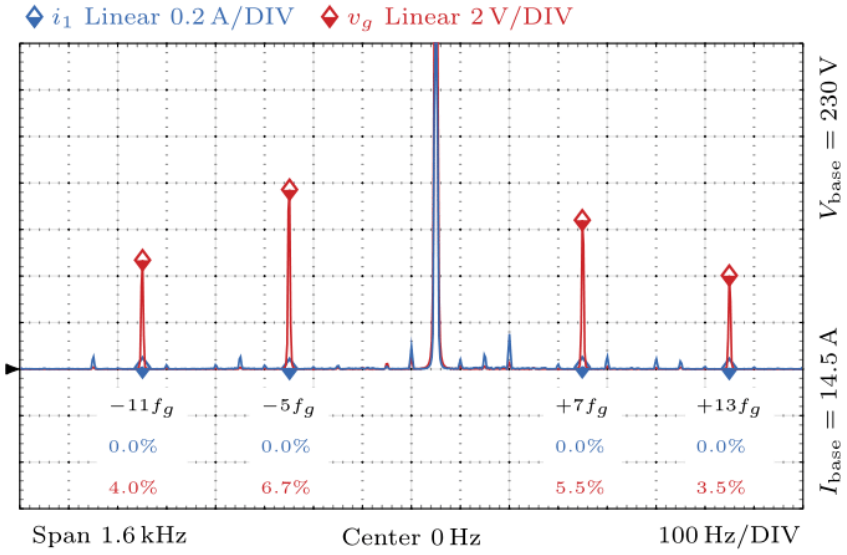

SS- Experimental Results. Disturbance Rejection

A 40%-depth type-C sag is generated.

- Design parameter Q defines transient duration (next slide).

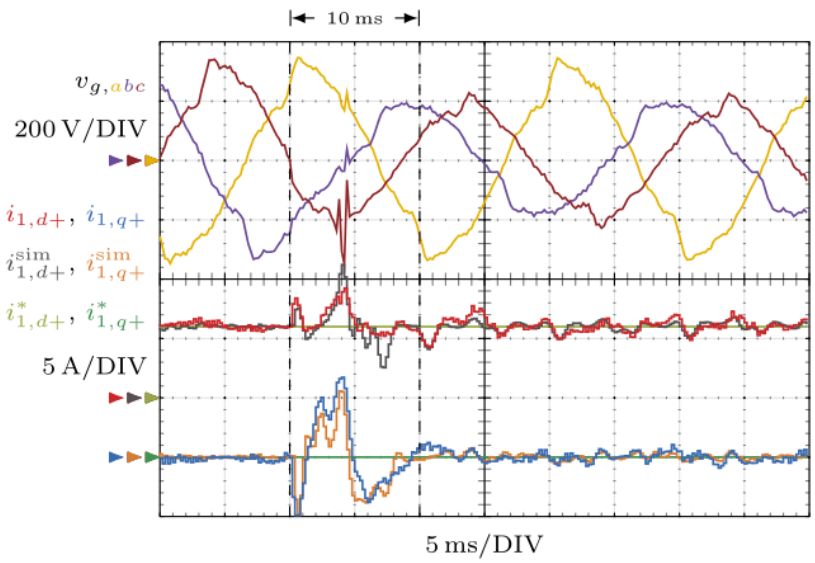

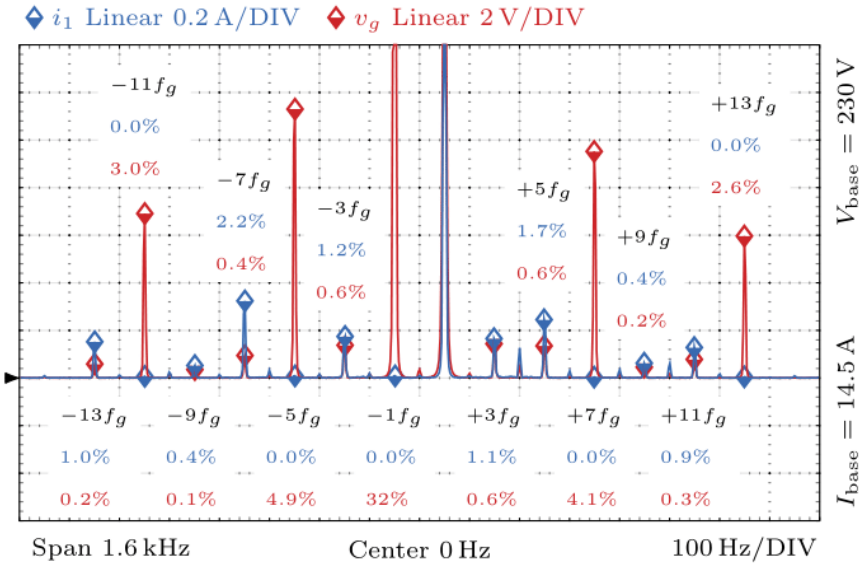

SS- Experimental Results. Observer Bandwidth

- $\boldsymbol{Q} = 0{,}1\%$

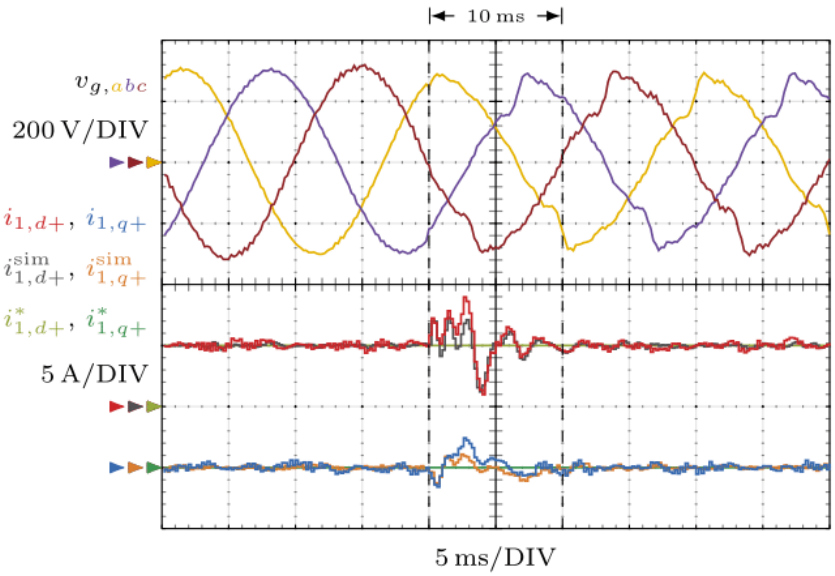

- $\boldsymbol{Q} = 0{,}01\%$

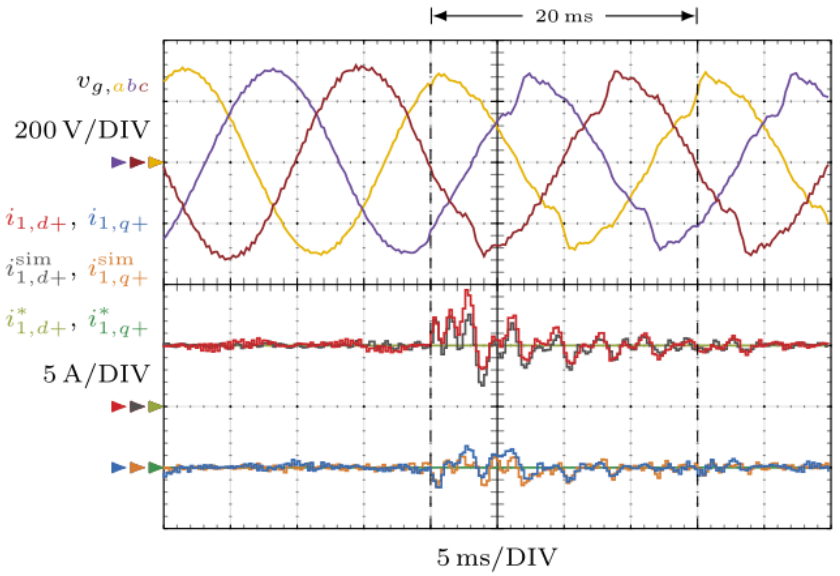

SS Multifrequency Current Controller. Summary

- A multi-frequency current controller based on a Kalman filter for grid-tied converters with LCL filter.
  - Consistent and fast transient response.
  - No overshoot.
  - Simple design process.

- The above properties are maintained irrespectively of:
  - The LCL filter used.
  - The number of current harmonics controlled.

Contents

- Background of microgrids
- AC current control of grid-connected converters
  - Plant model
  - Interface filter
  - Classical controllers
- Limitations of classical current controllers
- State-space based techniques applied to current controllers
- AC voltage control of standalone or weak grid-tied converters

Importance of a robust AC voltage controller

Robustness to load variations. Load can experience large variations depending on:

- The mode of operation: stand alone or grid connected.
- The type and number of loads and power converters connected at the PCC.

Load not included in the nominal plant model used to design the controller.

Load changes introduce unmodeled plant parameter variation that can:

- Degrade the transient response
- Introduce steady-state errors in v_g
- Cause instability.

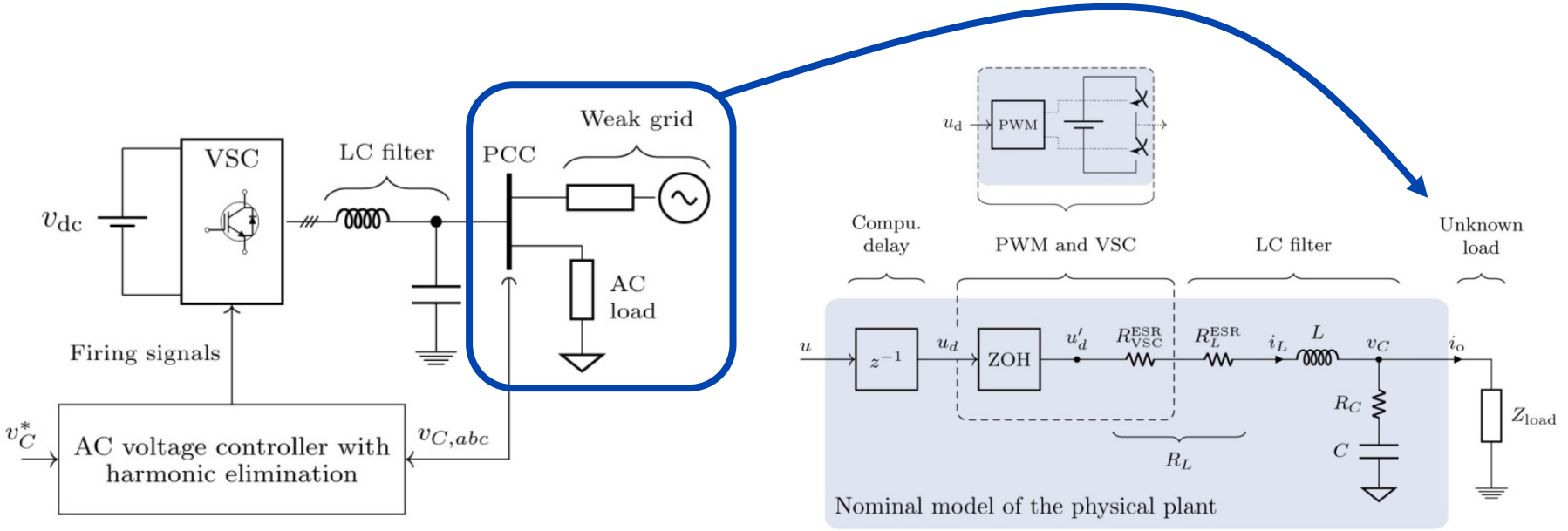

Previous literature of transfer-function-based voltage controllers

- Double-loop controllers:
  - Unstable when $f_{res} \geq f_s / 6$.

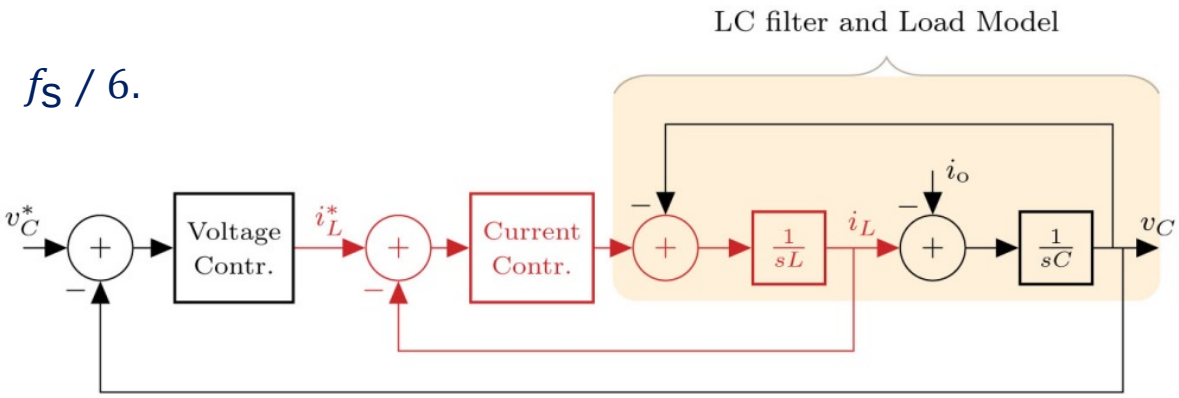

- Single-loop controllers:
  - Unstable when $f_{res} \leq f_s / 4$.

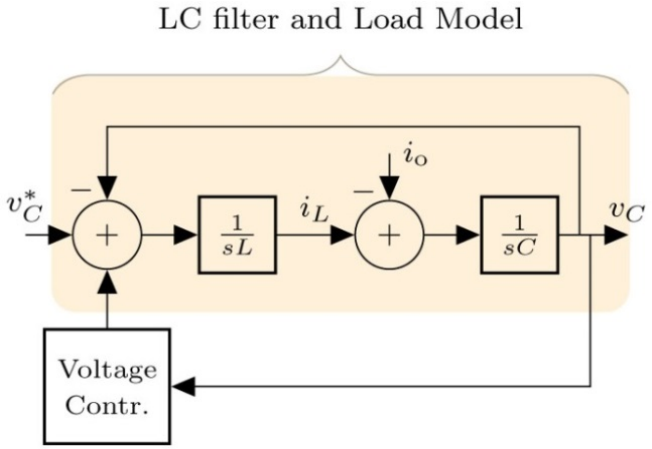

Performance of double-loop voltage controller. Disturbance rejection

Not enough degrees of freedom to remove sensitivity peaks.

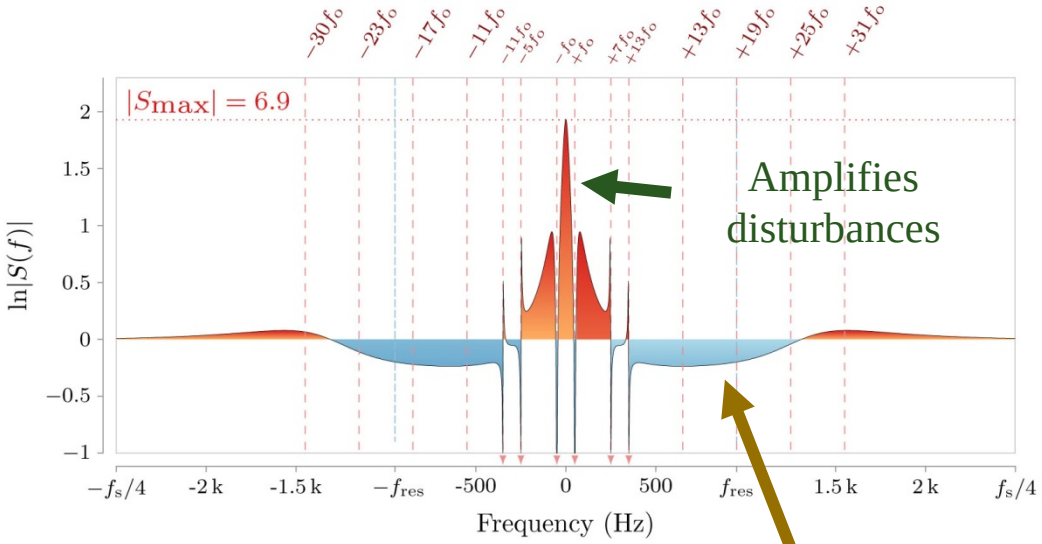

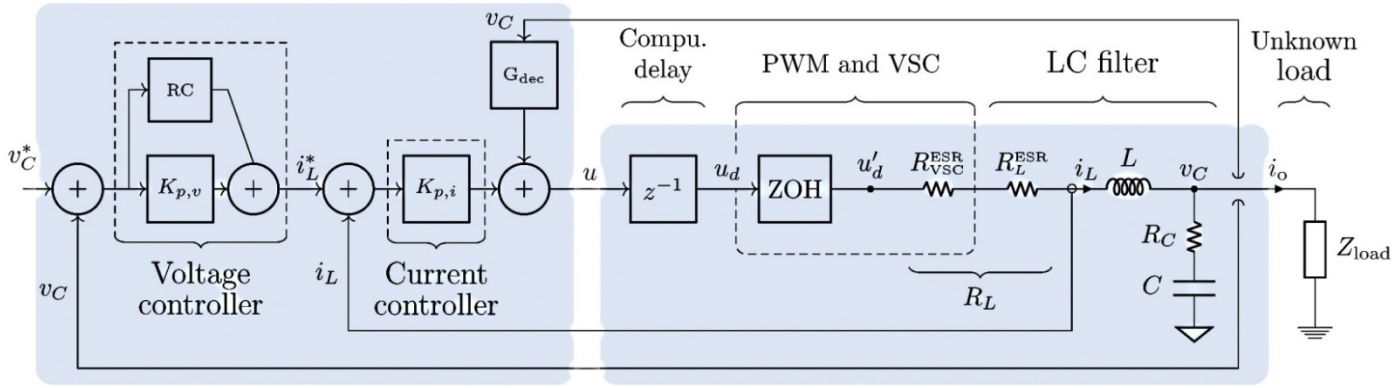

Block diagram of the SS voltage controller

- Linear design.
- State-space controller:
  - Observer uses a Kalman filter.
    - Inherent stability and robustness with simple design.
  - Compensator uses a pole placement technique.
    - Good transient response.

Proven solution applied to a current controller for a VSC with an LCL filter.

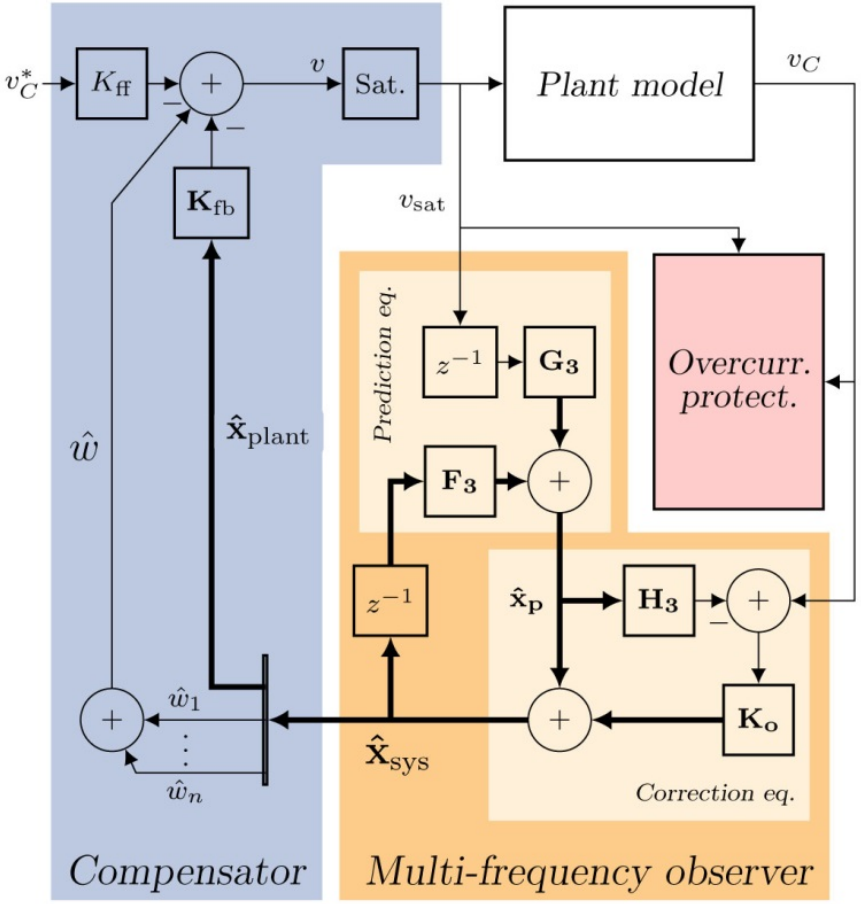

Performance of SS voltage controller. Reference tracking

The compensator uses a discrete-time pole-placement design:

- **Damps the resonant poles:** $p_1^{ol} \rightarrow p_1^{cl}$ and $p_2^{ol} \rightarrow p_2^{cl}$
- Establishes a **dominant pole:** $p_3^{ol} \rightarrow p_3^{cl}$

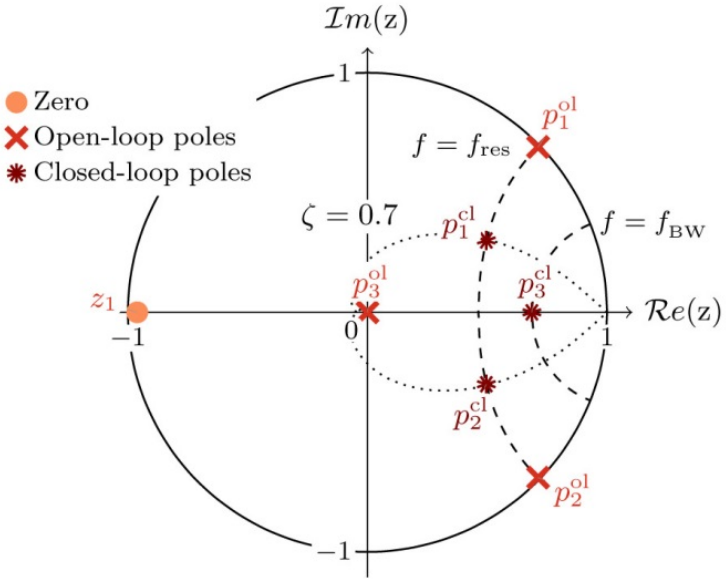

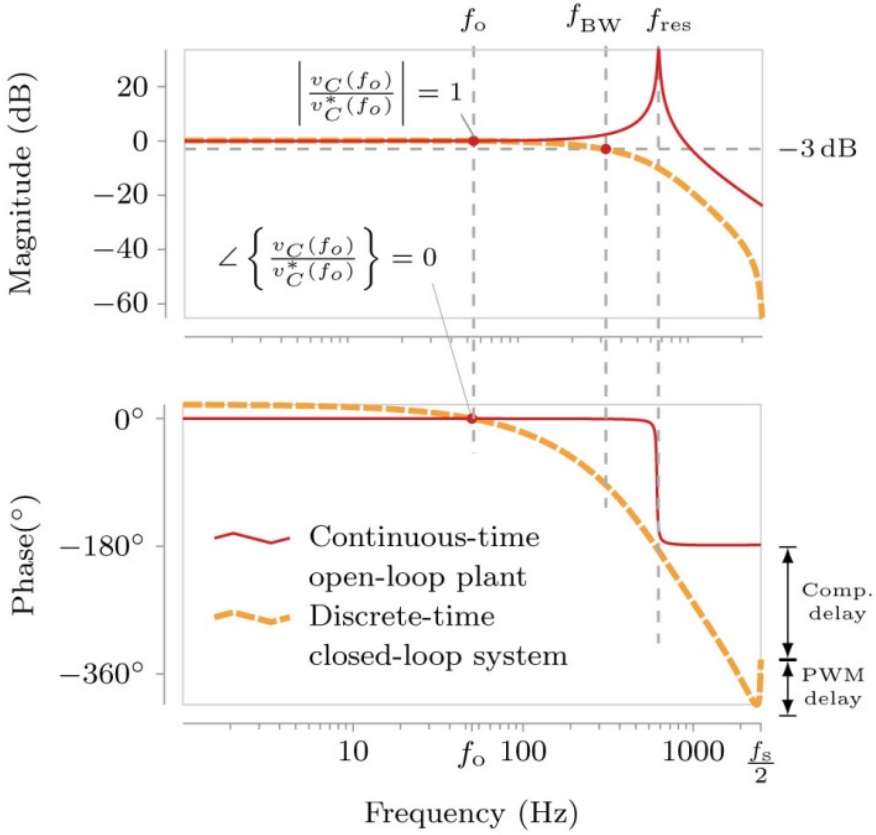

Performance of SS voltage controller. Disturbance rejection

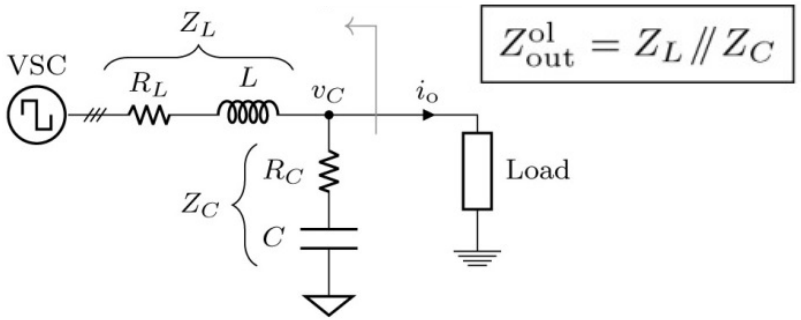

$$z_{out}^{cl} = S \cdot z_{out}^{ol}$$

Controller LC Filter

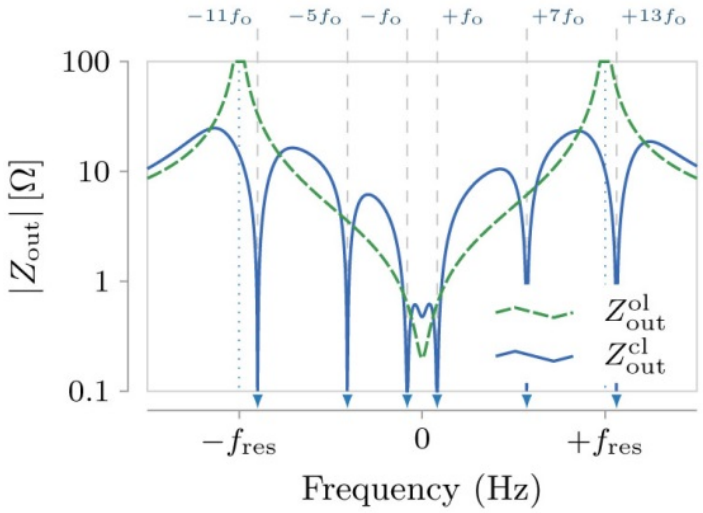

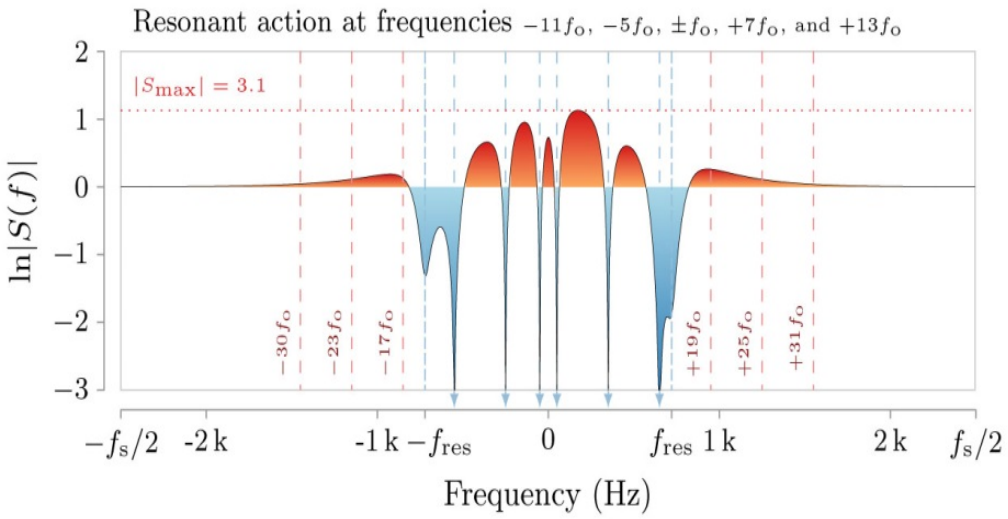

Performance of SS voltage controller. Disturbance rejection

The observer uses a Kalman filter:

- Simple design.
- Robust system.

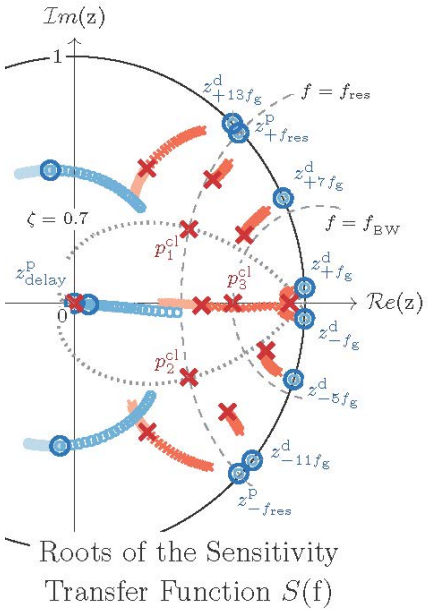

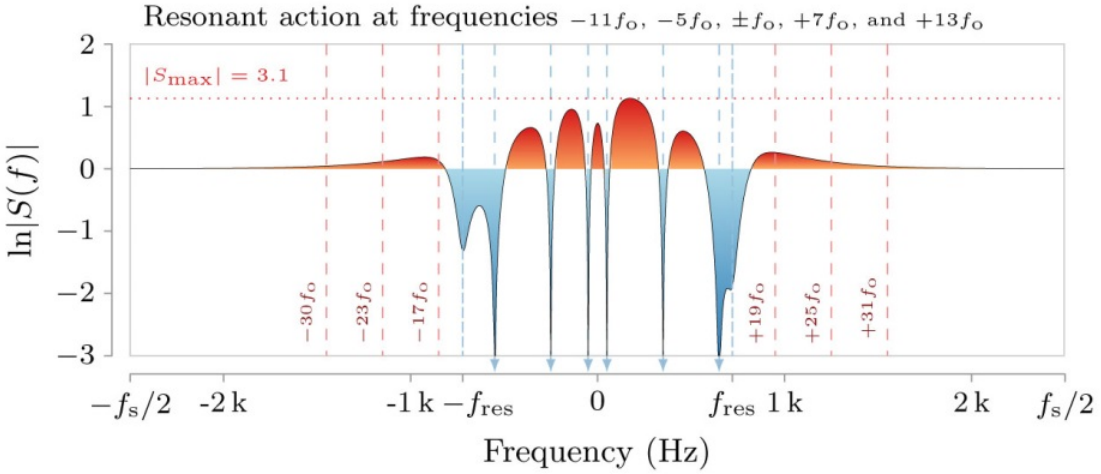

Bode's Theorem:

$$\int_{-\frac{f_s}{2}}^{+\frac{f_s}{2}} \ln|S(f)|df = 0$$

If sensitivity to disturbance is reduced at some frequency range, it is necessarily increased at some other range.

Performance of SS voltage controller. Robustness to load changes

Low disturbance-rejection capability.

Maximum robustness to load changes.

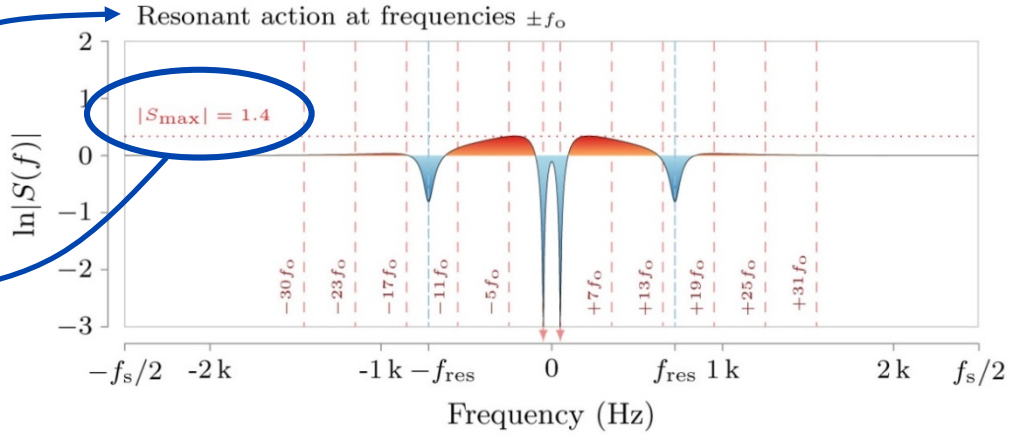

Good disturbance-rejection capability.

Robustness to load changes diminishes.

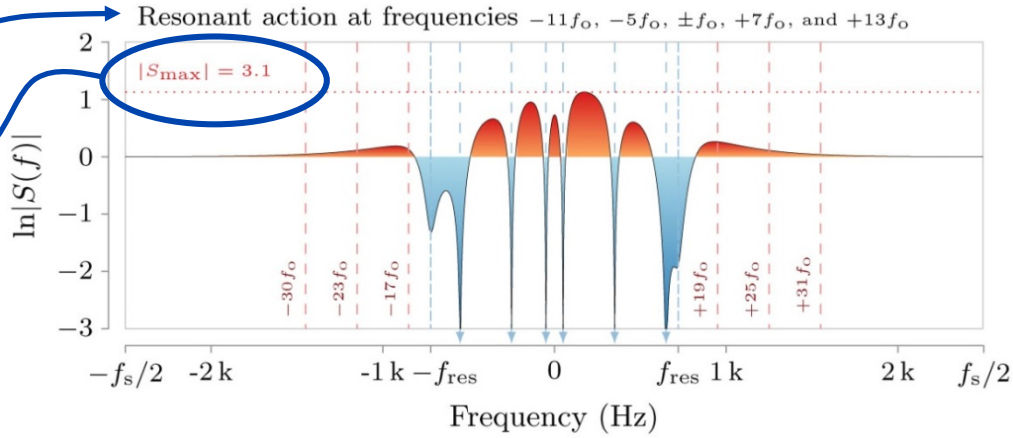

Performance of SS voltage controller. Robustness to load changes

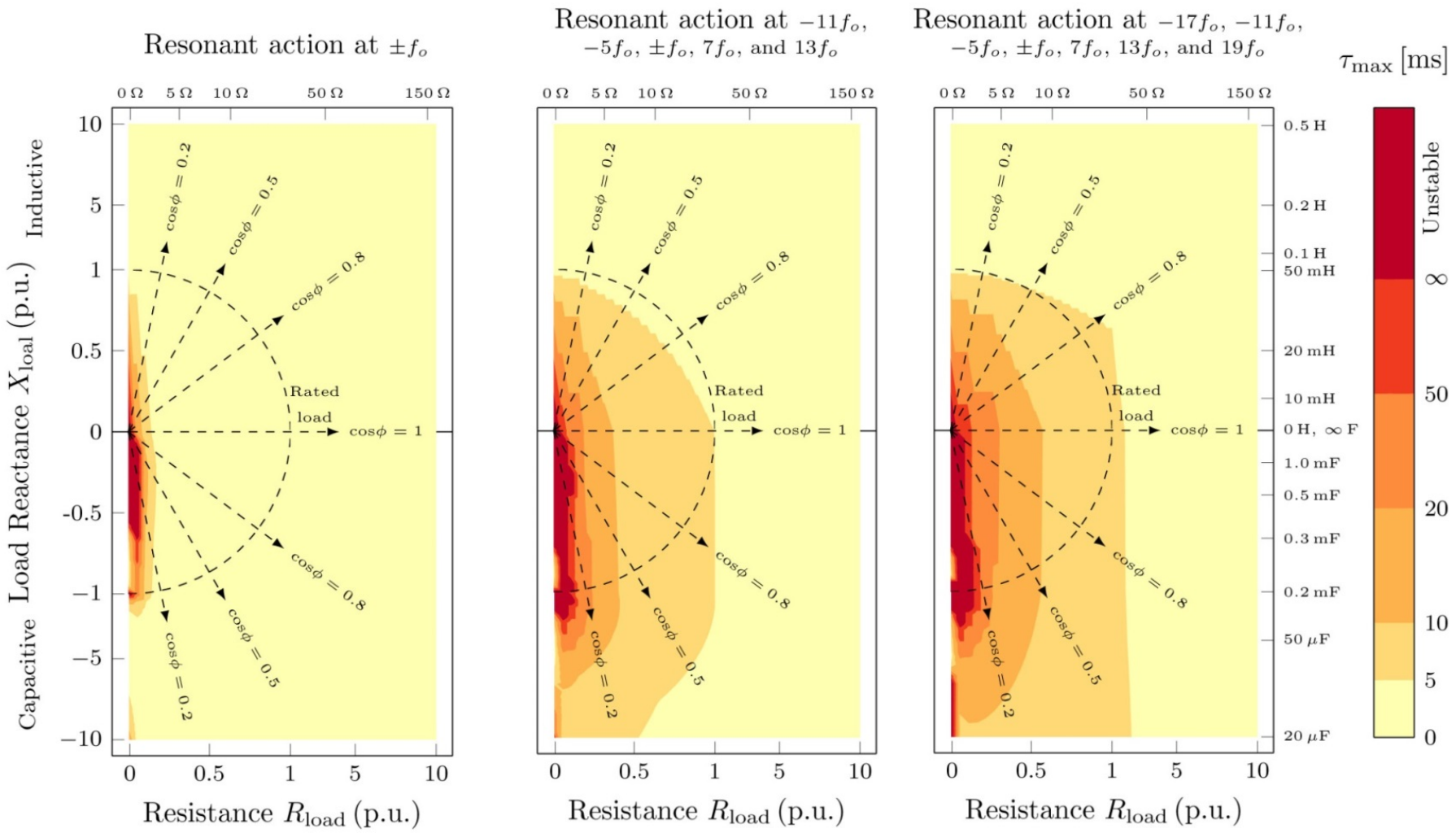

Experimental results. Setup

Tests

1. Disturbance rejection.
2. Operation in a weak-grid.

Base values: $P_o = 10\text{kW}$, $V_{oRMS} = 230\text{V}$, $f_o = 50\text{Hz}$.

VSC: $f_{sw} = 2.5$ kHz, $f_s = 5$ kHz.

LC filter: $f_{\text{res}} = 581$ Hz, $L_f = 2.5\text{mH}$ (5%,), $C_f = 30\mu\text{H}$ (14%).

Nonlinear load: 3-phase full-wave thyristor rectifier (DPF = 0.3).

Grid: 10.5% THD.

$\boldsymbol{Z_{out}^{cl} = 0}$ at $-17f_o$, $-11f_o$, $-5f_o$, $\pm f_o$, $+7f_o$, $+13f_o$, and $+19f_o$.

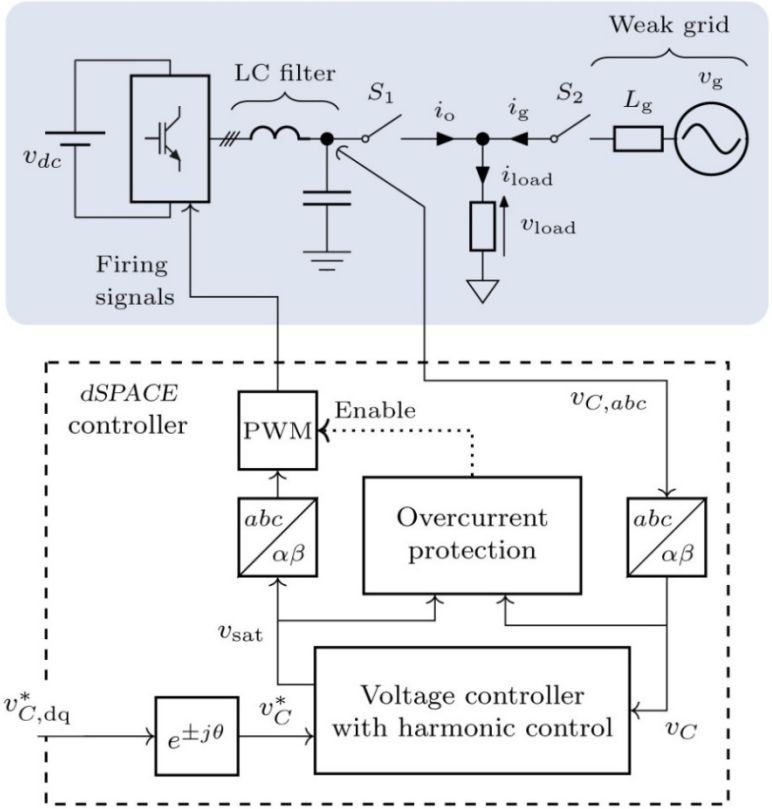

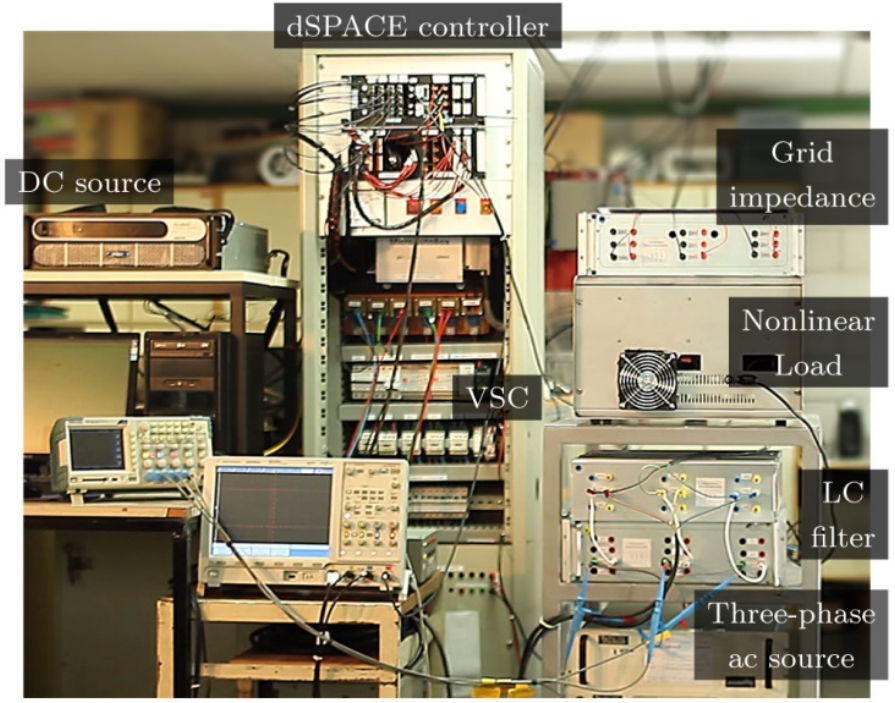

Experimental results. Disturbance rejection

Load step

Nonlinear load: 3-phase full-wave thyristor rectifier (DPF = 0.3).

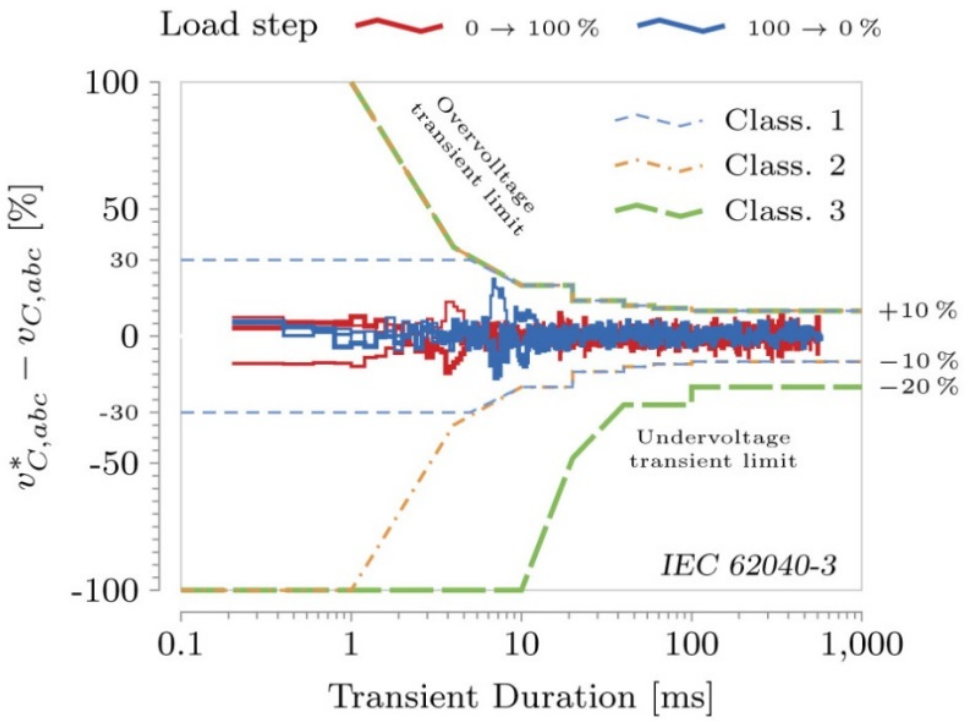

IEC 62040 – Part 3 Uninterruptible power systems (UPS): Method of specifying the performance and test requirements

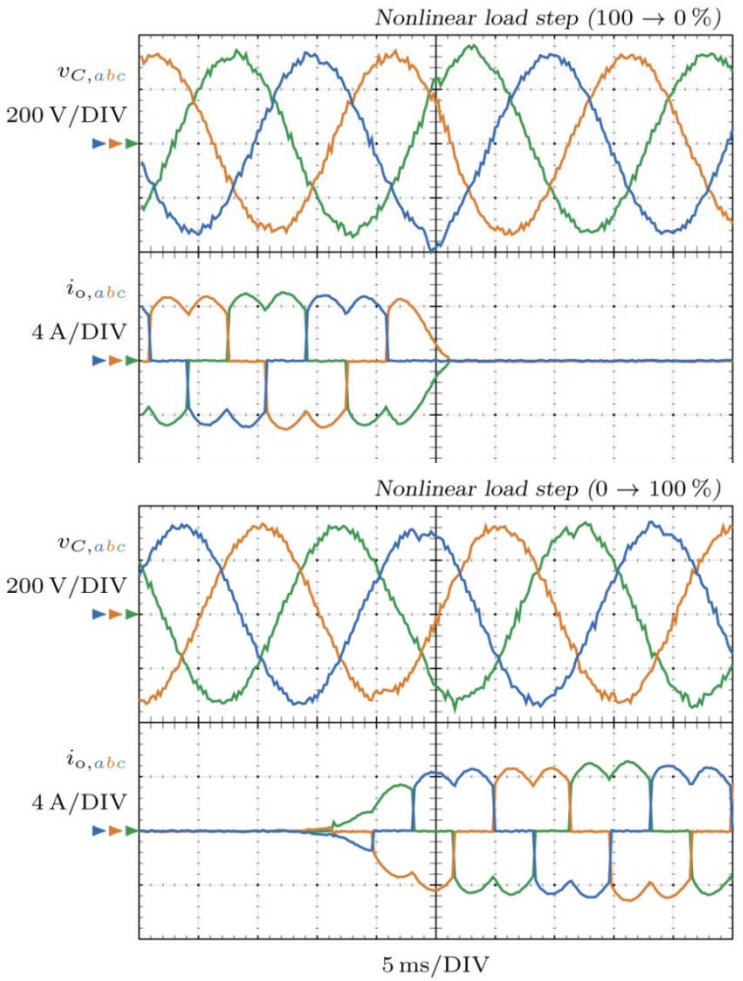

Experimental results. Weak-Grid connection

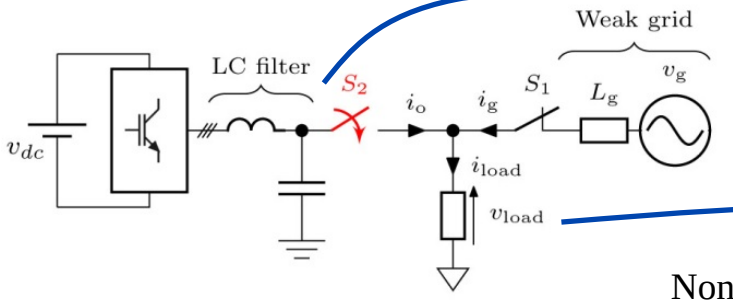

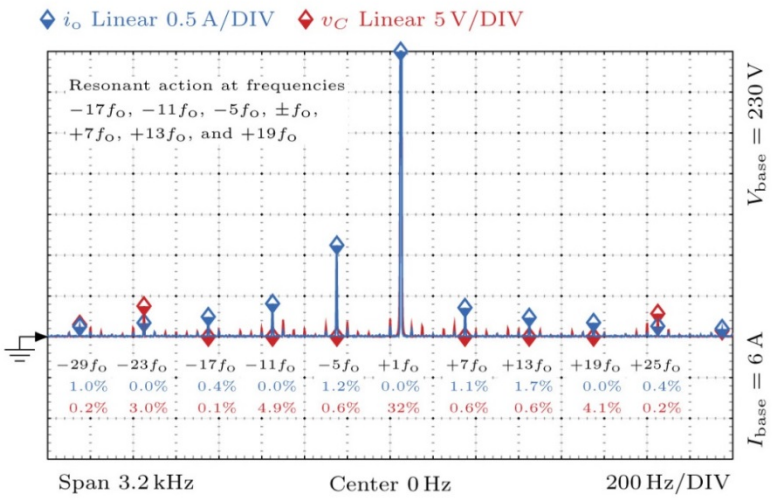

Nonlinear Load (SCR)

Weak grid:

- $L_g = 5.4$mH.
- THD = 10.5%.

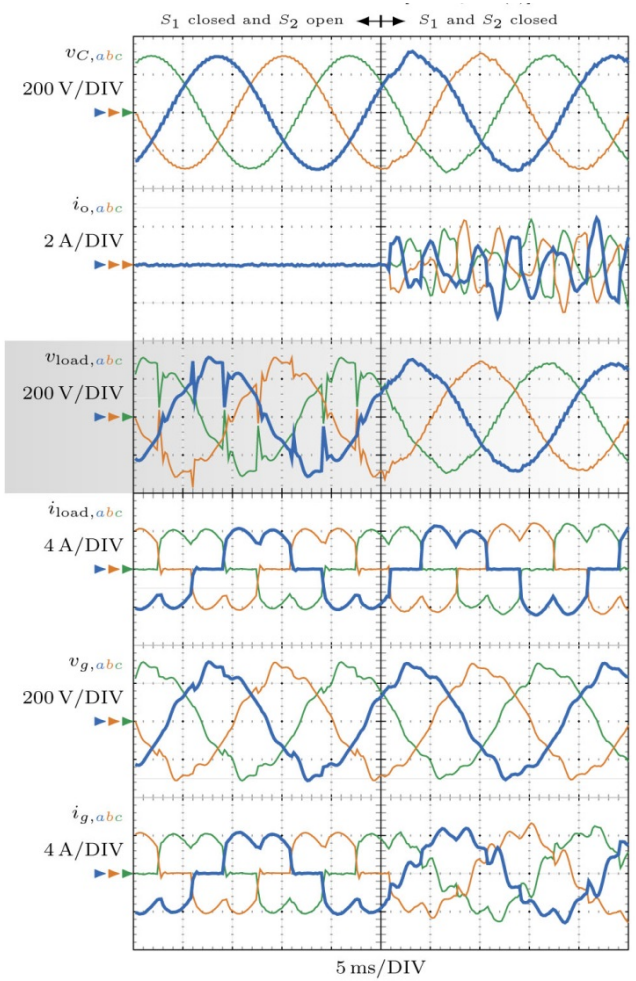

AC voltage controller. Summary

- Robust AC Voltage Controller With Harmonic Elimination for Stand-Alone and Weak-Grid-Connected Operation
  - Fast disturbances rejection capability with zero output impedance at a set of design-selected frequencies.
  - Simple design process based on direct discrete-time pole placement and a Kalman filter.
  - Good robustness to variations in the load impedance.
- Contrarily to a transfer-function-based design, a stable system is obtained irrespectively of the LC filter or the sampling frequency used.

References

PhD Theses

- D. Pérez-Estévez, “Control of Grid-Tied Converters in Microgrids”, PhD Thesis, University of Vigo, 2019.
- A. Vidal, “Transient Response Analysis and Design of Current-Controlled Grid-Tied Converters”, PhD Thesis, University of Vigo, 2015.
- S. Parker, “Discrete Time Current Regulation of Grid Connected Converters with LCL Filters”, PhD Thesis, RMIT University, 2014.
- A. G. Yepes, “Digital resonant current controllers for voltage source converters”, PhD Thesis, University of Vigo, 2011.

Books

- Ned Mohan, Tore M. Undeland, William P. Robbins, “Power Electronics. Converters, Applications and Design”, John Wiley and Sons, Inc, 2003.
- G. C. Goodwin, S. F. Graebe, and M. E. Salgado, Control System Design.1st ed. Englewood Cliffs, NJ, USA: Prentice-Hall, 2001.
- G. F. Franklin, J. D. Powell, and M. L. Workman, Digital Control of Dynamic Systems. 3rd ed. Reading, MA, USA: Addison Wesley Longman,1998.
- T. Hagglund K. J. Astrom. PID Controllers: Theory, Design and Tunning. Research Triangle Park, 1995.

Journal papers (I)

- D. Pérez-Estévez, J. Doval-Gandoy, A. G. Yepes, Ó. López and F. Baneira, "Generalized Multifrequency Current Controller for Grid-Connected Converters With LCL Filter," in IEEE Transactions on Industry Applications, vol. 54, no. 5, pp. 4537-4553, Sept.-Oct. 2018.
- D. Pérez-Estévez, J. Doval-Gandoy, A. G. Yepes, Ó. López and F. Baneira, "Enhanced Resonant Current Controller for Grid-Connected Converters With LCL Filter," in IEEE Transactions on Power Electronics, vol. 33, no. 5, pp. 3765-3778, May 2018.
- A. G. Yepes, J. Doval-Gandoy and H. Toliyat, "Multifrequency Current Control Including Distortion-Free Saturation and Anti-Windup With Enhanced Dynamics", IEEE Transactions on Power Electronics, vol. 33, no. 9, pp. 7309-7313, Sep. 2018.
- D. Pérez-Estévez, J. Doval-Gandoy, A. G. Yepes and Ó. López, "Positive- and Negative-Sequence Current Controller With Direct Discrete-Time Pole Placement for Grid-Tied Converters With LCL Filter,“ in IEEE Transactions on Power Electronics, vol. 32, no. 9, pp. 7207-7221, Sept. 2017.
- L. Harnefors, A. G. Yepes, A. Vidal and J. Doval-Gandoy, "Multifrequency Current Control With Distortion-Free Saturation", IEEE Journal of Emerging and Selected Topics in Power Electronics, Vol. 4, no. 1, pp. 116-125, Mar. 2016.
- A. Vidal, A. G. Yepes, F. D. Freijedo, O. López, J. Malvar, F. Baneira and J. Doval-Gandoy, "A Method for Identification of the Equivalent Inductance and Resistance in the Plant Model of Current-Controlled Grid-Tied Converters", IEEE Transactions on Power Electronics, vol. 30, no. 12, pp. 7245-7261, Dec. 2015.
- A. Vidal, A. G. Yepes, F. D. Freijedo, J. Malvar, O. López and J. Doval-Gandoy, "A Technique to Estimate the Equivalent Loss Resistance of Grid-Tied Converters for Current Control Analysis and Design", IEEE Transactions on Power Electronics, vol. 30, no. 3, pp. 1747-1761, Mar. 2015.

References

- Journal papers (II)

- L. Harnefors, A. G. Yepes, A. Vidal and J. Doval-Gandoy, "Passivity-Based Controller Design of Grid-Connected VSCs for Prevention of Electrical Resonance Instability", IEEE Transactions on Industrial Electronics, vol. 62, no. 2, pp. 702-710, Feb. 2015.
- L. Harnefors, A. G. Yepes, A. Vidal and J. Doval-Gandoy, "Passivity-Based Stabilization of Resonant Current Controllers With Consideration of Time Delay," in IEEE Transactions on Power Electronics, vol. 29, no. 12, pp. 6260-6263, Dec. 2014.
- Vidal,Ana et al., "Transient response evaluation of stationary-frame resonant current controllers for grid-connected applications" IET Power Electronics(2014),7(7):1714.
- A. G. Yepes, A. Vidal, O. López and J. Doval-Gandoy, "Evaluation of Techniques for Cross-Coupling Decoupling Between Orthogonal Axes in Double Synchronous Reference Frame Current Control," in IEEE Transactions on Industrial Electronics, vol. 61, no. 7, pp. 3527-3531, July 2014.
- S. G. Parker,B. P.McGrath, and D. G. Holmes, "Regions of active damping control for LCL filters," IEEE Trans. Ind. Appl., vol. 50, no. 1, pp. 424–432, Jan./Feb. 2014
- A. G. Yepes, A. Vidal, J. Malvar, O. López and J. Doval-Gandoy, "Tuning Method Aimed at Optimized Settling Time and Overshoot for Synchronous Proportional-Integral Current Control in Electric Machines," in IEEE Transactions on Power Electronics, vol. 29, no. 6, pp. 3041-3054, June 2014.
- A. Vidal et al., "Assessment and Optimization of the Transient Response of Proportional-Resonant Current Controllers for Distributed Power Generation Systems," in IEEE Transactions on Industrial Electronics, vol. 60, no. 4, pp. 1367-1383, April 2013.
- A. G. Yepes, F. D. Freijedo, Ó. Lopez and J. Doval-Gandoy, "Analysis and Design of Resonant Current Controllers for Voltage-Source Converters by Means of Nyquist Diagrams and Sensitivity Function," in IEEE Transactions on Industrial Electronics, vol. 58, no. 11, pp. 5231-5250, Nov. 2011.
- A. G. Yepes, F. D. Freijedo, Ó. Lopez and J. Doval-Gandoy, "High-Performance Digital Resonant Controllers Implemented With Two Integrators," in IEEE Transactions on Power Electronics, vol. 26, no. 2, pp. 563-576, Feb. 2011.
- H. Kim, M. Degner, J. Guerrero, F. Briz, and R. Lorenz, "Discrete-time current regulator design for ac machine drives," IEEE Trans. Ind. Appl.,vol. 46, no. 4, pp. 1425–1435, Jul./Aug. 2010.
- A. G. Yepes, F. D. Freijedo, J. Doval-Gandoy, Ó. López, J. Malvar and P. Fernandez-Comesaña, "Effects of Discretization Methods on the Performance of Resonant Controllers," in IEEE Transactions on Power Electronics, vol. 25, no. 7, pp. 1692-1712, July 2010.
- M. Liserre, F. Blaabjerg, and S. Hansen, "Design and control of an LCLfilter- based three-phase active rectifier," IEEE Trans. Ind. Appl., vol. 41, no. 5, pp. 1281–1291, Sep./Oct. 2005.
- F. Briz, M. Degner, and R. Lorenz, "Analysis and design of current regulators using complex vectors," IEEE Trans. Ind. Appl., vol. 36, no. 3, pp. 817–825, May/Jun. 2000
- Lennart Harnefors and H.-P. Nee. Model-based current control of ac-machines using the internal model control method. IEEE Trans. Ind. Appl., vol. 34, no. 1, pp. 133–141, Jan. 1998.

¿Questions?

Jesús Doval Gandoy
jdoval@uvigo.es
http://webs.uvigo.es/jdoval